Model Predictive Voltage Regulation in Active Medium Voltage Distribution Grids

András Zöllner

TU Delft
Delft University of Technology

Delft Center for Systems and Control

Model Predictive Voltage Regulation in Active Medium Voltage Distribution Grids

MASTER OF SCIENCE THESIS

For the degree of Master of Science in Systems and Control at Delft University of Technology

András Zöllner

October 30, 2023

Faculty of Mechanical, Maritime and Materials Engineering (3mE) · Delft University of Technology

Abstract

The renewable generation capacity, particularly solar and wind power installations, has increased steadily in the Netherlands over the course of recent years. Due to the local, small-scale nature of these power plants (compared to conventional power plants), a large share of this generation capacity is installed into the medium- and low-voltage distribution grids. This trend acts as the source of several challenges for distribution system operators (DSOs) such as Stedin Netbeheer B.V. (a DSO in the Netherlands, supporting this project). One of the main problems is the fact that voltage limit violations, particularly upper voltage limit violations, become more frequent.

Conventional voltage control schemes assume a unidirectional power flow (i.e., consumption only) in distribution grids and are unable to keep the limits in case a large share of generation capacity is installed. This is further complicated by the fact that underground cable networks, typical in Western European electricity distribution grids, have lines with large R/X ratios, which reduces the effectiveness of reactive power injection-based voltage control methods.

This MSc project intends to solve the issue of voltage limit violations with a model predictive control (MPC) policy. The considered control actions coordinated by the model predictive controller are the switching of the on-load tap changer (OLTC) mechanism mounted to the primary substation's transformer, setpoint adjustments of the low-level OLTC control relay, and the active power curtailment of larger photovoltaic plants. A linear, sensitivity-matrix-based model is used for the grid's state prediction; and the sensitivity values are re-calculated at each sampling time step of the MPC. To avoid the curtailment of photovoltaic (PV) plants when not justified, a conditional curtailment logic is incorporated into the MPC policy: PV plants are only allowed to be curtailed if their local voltage magnitude is above a tuneable threshold. This logic is described and incorporated into the model predictive controller's optimization problem with the help of binary variables and mixed-integer linear (MIL) constraints. The benefit of incorporating knowledge about future disturbances (load, generation, and external grid voltage profiles) is also tested, in order to assess the potential benefit DSOs could get from forecasting these quantities.

A case study was conducted in which the considered controllers were tested on a section of a Stedin grid that carries the characteristics of a typical Western European medium voltage

distribution grid: large R/X ratios and a large installed PV generation capacity both in the form of household generation and larger PV plants. All controllers were simulated in 4 different test cases: a typical summer day, a summer day with the external grid's overvoltage, a summer day with 2 out of 3 large PV plants not operating, and a typical winter day. All test cases have the control goals of mitigating limit violations and ensuring that the nodal voltage magnitudes are as close as possible to the nominal 1 per unit throughout the day. The winter day test case has the additional goal of avoiding excessive curtailment as PV energy is worth considerably more during these days. All profile data is based on real Stedin measurements. The designed model predictive control policies are compared to two simple control schemes: current compounding, i.e. when the primary substation's automatic voltage control relay's setpoint is adjusted based on the active power delivery through the substation's transformer, and another scheme when current compounding is combined with local active power curtailment controllers for large PV plants. The most important metrics used for comparison are voltage root mean square error (RMSE), the total voltage limit violation area, the percentage of curtailed PV energy, and the number of tap changes over the considered day. The simulations were carried out using Python and DIgSILENT PowerFactory.

The simulation results show that the MPC policy can perform better than the simple control schemes but only when exact knowledge of future profiles is available. In this case, the MPC results in lower voltage RMSE, smaller violation areas, and lower curtailment percentage values, at the expense of using more tap changes in all 4 test cases. In 3 of the 4 test cases, MPC was completely able to eliminate voltage limit violations, showing clearly the advantages of good quality forecasts on future disturbances. Since this exact knowledge about the near future fluctuations is quite ideal, more realistic MPC policies were also tested with no future knowledge and tightened voltage constraints. These simulations brought mixed results when compared with the simple schemes, performing better in terms of voltage RMSE, but sometimes worse in terms of the total voltage limit violation area, PV curtailment, and total number of tap changes.

Table of Contents

Bibliography **103**

Glossary **113**

Acknowledgements

This thesis marks the end of a long and interesting journey: my MSc training in Systems and Control at the Delft University of Technology. I am writing these acknowledgments to express my immense gratitude for this experience.

There are a few very important people without whom this project would not exist in its current form. I would like to thank Prof. Dr. ir. Bart De Schutter, my supervisor at TU Delft, for suggesting me this interesting thesis topic, and for his comments and guidance, which always helped me go in the right direction. I would like to thank my two supervisors at Stedin, Dr. ir. Edward Coster and ir. Bart Kers, for the immense amount of help, guidance, and encouragement they have given me while I was working at the company. I would also like to thank them for all the incredible experiences I had at Stedin, such as being able to visit a substation or being given the chance to attend CIRED2023.

I would also like to thank my mother Márta Szabó and my father Zoltán Zöllner, for all their support, love, and encouragement they have given me during my studies. I would like to express my gratitude to my girlfriend Anna Varga, for being there for me and listening to all my concerns with love, empathy, and a positive attitude. Lastly, I would like to thank my friends, family, professors, teachers, and anyone who has helped me in any way throughout my studies but could not be listed here by name due to sheer lack of space.

Thank you all very much! I truly consider myself very lucky to have had this amazing experience.

Delft, University of Technology   András Zöllner
October 30, 2023

Chapter 1

Introduction

1-1 Background Information

The modern electric power grid is the backbone of today's society. By looking at the role of electricity throughout history, it can be seen that its function has transformed significantly from a luxurious novelty way of lighting the home of the privileged to an absolute necessity. Nowadays millions of residential, commercial, and industrial customers consume electric power, and other critical infrastructure (e.g. water supplies, hospitals) also depends on it. Knowing the vital role of electricity and the electric power grid, the ongoing trends and changes due to the increasing popularity of distributed renewable energy resources will be discussed in this chapter, with the main focus being on European power networks, more specifically power grids in the Netherlands.

Traditionally, electric power production has three main stages: generation, transmission, and distribution. Figure 1-1 gives a visual representation of these three stages. Conventional power plants have a large generation capacity and are usually located far from the consumers. These plants generate three-phase AC voltages with a nominal frequency of 50 Hz, which is
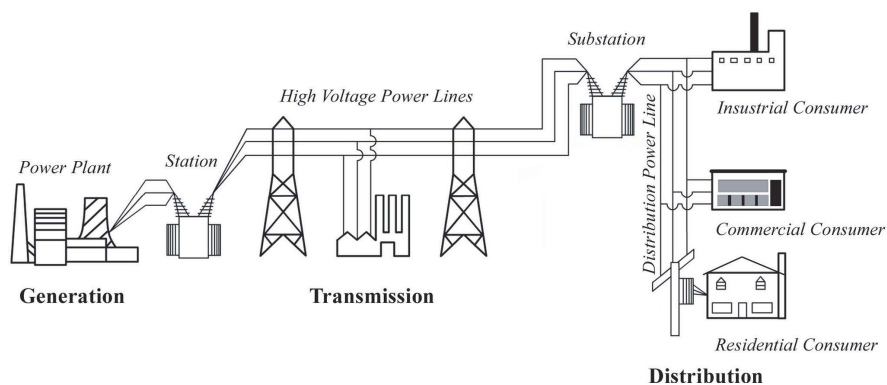
Figure 1-1: Overview of the Electric Power System, Source: [12]

constant throughout the whole network. This is achieved by synchronous generators whose speed is always proportional to the grid's frequency through a fixed ratio. The generators are driven by the so-called prime movers (turbines), which often use coal, natural gas, nuclear fission, hydropower, etc. as their source of energy. A synchronous machine's active power production can be changed by altering the amount of mechanical power delivered by the prime mover. This is done by the prime mover's governor, which is a local control device ensuring the right rotational speed of generators, hence also ensuring the right amount of active power is produced at all times (the demands of the consumers are met). The common grid frequency, i.e. the grid's synchronism is achieved by the dynamic interaction of governors of large generators, so it is essential that these devices are designed appropriately. The synchronous machines' excitation can also be adjusted which allows the setting of the right voltage magnitude at the power plant's grid connection point locally by injecting an adequate amount of reactive power into the grid.

In a traditional setting, the power plants are located far from the consumers for the following reasons: their prime energy source pinpoints their location (e.g. the location of a dam in case of a hydropower plant), their pollutant operation (e.g coal plants) requires them to be far from residential areas, or they require a lot of land and other infrastructure due to the grandiose scales on which they operate (e.g. nuclear plants). Considering this, electric power has to be efficiently transmitted to the customers over long distances. To minimize losses caused by the transmission grid's resistance, the generated AC voltages are stepped up, usually into the range of hundreds of kilovolts (high-voltage, i.e. the HV range) by transformers. After transmission, this high voltage has to be converted back to medium- (MV) and then low-voltage (LV) in order to be safely used by the customers. The HV transmission network's voltage is stepped down to MV at primary distribution substations by larger distribution transformers, and further down to LV at secondary substations by smaller distribution transformers that are close to the customers' points of connection.

A transmission grid is controlled and operated by a Transmission System Operator (TSO), and a distribution grid is controlled and operated by a Distribution System Operator (DSO) company. The national TSO of the Netherlands is TenneT TSO B.V. with its headquarters located in Arnhem. Stedin Netbeheer B.V. (in the following: "Stedin") is a Dutch DSO currently serving more than 2 million customers mainly in the Randstad area with its headquarters located in Rotterdam. The work in this graduation assignment was supported by Stedin as it intends to explore solutions to the voltage problems the DSO is facing in its grids due to the increasing share of renewable energy-based distributed generation.

In recent decades the popularity of renewable energy sources has increased rapidly, mainly due to environmental and sustainability concerns. Increasing energy prices are also a strong driving force toward the exploration of alternative energy sources. Statistics Netherlands (CBS), the Dutch Government's central statistics bureau, has reported a 20% growth of renewable generation in the country in 2022 [96]. This growth is also shown in Figure 1-2, where it can be seen that while renewable energy production grew in the Netherlands, overall energy production stagnated between 2020 and 2022. This means that conventional fossil fuels were replaced with renewable sources. The 20% growth is further differentiated in [96]: solar power production grew by 54% and wind power production by 17% in 2022 while hydropower and biomass-based renewable production has seen a decline. The main reasons listed in [96] for this growth are the extra 4 GW of solar and 1 GW of wind generation capacity installed during the year and the favorable weather conditions.
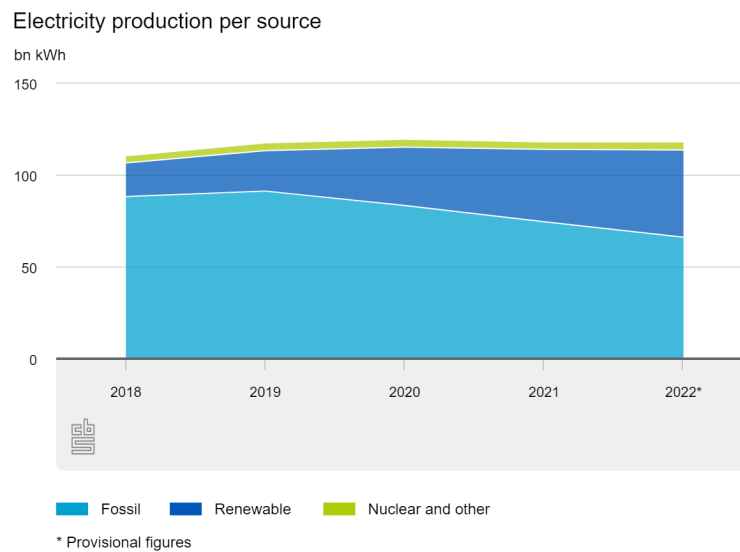
Figure 1-2: Electric Power Production in the Netherlands, Source: [96]

Compared to conventional power plants these renewable units are small-scale power generators, usually closer to the consumer's location. For this reason, these energy sources are often connected to the (medium or low voltage) distribution grids. The operation of small-scale power sources that feed power directly into the distribution grid is called Distributed Generation (DG) and it is a rapidly growing trend reshaping modern distribution networks. Distribution grids that also feature generation capacity and control systems that manage such resources are called active distribution networks (ADNs) as the definition in [19] also states: "Active Distribution Networks (ADNs) are distribution networks that have systems in place to control a combination of distributed energy sources (generators, loads and storage)." The control setups of ADNs are often referred to as Active Network Management (ANM) schemes.

According to [34, 78] the International Energy Agency (IEA) lists several reasons for the growing popularity of DG and the increasing number of ADNs in its 2002 report titled "Distributed Generation in Liberalised Electricity Markets". These reasons include the fast-paced advancements of DG technology, the challenges of constructing new transmission grids, the consumers' increased demand for a reliable connection, a liberalized electricity market and the increasing concerns about environmental issues such as climate change. Besides having many advantages such as cleaner power generation and lower transmission losses, DG also leaves DSO companies with several challenges. The issue of voltage limit violations is one of such challenges that is discussed in the next section of this chapter in the form of a detailed problem statement that serves as the main motivating factor behind this graduation project.

1-2 Problem Statement: Impact of Distributed Generation on Voltage Control

According to [80], the presence of DG causes the following problems in distribution grids: more frequent voltage limit violations (particularly upper limit violations), the possibility

of bi-directional power flow, increased short circuit currents (mainly with DG units using rotating machines such as wind turbines), more difficult network protection (harder to set protective relays, possible islanding), and possible imbalances due to small single phase DG units.

This thesis only focuses on the issue of voltage limit violations. The motivation behind this is the fact that many DSOs, including Stedin, experience voltage problems in their networks due to the growing number of DG units, mainly solar plants. At the moment, Stedin is conducting a pilot study in one of its MV distribution networks located in South Holland province, which focuses on finding a refined control policy that uses the grid's existing installed control gear (On-Load Tap Changer (OLTC) and active power curtailment) and is capable of solving the voltage problems caused by DG. This graduation assignment's goal is to explore how model predictive control can be applied to medium-voltage distribution grids, particularly the section of a Stedin medium-voltage distribution grid featured in the case study, presented in Chapter 4.

Ensuring the right voltage magnitudes in electric power networks, especially at the customer's point of connection is a very important goal of grid control and operation. Too high voltages can cause problems such as lights burning out or solar plants not being able to supply energy back to the grid (due to their inverters switching off). Too low voltages could result, for example, in the failure of electric motors [13]. For this reason, different policies and standards set limits on the minimum and maximum allowable voltage limits. In the European Union, the EN50160 standard [17] specifies a tolerance of $\pm 10\%$ around the nominal value of 400V line-to-line at the low-voltage customer's connection point. 95% of the 10 min average RMS voltage values have to lie within these bounds over any measurement period of 1 week. The Dutch grid code, which is followed by Stedin, specifies additional requirements stating that besides being compliant with EN50160 all the 10 min average RMS voltage measurements over any measurement period of 1 week have to lie within the bounds of 0.85 and 1.1 per unit (i.e. -15% and $+10\%$) at the customer's point of connection.

This study only focuses on the voltage magnitudes in the medium voltage grid, as the low voltage customers are only modeled as lumped load and PV generator elements. For the MV grid's nodes, more strict limits of 0.975 and 1.025 per unit are considered as the lower and upper limits respectively that are intended to be kept by the several considered control policies at all times (within the time resolution of the simulation). The main reason behind these value choices is the fact that in case stricter limits are kept at higher (medium) voltage levels, the grid can tolerate more disturbances (e.g. household PV, EV charging, heat pumps) at the lower voltage levels (in the low-voltage grids in this case). The per unit voltage magnitude limits will be denoted the following way in this report with V_{low} being the lower and V_{high} being the higher limit respectively:

$$V_{\text{low}} = 0.975 \text{ pu} \qquad V_{\text{high}} = 1.025 \text{ pu} \qquad (1\text{-}1)$$

1-2-1   Voltage Drop Approximation in a Simple Feeder

To illustrate how the presence of distributed generation affects the voltage profiles in distribution grids, the receiving end's voltage magnitude in the commonly used 2-bus feeder example will be shown here based on [80]. The simplified feeder circuit and its phasor diagram are

shown in Figure 1-3. $\mathbf{V}_S$ is the per unit voltage phasor at the supply side, and $\mathbf{V}_R$ is the receiving end's per unit voltage phasor. The supply side is assumed to have a constant $\mathbf{V}_S$ voltage phasor. This is a realistic assumption in a distribution grid, as the feeder's starting point is at the primary substation, where the feeder connects to a very stiff external high-voltage grid through a transformer, that is equipped with an automatic OLTC. For more information on OLTCs and Automatic Voltage Control (AVC) relays refer to Subsection 2-1-2 of Chapter 2 or [40, 80]. The load (receiving) side is assumed to consume P active and Q reactive power regardless of any other external factor, i.e. a constant power load model [57, 14] is assumed. The cable between the supply and the load is modeled as a series interconnection of a lumped R resistance and X reactance, and $\mathbf{I}$ denotes the per unit current phasor flowing from the supply to the load. The quantity of interest is the V_R voltage magnitude of the feeder's voltage drop and its dependence on other quantities.

(a) Simplified Feeder Circuit   **(b)** Phasor Diagram
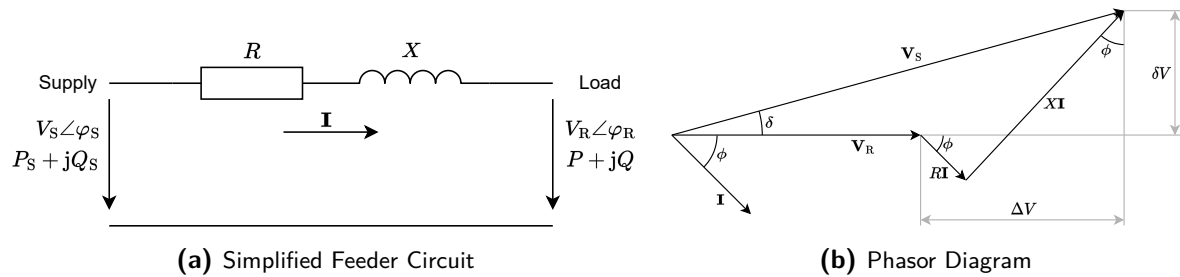
Figure 1-3: Illustrative Example for Feeder Voltage Drops, Source: [80]

Assuming the δ angle in Figure 1-3b is quite small (which is realistic for distribution grid feeders), the following approximation of Equation 1-2 can be derived for V_R. For the full derivation refer to [80].

$$V_R \approx V_S - \frac{R}{V_R}P - \frac{X}{V_R}Q \tag{1-2}$$

Looking at Equation 1-2 it can be seen that the receiving end's V_R voltage magnitude depends on the P active and Q reactive power consumption: the more power consumed, the smaller V_R becomes. The inaccuracies of the supply side's local voltage control cause fluctuations in the V_S magnitude which can also be observed at the feeder's receiving side. The goal of voltage control is to keep all nodal voltages as close to nominal as possible, so keep both V_S and V_R close to nominal (1 pu). Looking at Equation 1-2, the following conventional solutions to voltage problems can be listed:

- Suppressing the fluctuations of V_S with a well-selected OLTC equipped transformer and AVC relay at the feeder's supply side (primary substation), also results in a smoother V_R profile. For more information refer to Section 2-1-2 of Chapter 2 or [80, 40].

- Line Drop Compensation (LDC): raising V_S during heavy loading (when P and Q are large), helps keep V_R closer to nominal. For more information refer to Section 2-2 of Chapter 2 or [77].

- Changing the Q reactive power consumption at the receiving end with the help of a compensator device. This could mitigate V_R fluctuations without disturbing the load's P active power consumption. For this scheme to be feasible, the feeder cannot have

large R/X ratios as it would make the V_R voltage less sensitive to changes in Q. For more information refer to Section 2-2 of Chapter 2 or [78].

- Grid reinforcement, which results in smaller R and X values, and effectively a smaller difference between V_S and V_R. This requires the laying of new cables, which is a very costly procedure and hence should be avoided if possible.

These observations from Equation 1-2 generalize to more complex feeders and distribution grids the following way: The voltage fluctuations of the supply side, i.e. voltage fluctuations at the primary substation caused by the stiff external grid's fluctuation and the inaccuracy of the local voltage controllers are - to some extent - felt at all nodes of the distribution grid, and should therefore be suppressed. The larger the R/X ratios of lines in a grid, the less effective conventional reactive power injection-based voltage control/support schemes become. With these conclusions in mind, the next subsection illustrates the effect distributed generation has on grid voltages.

1-2-2 Effect of Distributed Energy Resources

To illustrate the effect of distributed energy resources on voltages in a distribution grid, a photovoltaic generator and a reactive power-injecting compensator device are added to the receiving end of the simple feeder presented in the previous subsection. This is shown in Figure 1-4. The PV plant injects P_{PV} amount of active power and the compensator device injects Q_c amount of reactive power at the discussed feeder's receiving end. In case the PV plant's inverter is also capable of handling reactive power exchange, they could take up the role of reactive power compensators, and therefore Q_c injection is not necessarily handled by separate devices, but in Figure 1-4 they are shown this way for clarity. Similarly to the previous case, a load is also connected to the receiving end consuming a P_l amount of active and Q_l amount of reactive power. The stiff external grid connection and the transformer equipped with an automatic on-load tap changer are also shown in Figure 1-4 as these devices are responsible for keeping the V_S magnitude relatively constant. It has to be noted that the supply side's voltage control scheme is only "aware" of this V_S magnitude and is unaware of all other nodal voltages (V_R in this case).
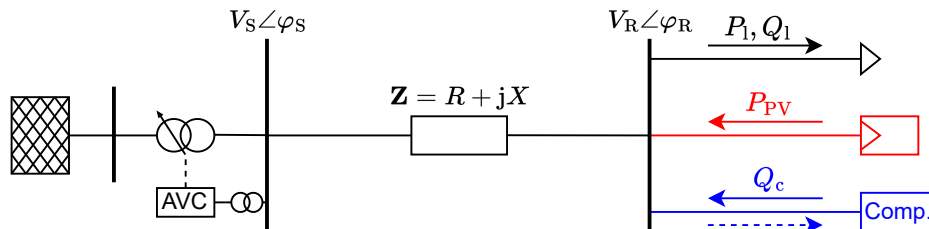

Figure 1-4: Simplified Feeder Diagram with Distributed Generation, Based on [48, 80]

The active power usage at the receiving end becomes $P = P_l - P_{PV}$, and a similar expression can be written for the receiving end's reactive power usage: $Q = Q_l - Q_c$. Plugging these power expressions into Equation 1-2 results:

$$V_{\mathrm{R}} \approx V_{\mathrm{S}} - \frac{R}{V_{\mathrm{R}}}\left(P_{\mathrm{l}} - P_{\mathrm{PV}}\right) - \frac{X}{V_{\mathrm{R}}}\left(Q_{\mathrm{l}} - Q_{\mathrm{c}}\right) \tag{1-3}$$

In grids where cables, in general, have lower R/X ratios (e.g. transmission and overhead distribution cables), the fluctuations in the V_R receiving end's voltage magnitude caused by the changes in P_l and Q_l loadings and P_{PV} photovoltaic generation can be effectively counteracted by injecting or absorbing the right amount of Q_{c} reactive power with the compensator device. However, in underground MV distribution grids typical in Western Europe, the R/X ratios are too high for these schemes to be feasible. In case the R/X ratio is roughly close to 1, the amount of reactive power flow necessary to solve voltage issues would have to be in the same order of magnitude as the feeder's active power flow resulting in a low power factor and inefficient energy transport. Furthermore, if $R/X >> 1$ the voltage magnitudes in the grid become practically insensitive to reactive power flow.

Equation 1-3 shows that the presence of distributed generation increases the voltage at the feeder's receiving end. The same physical principles, i.e. the fact that distributed energy resources increase voltage magnitudes locally and that voltage magnitudes are mainly determined by active power flow in case $R >> X$, scales to larger, more complex distribution networks as well. However, the voltage magnitudes for those networks can usually only be calculated with the help of power system simulation software by numerically solving the so-called power flow equations [40].

Conventional voltage control with automatic transformer on-load tap changers at the primary substation relies on a local voltage measurement at the primary substation or compensates for the feeder's voltage drop assuming a unidirectional power flow (only consumption at the receiving end). Figure 1-5 illustrates such a feeder's voltage profile with two tap-changing transformers. It can be seen that without distributed generation at the feeder's end, the conventional controllers are able to keep the voltage limits during peak load. During off-peak load, the upper voltage limit is violated both with and without DG. In the case when no DG is present, the upper limit's violation only happens close to the transformer, which could likely be attributed to the fact that the transformer controller's line drop compensation [77] assumes that all the load is at the feeder's end. On the other hand, when distributed generation is present, the upper voltage violation is present not only close to the transformer but on the 11 kV section's whole length. It can also be seen, that thanks to the presence of distributed generation, the voltage magnitude can not only drop but also increase from the last substation towards the feeder's end due to the possibility of bi-directional power flow.

Voltage issues caused by the presence of renewable energy-based DG are further complicated by the fact that renewable sources are inherently volatile and therefore offer less controllability and predictability to operators compared to traditional means of power generation. This stochastic behavior is illustrated by a generation profile of a photovoltaic plant shown in Figure 1-6. Even though some trends can be seen in this profile, especially on clear days, sudden changes i.e. power dips due to clouds can happen anytime. Besides being able to handle reverse power flows, modern active network management schemes also have to anticipate and/or be resilient against these fluctuations.

As illustrated in this problem statement by the simple feeder example, conventional voltage controllers struggle to keep voltage limits in the presence of DG so the voltage control schemes of modern distribution grids need new approaches. The purpose of this graduation project
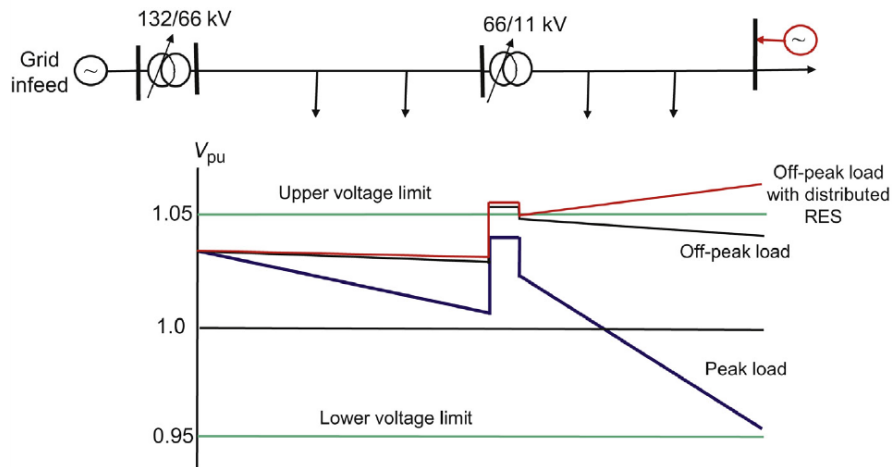
Figure 1-5: Illustration of Voltage Rise due to Distributed Generation, Source: [80]
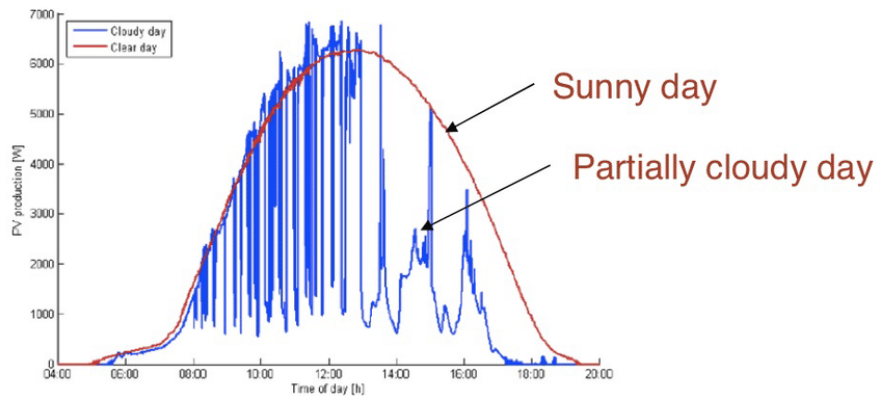
Figure 1-6: Geneartion Profiles of a Solar Power Plant, Source: [3]

is to investigate Model Predictive Control (MPC) based solutions for the voltage regulation problems of active distribution grids that incorporate a lot of generation, due to the increasing widespreadness of renewable energy and have high R/X ratios due to the usage of underground cables. The final goal is to design a MPC scheme for a section of a Stedin MV distribution grid, which is expected to solve the problem of voltage limit violations, particularly upper limit violations. This will be achieved by the coordination of two control resources: the primary substation transformer's OLTC and the active power curtailment of larger PV plants. The MPC's performance will be compared to simple control schemes that intend to solve the same problem, more specifically current compounding (CC) and current compounding in combination with local active power curtailment (CC+APC).

1-3   Formulation of Research Questions

Considering the problem statement the following research questions are investigated in this thesis:

- How can complex distribution networks (like Stedin's medium voltage distribution networks) be modeled and simplified to be effectively used with MPC-based voltage regulation?

- How effective is a MPC-based voltage control policy in mitigating the voltage disturbances caused by load, DG, and external grid voltage variation in an active MV distribution grid?

1-4 Contributions

This MSc project features the following contributions to the state of the art in research on model predictive voltage regulation in active medium voltage distribution grids:

- Conditional active power curtailment is used in the considered MPC policies. Similarly to local droop active power curtailment controllers, the active power output of a PV plant can only be limited in case their local voltage magnitude is above a certain tuneable threshold. This logic is incorporated into the developed MPC policies with the help of binary variables and mixed-integer linear (MIL) constraints [9]. This logic ensures that the otherwise useable energy output of curtailable PV plants is only wasted in cases when said action is justified, i.e. when said PV plant's output contributes to overvoltage issues in the plant's area. To the author's best knowledge, this is the first time that conditional curtailment (based on local voltage) is used in a model predictive voltage control policy with the help of MIL constraints. For more details, see Section 3-2 of Chapter 3.

- The benefit of incorporating exact knowledge about the fluctuation of load, generation, and the external grid's voltage into the model predictive voltage control policy is tested. The resulting intersample limit violation phenomena are analyzed, and two solutions are proposed, namely the consideration of intersample voltage values and the deactivation of the automatic voltage control relay at the primary substation. The results illustrate the benefit distribution system operators could get from further research on accurately forecasting said fluctuations. To the author's best knowledge, this is the first time an exact forecast is assumed on all quantities that affect grid voltages. Similar work can be found in [29], however, that study only considers the incorporation of forecasted and exact future knowledge on photovoltaic generation profiles and not the changes in consumption and the external grid's voltage. For more information on this contribution, refer to Section 3-4 of Chapter 3.

- A case study is conducted in which the considered controllers are applied to a section of a Stedin medium voltage underground distribution grid in South Holland province. This grid section carries the typical features of Western European medium voltage distribution grids, as it features a large photovoltaic generation capacity and it is composed of underground cables with large R/X ratios, making nodal voltage magnitudes insensitive to reactive power injections. The model predictive voltage control policies are simulated in 4 test cases (normal summer day, summer day with the external grid's overvoltage, summer day with 2 of 3 large PV plants not operating, normal winter

day) and their performance is compared to two simple uncoordinated control schemes: current compounding (CC) and current compounding in combination with local active power curtailment (CCAPC). The profile data used for the simulations is based on real measurements of Stedin. The low voltage load and generation profiles were only available with a temporal resolution of 1 hour, which was increased to 5 minutes using the Super Resolution General Adversarial Network (SRGAN) found in [100]. Other papers citing [100] show that this is the first time this interpolation method is used to enhance the quality of profile data in model predictive voltage control simulations. The studied grid, profile data, and the results of the conducted case study are presented in Chapter 4.

1-5   Structure of This Thesis

This report is divided into 5 chapters. Chapter 1 introduces the topic by presenting the necessary background information alongside a problem statement. The research questions of this project alongside the list of contributions in this thesis are also provided. Chapter 2 presents essential knowledge on power grid modeling alongside the current state-of-the-art research on voltage control in active medium voltage distribution grids that have a high penetration of distributed renewable energy sources, with a particular focus on model predictive control-based methods. Chapter 3 contains a detailed description of the model predictive voltage controllers that are designed and analyzed in this project. Two alternative methods, namely Current Compounding (CC) and CC combined with Active Power Curtailment (APC), against which the designed MPC controllers will be compared; are also presented in this chapter alongside the metrics that are used for comparison. Chapter 4 starts with presenting the medium voltage distribution grid section that served as the basis of the case studies. Afterward, a brief explanation of the Python-PowerFactory co-simulation framework that was created and used to produce the numerical results of this thesis is given. The different test cases and the numerical results are also presented in this chapter. An in-depth analysis of the numerical results is also given in Chapter 4. Chapter 5 concludes the report and gives recommendations for future research directions.

Voltage Regulation in the Presence of Distributed Generation

This chapter focuses on presenting the state of the art on the topic of voltage regulation in active distribution networks. To give a solid theoretical background, the chapter's first section presents the relevant topics of power grid modeling, namely power flow equations, tap-changing transformers alongside the dynamic behavior of their control relays, and the sensitivity-matrix-based model for voltage dynamics. The information shown in the first section is inherent to conducting a simulation-based case study on power system voltage control, particularly, model predictive voltage control. The chapter's second subsection gives a literature overview of solutions that intend to solve the voltage problems caused by the high penetration of distributed energy resources. A vast variety of solutions are presented excluding model predictive control. The chapter's third section focuses solely on applying model predictive control to power system voltage regulation. A literature review is presented, in which the discussed works use this control method. The review is done based on different aspects that all form the basis of important decisions during the design of a model predictive voltage control policy. The last (fourth) section concludes the chapter.

2-1 Power Grid Modeling

Many different dynamic phenomena are happening in the electric power grid at vastly different timescales from incredibly fast (e.g. lightning strikes, electromagnetic transients), to quite slow (e.g. load variability). Figure 2-1 gives an overview of the different timescales that are considered in the broad field of power system analysis. It can be seen that they are quite decoupled, meaning, that it is possible to only focus on the scale relevant to the dynamic phenomena of interest and neglect anything faster or slower.

This focusing is done using a set of differential-algebraic equations (DAEs) the following way:

$$\dot{x} = f(x, y, u) \tag{2-1}$$
$$0 = g(x, y, u) \tag{2-2}$$
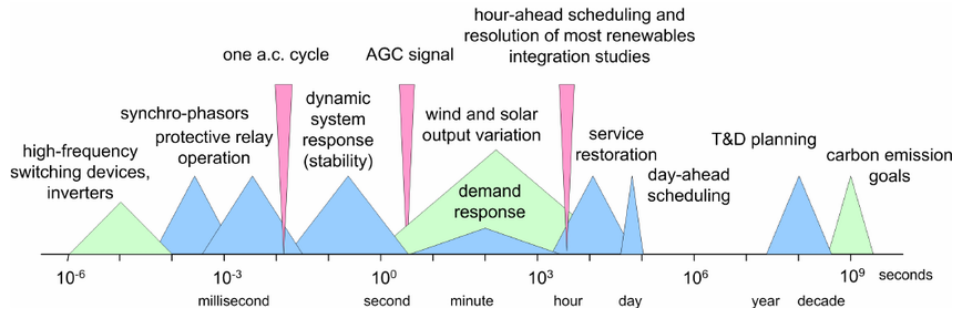
Figure 2-1: Different Time Scales in Power Systems, Source: [70]

where x and y are vectors of relevant state variables and u is the vector of exogenous inputs. Vector x contains the state variables whose dynamic behavior is modeled with more temporal accuracy thanks to the help of differential equations. The f vector function describes how these variables evolve in time. The states in vector y are assumed to be stationary throughout the considered timespan, and thus their values are determined with the set of algebraic equations that are given by equating the g vector function to zero. A detailed explanation and example for the usage of differential-algebraic equation systems as a power system modeling tool can be found in [93].

By setting $\dot{x}$ to zero in the DAEs, the system's equilibrium (steady-state) can be computed. With only very slowly varying u exogenous inputs, a series of steady-state computations is sufficient to describe the grid's response. This type of study is called the quasi-dynamic simulation (QDS), and is very commonly used e.g. in case of long-term load variability studies which can cover a timespan of multiple years, with timesteps often in the range of hours. This type of study is used to examine the progression of the slowest grid dynamics, as QDS can be solved much faster compared to other more detailed dynamic methods while still delivering the necessary results. [35] shows an example, where QDS is used to analyze the effect of distributed generation on an IEEE 13-bus benchmark network.

The simulations conducted in the case study of this MSc project are similar to a QDS in the sense that they focus on the network's slow voltage dynamics and assume the power grid is always in a steady state. They are however different in the sense, that the dynamic behavior of slow voltage control gear, more specifically the primary substation's automatic voltage control relay, are modeled and simulated in detail with the help of differential equations. This section presents a literature overview on the aspects of power system modeling that are necessary to conduct the simulations presented in Chapter 4 of this report: the power flow equations, on-load tap changers alongside their automatic voltage control relays, and the sensitivity-matrix-based models for slow voltage dynamics.

2-1-1   Power Flow Equations: The Steady State of a Power Grid

The power flow study, also referred to as a load flow study deals with calculating the steady state of the power system. More specifically, the voltage magnitudes and phase angles of each node in the studied network, by numerically solving a set of nonlinear equations, the so-called power flow equations. For these equations to be solved, the studied network's structure has to be known in the form of a $\mathbf{Y}$ admittance matrix alongside some other information about

each node (depending on its type). The power flow equations and their solution using the Newton-Raphson method is presented in great detail in [40], but the key concepts including the Newton-Rapshon algorithm are also briefly shown here. It has to be noted, that the power flow equations discussed in this study are all for balanced three-phase grids.

Power Flow Equations for a Single Node

The power flow of a single node (bus) i in the network can be expressed in the following so-called mismatch form (assuming there is a total of $i = 1, \ldots, N$ buses in the network):

$$\Delta P_i = P_{\mathrm{g}i} - P_{\mathrm{d}i} \underbrace{- V_i^2 G_{ii} - \sum_{\substack{n=1 \\ n \neq i}}^{N} V_i V_n Y_{in} \cos\left(\theta_{in} + \delta_n - \delta_i\right)}_{-P_i} = 0 \tag{2-3}$$

$$\Delta Q_i = Q_{\mathrm{g}i} - Q_{\mathrm{d}i} \underbrace{+ V_i^2 B_{ii} + \sum_{\substack{n=1 \\ n \neq i}}^{N} V_i V_n Y_{in} \sin\left(\theta_{in} + \delta_n - \delta_i\right)}_{-Q_i} = 0 \tag{2-4}$$

where ΔP_i and ΔQ_i are the (active and reactive) power mismatches of node i which are zero due to the node's power balance. $P_{\mathrm{g}i}$, $Q_{\mathrm{g}i}$ are the generated, and $P_{\mathrm{d}i}$, $Q_{\mathrm{d}i}$ are the demanded active and reactive powers at said bus. The $P_{\mathrm{g}i} - P_{\mathrm{d}i}$ and $Q_{\mathrm{g}i} - Q_{\mathrm{d}i}$ terms are often referred to as the node's scheduled power which is the power that is transmitted from bus i towards the rest of the network. The terms P_i and Q_i are the same scheduled powers expressed as a function of the network's $\mathbf{V}_n = V_n \angle \delta_n$ ($n = 1, \ldots, N$) voltage phasors and admittances contained in the $\mathbf{Y}$ admittance matrix. $\mathbf{Y}_{ii} = G_{ii} + \mathrm{j}B_{ii}$ is the ith diagonal element of $\mathbf{Y}$, and an arbitrary element in the ith row and n^{th} column of $\mathbf{Y}$ is denoted $\mathbf{Y}_{in} = Y_{in} \angle \theta_{in}$.

The admittances of individual network components are calculated using the lumped π-models of different components (lines, buses, transformers, etc.). For more information on the π-models of lines refer to [41]. For more information on transformer π-models see the next section of this chapter or [40]. The $\mathbf{Y}$ matrix can be constructed knowing the admittances of components using the following rules in [42]: The $\mathbf{Y}_{ii}$ diagonal elements are composed by summing all admittances that are connected between bus i and the (possibly virtual) neutral line. The $\mathbf{Y}_{ij} = \mathbf{Y}_{ji}$ elements are the negative of the admittance that connects bus i to bus j. The equality implies that matrix $\mathbf{Y}$ is symmetric.

System of Power Flow Equations

It can be seen that for each bus in the network, it is possible to write two power flow equations: one concerning the active (Equation 2-3) and the other concerning the reactive (Equation 2-4) power flow. The bus type plays a vital role in the load flow study, as it determines whether both, one or no power flow equations hold true for the bus. Based on this there are the following three types of nodes:

- Load bus (PQ bus): Scheduled active and reactive powers ($P_{\mathrm{g}i} - P_{\mathrm{d}i}$ and $Q_{\mathrm{g}i} - Q_{\mathrm{d}i}$) are specified and both Equation 2-3 and Equation 2-4 hold true. The voltage magnitude V_i and phase angle δ_i are unknowns.

- Voltage supported bus (PV bus or generator bus): The scheduled active power ($P_{\mathrm{g}i} - P_{\mathrm{d}i}$) and the bus voltage magnitude (V_i) are specified, only Equation 2-3 holds true with the δ_i phase angle and Q_i reactive power injection being unknowns. The amount of reactive power injection is always equal to the exact amount that ensures the node's set voltage magnitude, and it is determined using the expression for Q_i in Equation 2-4 once the voltage phasors have been obtained. Buses with large synchronous generators are typically modeled this way.

- The slack bus (also called the swing bus): The voltage magnitude (V_i) and angle (δ_i) are specified. None of the power flow equations hold true, as the scheduled active and reactive power of this bus are determined based on the losses in the rest of the network (power coming from this bus compensates for these deficits). The network's losses and hence the power deficits are not known in advance, so the scheduled power of this bus can only be obtained once all bus voltage magnitudes and angles are calculated. In a typical AC power flow study there can only be one slack bus, and in case of distribution grids, this is the bus at the primary substation that connects to the external high-voltage network. The angle of the slack bus voltage phasor is often specified to be 0° and other voltage phasor angles are referenced to this angle.

It is clear that PQ nodes introduce two unknowns alongside two equations, and PV nodes introduce one unknown alongside one equation. The slack bus introduces no unknowns and no equations into the power flow study. For this reason, the system of power flow equations can be solved.

The Newton-Raphson Algorithm

Distribution networks are typically composed of PQ load buses (which can also have distributed energy sources connected) and one slack bus, which is connected to the transmission/subtransmission grid. Power flow equations can be solved with the Newton-Raphson method [40], which will be briefly presented in the following, for a grid where bus 1 is the slack bus and the rest $2, \ldots, N$ buses are PQ buses. Knowing this, the vector of unknowns which has to be determined is:

$$x = \begin{bmatrix} \delta_2 & \ldots & \delta_N \mid V_2 & \ldots & V_N \end{bmatrix}^{\mathrm{T}} \qquad (2\text{-}5)$$

The basis of the Netwon-Raphson method is the first-order Taylor expansion of the power flow equations in the power mismatch form (given in Equation 2-3 and Equation 2-4), and the fact that these mismatches are zero in case of power balance. The Taylor expansion takes

the following form:

$$
\underbrace{\left[
\begin{array}{ccc|ccc}
\frac{\partial P_2}{\partial \delta_2} & \cdots & \frac{\partial P_2}{\partial \delta_N} & V_2\frac{\partial P_2}{\partial V_2} & \cdots & V_N\frac{\partial P_2}{\partial V_N} \\
\vdots & J_{11} & \vdots & \vdots & J_{12} & \vdots \\
\frac{\partial P_N}{\partial \delta_2} & \cdots & \frac{\partial P_N}{\partial \delta_N} & V_2\frac{\partial P_N}{\partial V_2} & \cdots & V_N\frac{\partial P_N}{\partial V_N} \\
\hline
\frac{\partial Q_2}{\partial \delta_2} & \cdots & \frac{\partial Q_2}{\partial \delta_N} & V_2\frac{\partial Q_2}{\partial V_2} & \cdots & V_N\frac{\partial Q_2}{\partial V_N} \\
\vdots & J_{21} & \vdots & \vdots & J_{22} & \vdots \\
\frac{\partial Q_N}{\partial \delta_2} & \cdots & \frac{\partial Q_N}{\partial \delta_N} & V_2\frac{\partial Q_N}{\partial V_2} & \cdots & V_N\frac{\partial Q_N}{\partial V_N}
\end{array}
\right]}_{J}
\underbrace{\left[
\begin{array}{c}
\Delta\delta_2 \\ \vdots \\ \Delta\delta_N \\ \frac{\Delta V_2}{V_2} \\ \vdots \\ \frac{\Delta V_N}{V_N}
\end{array}
\right]}_{C}
=
\underbrace{\left[
\begin{array}{c}
\Delta P_2 \\ \vdots \\ \Delta P_N \\ \Delta Q_2 \\ \vdots \\ \Delta Q_N
\end{array}
\right]}_{M}
\tag{2-6}
$$

where J is the (modified) Jacobian matrix, C is the vector of corrections with $\Delta\delta_i$ and ΔV_i being the amounts with which the voltage angles and magnitudes of node i have to be changed between iterations, and M is the vector of power mismatches that have to converge to zero over the course of iterations. The partial derivatives with respect to voltage magnitudes in J are multiplied and the voltage corrections in C are divided by the voltage magnitudes for numerical robustness [40].

In order to obtain the solutions for the power flow equations, the Newton-Raphson method performs the following steps iteratively, where k is the iteration counter, and when placed in the superscript of a quantity it denotes a certain quantity's value at step k.

1. Come up with a good initial guess for the calculated variables: x^0.

2. Start iteration step k (with $k = 1$ at the first iteration): Calculate the M^k mismatches using Equation 2-3 and Equation 2-4, then calculate the J^k Jacobian using the voltage and phase angle values in x^{k-1} (obtained at the previous iteration).

3. Using Equation 2-6 calculate the C^k correction vector.

4. Calculate the current iteration's x^k solution using Equation 2-7.

5. If all mismatches in M^k are smaller than some pre-specified threshold, then stop the algorithm and consider x^k as the final solution. Else continue from Step 2 with $k := k+1$.

The update equations for the ith node's voltage angle and magnitude:

$$
\delta_i^k = \delta_i^{k-1} + \Delta\delta_i^k \qquad\qquad V_i^k = V_i^{k-1}\left(1 + \frac{\Delta V_i^k}{V_i^k}\right)
\tag{2-7}
$$

The Newton-Raphson method was shown here for two main reasons: Firstly it is a numerically robust method that provides fast convergence and is used by many power system analysis software including DIgSILENT PowerFactory [26]. The other reason this method was shown in detail, is the fact that the sensitivity matrix-based (quasi-) dynamic model for voltages is based on the J Jacobian matrix used in this method. While not strictly relevant to this project, other power flow solvers also exist such as fast decoupled load-flow (FDLF) [98, 40], the Gauss-Seidel Method [40], or other efficient methods particularly suitable for weakly meshed systems [95, 61].

2-1-2 Transformer On-Load Tap Changers and Automatic Voltage Control Relays

Tap changers are mechanisms that give transformers the ability to change their turns ratio. They are considered to be among the most important means to influence voltage in electric power grids, particularly distribution grids. The working principle of tap-changers is presented in this subsection based on [80, 40] with a special focus on On-Load Tap Changer (OLTC)s and their control devices, the so-called Automatic Voltage Control (AVC) relays.

Working Principle and Modeling

The two types of tap changer mechanisms are shown in Figure 2-2. Both types are usually fitted to the transformer's high voltage side, as the current flowing there is lower, resulting in less wear on the mechanism's contact points. For this reason, the tap changers in Stedin grids are all fitted to the higher voltage side of transformers. Off-load tap changers shown in Figure 2-2a can only be moved when the transformer is de-energized. Their position is determined at the time of installation and is seldom changed afterward by skilled technicians only. On-load tap changers (shown in Figure 2-2b) allow the alteration of the turns ratio, without the interruption of the transformer's load current, i.e. without interrupting power delivery. It can be seen that there are two selector switches that move one after the other, and the circulating current that flows during switching superimposed to the transformer's load current is limited thanks to the usage of reactor coils. In other words, the reactor coils prevent shorting of subsequent taps during switching. Larger transformers of primary (high to medium voltage) substations are usually equipped with on-load while smaller transformers of secondary (medium to low voltage) substations are typically only fitted with off-load tap changers.

(a) Off-Load Tap Changer

(b) On-Load Tap Changer
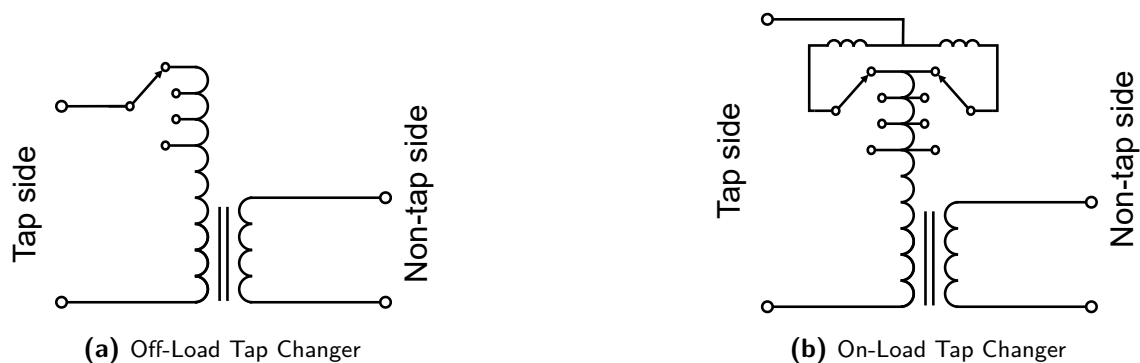
Figure 2-2: Illustration for the Working Principle of Tap Changers, Based on [80]

OLTCs have three main drawbacks: the inherent discreteness due to the finite number of taps, and the slow and maintenance-heavy operation due to them being mechanical devices actuated by electric motors. To overcome these issues, the development of solid-state tap changers is a heavily researched topic [7, 32, 66, 104]. These designs use fast semiconductor switches (e.g. thyristors, IGBTs, etc.) which allow more sophisticated and faster control actions e.g. modulation, and require less maintenance, but they are not yet common in commercial settings. OLTCs found on commercial transformers are still electromechanically

actuated, relatively slow discrete mechanical switches. For this reason they can only change the transformers' $\mathbf{a} \in \mathbb{C}$ off-nominal turns ratio in discrete steps:

$$\mathbf{a} = \mathbf{a}_{\text{nom}} + \Delta\mathbf{a}\,(n - n_{\text{nom}}) \tag{2-8}$$

where $\mathbf{a}_{\text{nom}} \in \mathbb{C}$ is the transformer's nominal turns ratio, $\Delta\mathbf{a} \in \mathbb{C}$ is the amount with which the turns ratio changes between two taps and $n, n_{\text{nom}} \in \mathbb{Z}$ are the selected and nominal tap positions respectively (denoted by integer numbers). In case the transformer does not do any phase shifting $\mathbf{a}$, $\Delta\mathbf{a}$ and $\mathbf{a}_{\text{nom}}$ are real numbers and can be denoted as their absolute values as a, Δa and a_{nom} respectively.

Tap changing transformers are often modeled as an ideal transformer that has a turns ratio $\mathbf{a} : 1$ connected in series with the real transformer's $\mathbf{y}_{\text{t}}$ short-circuit admittance [40], as it can be seen in Figure 2-3a. The tap changing transformer in this case is connected between the nodes with $\mathbf{V}_j$ and $\mathbf{V}_i$ voltage phasors, and the node with $\mathbf{V}_x$ voltage phasor only exists virtually. In power-flow calculations tap changing transformers are represented with the transformer's π-model [40] that is shown in Figure 2-3b.

(a) Equivalent Circuit **(b)** π-model
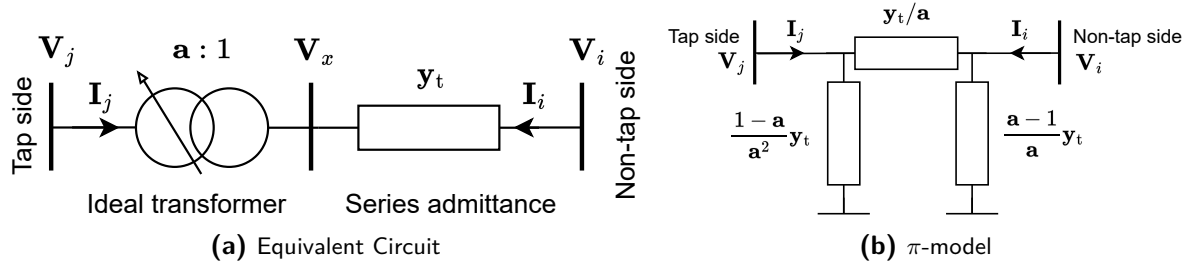
Figure 2-3: Tap Changer Modeling, Based on: [52]

Based on this π-model, the relationship between the currents and voltages of buses i and j can be derived, it is given in Equation 2-9. For a more detailed derivation and explanation [40] can be referred to.

$$\begin{bmatrix} \mathbf{I}_i \\ \mathbf{I}_j \end{bmatrix} = \begin{bmatrix} \mathbf{y}_{\text{t}} & -\mathbf{y}_{\text{t}}/\mathbf{a} \\ -\mathbf{y}_{\text{t}}/\mathbf{a}^* & \mathbf{y}_{\text{t}}/|\mathbf{a}|^2 \end{bmatrix} \begin{bmatrix} \mathbf{V}_i \\ \mathbf{V}_j \end{bmatrix} \tag{2-9}$$

where $\mathbf{y}_{\text{t}}$ is the transformer's series admittance and $\mathbf{a}$ is the off-nominal turns ratio. $\mathbf{a}^*$ is the conjugate of the off-nominal turn ratio. By looking at the relationship between the transformer's current and voltage phasors given in Equation 2-9, it can be seen that a change in $\mathbf{a}$ caused by a tap change, results in a change of the power system's $\mathbf{Y}$ admittance matrix and hence a change in the power flow equations.

Automatic Voltage Control Relays

The OLTCs of distribution grid transformers are switched by automatic voltage control (AVC) relays, i.e. control devices whose task is to keep their regulation point's V_{meas} voltage magnitude as close to their V_{ref} setpoint as possible. Frequent switchings cause the OLTC's contact points to wear out quickly, so almost all AVC relays use a deadband module and an integrator to avoid them.
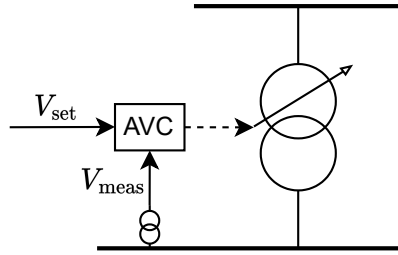
Figure 2-4: Simple Automatic Voltage Control (AVC) Relay Scheme

A conventional AVC relay connection is shown in Figure 2-4. It can be seen that the regulation point is the transformer's low-voltage side so in its simplest form the AVC relay is only capable of maintaining one local voltage. More advanced schemes exist that make the AVC relay to some extent "aware" of what is happening in the rest of the grid such as line drop compensation (LDC) or current compounding (CC). These will be discussed in more detail in Section 2-2 of this chapter.

Dynamic modeling of tap-changing transformers and their automatic voltage control relays is a non-trivial task. The simplest method only considers the integrator responsible for limiting excessive switching, and neglects discreteness:

$$\dot{n}_{\mathrm{cont}} = K_{\mathrm{i}} \left(V_{\mathrm{ref}} - V_{\mathrm{meas}} \right) \tag{2-10}$$

where $\dot{n}_{\mathrm{cont}}$ is the time derivative of the n tap position's n_{cont} continuous approximation, and K_{i} is the integrative gain of the controller. The sign of K_{i} depends on whether the tap changer is on the LV or HV side, and the amount of time necessary for a tap change is dependent on the absolute value of K_{i} as well as how big the $V_{\mathrm{ref}} - V_{\mathrm{meas}}$ error signal is. The transformer's **a** off-nominal turns ratio and therefore its voltage alteration is proportional to the selected n tap position, so the control device will reach equilibrium when the measured voltage error is zero. Many studies addressing the small-signal stability of the tap-changer controller focus on this continuous approximation of the tap position along with a simple integrative controller, such as [60].

More realistic tap changer and AVC relay models incorporate three more important characteristics: the discrete nature of tap changers, the saturation caused by minimum and maximum tap positions, and the deadband around the voltage setpoint. The deadband is necessary to keep the controller at rest in the close vicinity of the equilibrium, as the equilibrium cannot be reached exactly in practice, due to the discreteness of OLTC mechanisms. This modifies the simple model given in Equation 2-10 the following way:

$$\dot{n}_{\mathrm{cont}} = \begin{cases} K_{\mathrm{i}} \left(V_{\mathrm{ref}} - V_{\mathrm{meas}} \right) & \text{if } n_{\min} < n_{\mathrm{cont}} < n_{\max} \text{ and } |V_{\mathrm{ref}} - V_{\mathrm{meas}}| \geq V_{\mathrm{db}} \\ 0 & \text{otherwise} \end{cases} \tag{2-11}$$

$$n = \mathrm{round} \left(n_{\mathrm{cont}} \right) \tag{2-12}$$

where $n_{\min}$ and $n_{\max}$ are the minimum and maximum tap positions respectively and the round() function rounds the n_{cont} continuous position approximation to the nearest integer.

The AVC relay's dynamic behavior described by Equation 2-11 and Equation 2-12 can also be visualized in a block diagram shown in Figure 2-5. This shows that AVC relays can be modeled as a series interconnection of a deadband module, a saturated integrator, and a quantizer block. These blocks form the hybrid (switched) dynamic model of OLTCs that are controlled by AVC relays. Examples of studies that use these more complex models are [69, 72].
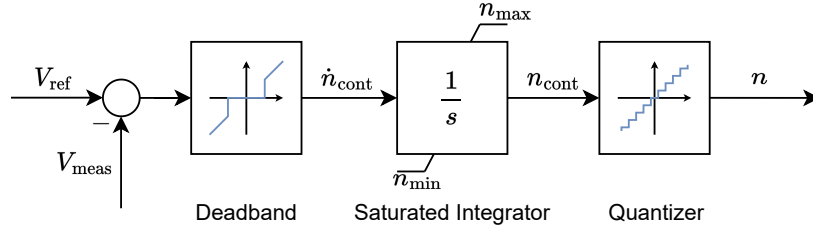
Figure 2-5: Block Diagram of an Automatic Voltage Control (AVC) Relay

In power flow studies and quasi-dynamic simulations, either a fixed tap position or an AVC relay setpoint can be specified for transformers with OLTCs. In the former case, the transformer is handled as if it had a fixed turns ratio corresponding to the given tap selection. In the latter case, the taps are changed and the power flow equations are re-calculated iteratively until the AVC relay's monitored bus voltage lies within the deadband around the specified setpoint.

The simulations in the case study of this thesis use the hybrid dynamics of AVC relays characterized in Equation 2-11 and Equation 2-12. The network's response to the tap change actions is obtained using fixed tap position power flow calculations. More information can be found in Section 4-2 of Chapter 4 about the implemented simulation framework and the simulation of OLTC-grid interactions. It is investigated in this thesis whether model predictive voltage controllers should account for the discreteness of OLTCs. The AVC relay used by Stedin is the a-eberle REG-D, more information about it can be found under [2].

2-1-3   Sensitivity Model

The sensitivity matrix-based voltage dynamics model is very commonly used with MPC-based voltage control; examples can be found in [6, 103, 75, 64, 62, 54, 30, 31]. This model stems from a Taylor-series expansion of the power flow equations, similar to the one used in the Newton-Raphson method. The model can characterize the slow voltage dynamics of a power system provided the changes of the factors that determine power flow solutions (power injections, OLTC positions, slack bus voltage) are known. It is only capable of telling the grid's next equilibrium (quasi-dynamic model) after said quantities have changed and does not incorporate transients in between. For this reason, the model's sampling time has to be large enough to ensure the model's accuracy, i.e. let grid states converge to their new equilibrium. The model can be expressed with the following discrete-time linear state equation:

$$x(k + 1) = x(k) + S\Delta u(k) + S_\mathrm{d}\Delta w(k) \tag{2-13}$$

where $x(k)$ is the state vector at time step k containing voltage magnitudes and phase angles of the measured buses. Contrary to the Newton-Raphson method used for power-flow solutions

k does not denote the iteration count in this case, but the number of the sampling time instant, i.e. when the time $t = k\tau$ with τ being the discrete time step of the model (sampling time). $\Delta u(k) = u(k+1) - u(k)$ with $u(k)$ being the vector containing the control inputs at time step k, namely tap position, active power curtailment, and reactive power injection. $\Delta w(k) = w(k+1) - w(k)$ with $w(k)$ being a vector of the non-controllable disturbances, i.e. the voltage fluctuation of the external grid (slack bus), changes in the consumption of loads and power production of non-curtailable distributed generators at time step k. S is called the power system's sensitivity matrix towards control actions and S_d is the sensitivity matrix towards disturbances.

The entries of the S and S_d matrices can be calculated using many methods. A very common approach is to invert the $\tilde{J}$ Jacobian of the power-flow equations, in an equation that is similar to Equation 2-6, although the partial derivatives and voltage magnitude changes are not multiplied here with voltage magnitudes:

$$\underbrace{x(k+1) - x(k)}_{\Delta x(k)} = \begin{bmatrix} \delta_2^{k+1} - \delta_2^k \\ \vdots \\ \delta_N^{k+1} - \delta_N^k \\ V_2^{k+1} - V_2^k \\ \vdots \\ V_N^{k+1} - V_N^k \end{bmatrix} = \underbrace{\left[\begin{array}{ccc|ccc} \frac{\partial P_2}{\partial \delta_2} & \cdots & \frac{\partial P_2}{\partial \delta_N} & \frac{\partial P_2}{\partial V_2} & \cdots & \frac{\partial P_2}{\partial V_N} \\ \vdots & \tilde{J}_{11} & \vdots & \vdots & \tilde{J}_{12} & \vdots \\ \frac{\partial P_N}{\partial \delta_2} & \cdots & \frac{\partial P_N}{\partial \delta_N} & \frac{\partial P_N}{\partial V_2} & \cdots & \frac{\partial P_N}{\partial V_N} \\ \hline \frac{\partial Q_2}{\partial \delta_2} & \cdots & \frac{\partial Q_2}{\partial \delta_N} & \frac{\partial Q_2}{\partial V_2} & \cdots & \frac{\partial Q_2}{\partial V_N} \\ \vdots & \tilde{J}_{21} & \vdots & \vdots & \tilde{J}_{22} & \vdots \\ \frac{\partial Q_N}{\partial \delta_2} & \cdots & \frac{\partial Q_N}{\partial \delta_N} & \frac{\partial Q_N}{\partial V_2} & \cdots & \frac{\partial Q_N}{\partial V_N} \end{array} \right]^{-1}}_{\tilde{J}^{-1}} \begin{bmatrix} \Delta P_2 \\ \vdots \\ \Delta P_N \\ \Delta Q_2 \\ \vdots \\ \Delta Q_N \end{bmatrix}$$

$$(2\text{-}14)$$

where $\tilde{J}^{-1}$ can be partitioned into S and S_d based on what is considered a controllable variable and what is considered a disturbance. In case the network contains a tap-changing transformer, the sensitivity to tap positions or to the tap changer controller's voltage setpoint can also be calculated (depending on the way the tap-changing transformer is considered in the network's power flow study). The slack bus's voltage magnitude and angle also appear in the power flow equations and affect their solutions. Consequently, sensitivities to the fluctuation of these quantities can also be obtained. For more details on power system sensitivity calculation refer to [5].

Effect of Load Models   In heavily loaded power systems, the voltage dependence of certain loads could affect the calculated power flow solutions and sensitivity values. More advanced models, e.g. ones shown in [57], characterize a dynamic load behavior while simpler load models, such as the exponential and ZIP models discussed in [78] only consider the load's static voltage dependence. The latter are also sufficient to show the load's voltage dependence's effect on power flow and sensitivity results. This study however will only use simple constant power loads, which simplification can be supported by the conclusion of [14], as authors of [14] compared the voltage dependence of different household consumers from 1999 and 2012 and found that the power usage of modern households is less dependent on the supplied voltage.

Calculation Methods   The main drawback of the sensitivity-matrix-based model is the fact that it is only valid in the close vicinity of the point of linearization, and therefore has to be

re-calculated frequently. This could increase the computational demand of control schemes using this model, especially with larger networks. There are several methods in the literature that reduce this complexity: [98] neglects the $\tilde{J}_{12}$ and $\tilde{J}_{21}$ off-diagonal blocks in the $\tilde{J}$ matrix and hence the Jacobian inversion becomes an easier task. This however only works in networks where those blocks are actually negligible, and therefore [98] does not perform exceptionally well with larger R/X ratios. [75] uses an artificial neural network (ANN) to approximate sensitivity matrices, which is fast but requires a lot of training data (pre-calculated sensitivities) beforehand. The enhanced Z-bus method [63, 64] is based on the simplification of the power system impedance matrix, and according to [63] it is computationally less demanding compared to power flow Jacobian inversion. [63] also mentions the very simple "perturb and observe" method, which is relatively time-consuming as it requires the solution of the power flow equations twice for each quantity to which sensitivities need to be obtained. [59] proposes and compares three multivariate least squares (MLS) algorithms for the online estimation of sensitivity matrices. In the case study of this thesis, the built-in calculation tool of DIgSI-LENT PowerFactory is used through its Python API. This software uses Jacobian inversion to calculate sensitivities against power injections as stated in [26]. Regarding sensitivities to transformer tap position, the user can choose whether to carry out the calculations based on linearization or a perturbation-based method; in this project, the former was chosen. The sensitivities to the external grid's (slack bus's) voltage magnitude fluctuation were calculated using a simple "perturb and observe" method, as the built-in PowerFactory tool does not calculate this quantity out of the box. The chosen amount with which the external grid's voltage magnitude was perturbed during the calculations of the case study is 0.01 pu.

2-2 Literature Overview on Voltage Regulation Methods in the Presence of Distributed Generation

Previously two possibilities were shown for influencing voltages in active distribution grids: on-load tap changers of distribution transformers in Subsection 2-1-2 and the active and reactive power injection of Distributed Generation (DG) units or compensator devices in the problem statement of Chapter 1. These means of voltage manipulation act as the control inputs (actuation possibilities) for many control schemes that intend to regulate the voltages in the grid in case a large share of distributed generation is present. Examples of said control schemes and policies found in the literature will be briefly presented in this section.

Line Drop Compensation   Simple AVC relays shown previously in Figure 2-4 only control tap changers based on a local voltage measurement and are unaware of other nodal voltages that could be vastly different due to the presence of DG. For this reason, simple schemes focus on making AVC relays aware of the primary substation's whole supplied network's voltage profiles. One such scheme is called line drop compensation (LDC) [77] which is visualized in Figure 2-6. By setting the correct R and X parameters, this scheme gives the opportunity to move the regulation point towards the end of long feeders by subtracting an estimated voltage drop from the AVC relay's local V_{meas} voltage measurement. It can be seen, that the LDC scheme requires a local current measurement and therefore the installation of a current transformer at the primary substation. A big drawback of these schemes is that they could result in suboptimal performance when the distribution transformer supplies more feeders at

once (in almost all distribution networks) and the setting of the R and X tuning parameters is also not self-explanatory with these complex networks. Other issues could also stem from the fact that older LDC schemes cannot account for the reversal of power flow due to excessive generation in the supplied feeder.
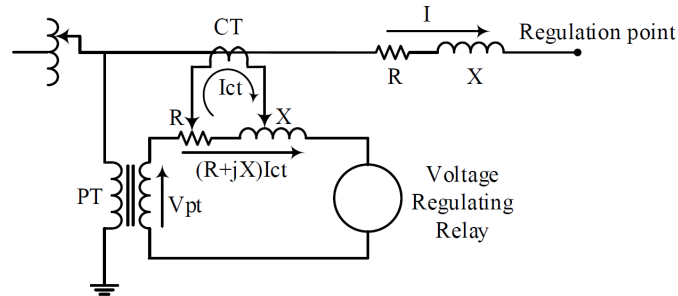
Figure 2-6: Illustration of Line Drop Compensation (LDC), Source: [77]

Current Compounding   Another scheme for making the AVC relay aware of voltages in the network besides the primary substation's local measurement is called Current Compounding (CC). This scheme can also be found in the literature under different names, however, PowerFactory (the simulation software of choice in this project) calls it this [26], so for this reason this study uses the same name. Similarly to LDC this method also requires a local current measurement, and having this obtained, the calculation of (usually active) power delivery through the primary substation's transformer ($P_{\mathrm{prim,supp}}$). The CC scheme adjusts the V_{set} voltage setpoint of the AVC relay based on the $P_{\mathrm{prim,supp}}$ supplied active power: If a lot of power is being consumed V_{set} is increased and if power is flowing back to the HV grid (a lot of PV generation) V_{set} is decreased. This scheme is quite easy to implement, proves to work well with multiple feeders, and is relatively effective against the voltage problems caused by distributed generation. For this reason, this is one of the control schemes against which Model Predictive Control (MPC) will be compared in this study. For more details on the design and the tuning of the CC scheme that was used in this project, refer to Section 3-5-1 of Chapter 3. One of the biggest drawbacks of CC is that the V_{set} ($P_{\mathrm{prim,supp}}$) function, i.e. the voltage setpoint's dependence on active power delivery has to be specifically tuned to the grid CC is applied to. To the author's best knowledge, no systematic method exists for the shaping of said function, and the tuning can only be done with trial and error using many simulations. An example of CC can be found in the literature under [53], where the authors use it at a (medium voltage) primary substation in order to lower voltage fluctuations at secondary substations and hence increase the DG hosting capacity of their low-voltage network.

Simple Local Power Injection Methods   After the presentation of two simple local OLTC based control schemes, simple local power injection schemes are shown. [78] mentions local active and reactive power injection-based methods that can be used in the presence of DG. Three schemes rely on the reactive power injection capabilities of distributed energy resources: Constant power factor schemes modify the generator's reactive power injection based on said unit's active power production. The second scheme modifies the DG unit's power factor based on active power output. The third method is the injection of reactive power based on the

unit's local voltage measurement. All three of these schemes provide local voltage support at the connection point of the DG unit but are ineffective in grids with high R/X ratios as it was also shown in Section 1-2 of Chapter 1. As the nodal voltages of grids with mainly resistive lines are practically only sensitive to active power flow, the only effective local power injection method presented in [78] is the Active Power Curtailment (APC) of DG units based on their local voltage measurement. This scheme seems to be effective against overvoltage issues, however, it comes at the cost of losing valuable energy. As the combination of CC and these local APC schemes is one of the alternative control methods used for comparison in this study, more details of APC, particularly the local APC designed in this project are given in Section 3-5-2 of Chapter 3. [101] discusses APC, particularly its implementation in household photovoltaic (PV) plants and their impact on low-voltage grids in more detail. Different active power curtailment rules are implemented for households that are located further from the substation. This modification of all installed household PV inverters would require a substantial investment and is therefore quite unrealistic. The method presented in [37] uses the combination of active and reactive power injection to regulate voltages. The reactive power injection is simply dependent on local voltage measurements (piecewise linearly). The active power injection however is more complex and uses Kalman filter-based solar forecasts to avoid unnecessary curtailments in case the simple reactive power injection is sufficient to keep voltage limits.

Other OLTC-based Control Methods   [92] is an overview paper that lists OLTC-based voltage control techniques and, alongside some conventional methods, lists 4 control schemes that work in the presence of DG units: SuperTAPP n + relay, artificial neural networks, fuzzy logic, and state estimation based voltage control relay. The SuperTAPP n + relay method estimates the current output of DG units by current measurements of feeders with DG and a ratio of load-share between feeders with and without DG. This way the voltage increases at the DG units' locations are determined, and the setpoint of the AVC relay is modified accordingly. Artificial Neural Networks (ANNs) [88] can be used to control tap changers and regulate voltages in the presence of DG units, however, these require many power-flow solutions to train the ANN and excessive testing to ensure its performance under all circumstances. Fuzzy logic control presented in [89] uses a rule base to calculate the tap changer controller's setpoint. These rules are similar to natural language and reflect an experienced operator's physical intuition and way of thinking. According to [92] these fuzzy controllers do not have to be re-adjusted in case new DG units are installed on the network. State estimation-based AVC relay [51] uses knowledge about the network structure and a few measurements to obtain all bus voltages in the system. The tap changer voltage setpoint is adjusted accordingly having this knowledge of the whole network's state.

Overview of Volt-Var Control Schemes   [76] gives an overview of voltage and reactive power (Volt-VAr) control in distribution grids. Both traditional and modern approaches are discussed. The presented traditional methods in [76] are the following: The first and most basic scheme is local tap changer control of transformers with or without line drop compensation which performs poorly with a lot of DG. A Supervisory Control and Data Acquisition (SCADA) based approach that uses measurements from the network (i.e. remote voltages) and a rule base to make decisions but suffers from limitations in case the feeder is reconfigured. The integrated or model-based approach is able to adapt to the changes in the network

configuration. This approach uses a dynamic model of the network and an optimization solver to determine a set of optimal control actions. Heuristics-based adaptive control algorithms do not use a model of the grid, only measurements such as voltages and power injections. The control actions are based on the changes in the monitored quantities and previous control actions, and this control scheme is successfully able to adapt to changes in the grid structure as well as the generation of renewable energy sources. The advanced Volt-VAr control schemes in [76] are smart inverters with voltage support/control capabilities (similar to the local methods in [78]), smart inverters with energy storage, distributed secondary side voltage regulation devices and the usage of data coming from advanced metering infrastructure.

Additional Overview Papers   Additional overview papers on the topic of distribution grid voltage control are [48, 46, 30]. Control methods in [48] are grouped based on whether they operate in a centralized or distributed manner. Centralized approaches are claimed to require extensive communication infrastructure and hence they are said to come at a higher cost. On the other hand, these methods offer better systemwide results compared to their distributed counterparts. The categories of centralized control schemes considered in [48] are: the distribution management system (DMS) schemes, coordination control for distribution system components, and intelligent (neural network, fuzzy, genetic algorithm, etc.) methods. Distributed schemes listed in [48] are based on active and reactive power injection, some use OLTCs, and some of them apply intelligent methods based on local measurements. It is claimed that local controllers are seldom able to solve the voltage limit violations in the whole distribution grid. [46] develops a system of metrics to assess different distribution grid voltage control methods. This system is based on many technical and market-adopting aspects. The paper assesses two local DG controllers, a hierarchical coordination controller for DGs and tap changers, and two fault-tolerant hierarchical voltage controllers. [30] categorizes voltage controllers according to multiple "levels". The first level is whether the controller is local or coordinated, and it is stated that the problems of a modern active distribution grid increase the demand for coordinated approaches. The second most important categorization aspect of the paper is whether the control scheme is centralized, distributed or decentralized. The control algorithms mentioned in [30] are model predictive control, consensus-based distributed control, droop control and its derivatives, tie-line bias control, containment-based control, sensitivity analysis-based techniques, game theoretic control, volt-var optimization, average current sharing, cooperative control, PI / state-feedback / $\mathcal{H}_2$ / $\mathcal{H}_\infty$ controllers, SMC-based current loop control, multi-layer control techniques, fuzzy control and state estimator based control techniques.

A Novel Voltage Control Scheme for the CIGRÉ MV Benchmark Grid   [78] presents a novel voltage controller for the CIGRÉ MV [10] benchmark grid. This scheme uses OLTCs and intelligent nodes with battery storage. The tap-changer controller monitors all nodal voltages in the transformer's supplied area and determines how a tap-change would influence each nodal voltage's deviation from the reference. If the minimum or maximum measured voltage violates the set limits for more than 40 seconds, a corrective tap change action is possible regarding the minimum and maximum tap position, and the corrective selection would not result in the other voltage limit's violation, the change is executed. In case the voltage profiles cannot solely be controlled by the tap changer, the intelligent nodes' help (active power injection or absorption) is requested. The control scheme presented in [78]

introduces two important concepts: the controller considers (predicts based on a model) how
one tap change would affect each nodal voltage in the network, however, it is assumed that
each nodal voltage would change by the same amount. This could be refined by using a more
detailed model for the effect of tap changes (e.g. sensitivity model), and by looking multiple
timesteps ahead in the future in a receding horizon manner instead of the used one-step-ahead
prediction. The other important concept is that certain types of control actions, i.e. tap
changes, are more desired compared to the intelligent node's power injections. These aspects
and the considered improvements to [78] alongside the model-based approaches presented in
[76] would lead to a model predictive voltage control scheme for the distribution grid, which
is the main focus of this MSc project. Model predictive control with a particular focus on
its application to distribution grid voltage regulation will be discussed in detail in the next
section of this chapter.

2-3 Application of Model Predictive Control for Voltage Regulation in Active Medium Voltage Distribution Grids

Model Predictive Control (MPC) is an optimal control method that first appeared in the
1960s. Back then MPC policies took a long time to compute (they require the online solution
of optimization problems) which meant that they could only be applied to "slow" dynamical
systems. MPC has the ability to minimize operational costs and maintain operational con-
straints. These three factors made MPC first only popular in the process industry [81] as
large chemical reactor plants have relatively slow dynamics (e.g. consider their large ther-
mal time constants), are very costly to operate, and could be relatively safety critical and
therefore subject to many operational constraints. As the amount of embeddable computing
power increased, MPC gained more use and interest in a vast variety of fields such as aviation
[21], the automotive industry [15], or power electronics [86], where system dynamics are much
faster. This section gives a brief literature overview on the application of MPC to the problem
of voltage regulation in active medium-voltage distribution grids. Due to lack of space, the
section only focuses on application, and the detailed theoretical foundation of MPC can be
found for example under [82, 83] or for a brief summary Chapter 3 could be referred.

System States The definition of the controlled system's state variables, inputs and outputs
is usually one of the first steps of every model-based control design procedure. Since the
controller's goal is to regulate the magnitudes of nodal voltages, these quantities definitely
have to be in the set of state variables. Depending on the controlled network, other variables
such as the state of charge for a battery [6, 62, 54] or the position of an OLTC [64, 108, 54]
could also be needed to accurately describe the system's state. Complete knowledge of a power
grid's state could be achieved by using a state estimator (observer) algorithm [43] and/or a
complex sensor and communication network. Since power system state estimation is a very
broad and complex field on its own, this study and all MPC papers surveyed here assume an
accurate full state measurement, i.e. exact knowledge of all the nodal voltages in the network.
With larger grids, dimension reduction of the prediction model, and the resulting reduction
of the controller's computational complexity might be a necessity. To tackle this, the MPC
policies in [103, 6] only monitor certain strategically selected bus voltages in the network, and
[62] represents low-voltage areas with simple lumped models. In this MSc project, all nodal

voltages of the studied grid will be monitored and the low-voltage areas will be represented with the MV-Load elements of PowerFactory as this study only deals with the nodal voltage magnitudes in the medium voltage network.

Inputs   Control actions, i.e. the different means of influencing voltages in the grid, depend heavily on the considered network. Almost all distribution grids contain transformers equipped with on-load tap-changers, so either the selected tap position [64, 108, 54] or the setpoint [6, 103, 33, 75, 30, 31] of the lower-level tap-changer controller (AVC relay) can be a control input for the MPC-based voltage control policy. The consideration of the tap changer's discreteness is an important decision from an MPC designer's point of view, as integer n tap positions could complicate the control policy's optimization problem. Other control inputs are mostly based on the active- and reactive power injection of distributed energy resources. The produced active power of these resources can be curtailed [64, 54, 75, 30, 31], however this results in wasting energy that could have been used otherwise, so this, in general, should be avoided and only used if well justified. Limiting the active power export of DG units also means that the operators of such resources lose potential revenue, and the DSO is obliged to pay compensation in exchange, making curtailment an expensive control action in quite the literal sense. Battery-based systems are capable of both injecting and consuming active power [6, 62, 54], with the big advantage, that a large share of excess energy can be reused as opposed to curtailment. This action however still results in losses due to battery chargers' and inverters' efficiency being lower than 1. To this day, Dutch grid operators, including Stedin, are legally forbidden from installing battery systems in order to prevent their interference with the energy market. For this reason, battery systems are not considered in this study. The reactive power injection of a distributed energy resource or compensator device can also be a control input if the said source is able to produce/consume reactive power. This can happen in two ways: either the reactive power injection is determined directly by the MPC-based grid controller [6, 103, 108, 54, 75], or the local reactive power injection law is modified by a higher-level model predictive controller [64, 33, 31]. Reactive power flows can also be influenced by connecting/disconnecting capacitor banks [36, 8]. The last resort concerning voltage control inputs is called load-shedding [109, 36, 8, 107]. This refers to the practice used in case of very low voltages and involves temporarily shutting off certain customers, to ensure the necessary voltage levels in the grid. In general, load shedding should only be used as a last resort and voltage problems should be solved differently if possible. The installation of distributed energy resources, in general, increases bus voltages, so the installation of these sources could reduce the necessity for load-shedding. Capacitor bank switchings and load shedding are both discrete control actions and similarly to OLTCs the consideration of their discreteness in MPC policies are important design decisions.

Prediction Models   MPC works best with linear or linearized system models, as the cost function minimization problem can only be convex this way (the system dynamics is specified with the help of linear equality constraints, and in a convex problem equality constraints can only be linear). For this reason, many studies in the literature [6, 103, 75, 64, 62, 54, 30, 31] use the sensitivity-matrix-based quasi-dynamic model of power systems which is introduced in Subsection 2-1-3 of this chapter. As discussed there, several methods exist for obtaining the network's sensitivity matrices. These sensitivities have to be recalculated frequently which increases the computational cost of MPC. Although a lot less common, some MPC-based

works characterize power system voltage dynamics with different models: [102] uses sparse
identification of nonlinear dynamics (SINDY) to formulate a nonlinear model of the voltage
dynamics. [33] uses an impulse response model, which even though being linear requires
experiments to identify contrary to the sensitivity-based model which can be derived by
using only the underlying physical laws of the power system. [36] approximates the nonlinear
grid dynamics with a piecewise affine function. In this MSc project, the sensitivity model
will be used, with the sensitivity matrices recalculated at every sampling time instant of the
MPC policies.

Constraints and Relaxation   The constraints in case of distribution grid voltage control can
come from many physical limitations. As far as control inputs are concerned, tap-changers
have minimum and maximum positions, and the active and reactive power injections of DG
units can also be subject to limitations. The rate with which these inputs are allowed to change
between two time steps can also be limited. These limitations all result in linear inequality
constraints in the optimization problem. One really important and critical constraint of the
voltage control task is the upper and lower constraint on the monitored bus voltages. In
extreme cases, it might be physically impossible to drive all the monitored grid voltages
within the specified lower and upper values, which from an optimization point of view means
that the cost function minimization problem becomes infeasible. This issue can be solved by
voltage limit relaxation (also called soft voltage constraints) used in [103, 33, 30, 31, 8]. The
ε_{low} and $\varepsilon_{\text{high}}$ non-negative decision variables, the so-called slack variables are added to the
cost function minimization problem and instead of the V_{low} lower and V_{high} higher voltage
limits, the nodal voltages are subjected to the $V_{\text{low}} - \varepsilon_{\text{low}}$ lower and $V_{\text{high}} + \varepsilon_{\text{high}}$ upper limits.
To avoid unjustified limit violations, high slack variable values are "punished" by adding the
$w_{\text{low}}\varepsilon_{\text{low}}$ and $w_{\text{high}}\varepsilon_{\text{high}}$ terms to the cost function, where w_{low} and w_{high} are both non-negative
tuneable weights that basically express how much of a problem a limit violation is. In order
to avoid extending the limits for the whole prediction horizon in case the limits cannot be
kept, each future time step has its own lower and upper slack variable in the relaxed voltage
constraints of the MPC policies that were designed in this study.

Direct MPC vs. Cascade Structure   An important aspect of applying MPC for distribution
grid voltage regulation is whether it will be the sole controller responsible for regulating nodal
voltages or whether it only provides coordinating reference signals for low-level controllers in
a cascade structure. The work under [6] implements a cascade structure where the high-level
MPC coordinates the low-level controllers of tap-changers (AVC relays) and a battery en-
ergy storage system (BESS). All low-level controller dynamics are considered in the MPC
policy, including the storage capabilities of the BESS. [103] also uses a cascade structure,
but only the tap-changer controller's dynamics are known by the MPC policy, the DG power
injections are directly modified by the MPC (the low-level controllers of the DG units are
neither modeled nor considered). The MPC developed in [64] adjusts the tap positions di-
rectly, and modifies the low-level local $Q(V)$ reactive power injection curve of the distributed
generators. The model predictive policies in [30] and [31] adjust the voltage setpoint of the
tap changer's low-level voltage control relay and directly adjust the active power curtailment
of DG units. The controller in [31] also controls the voltage setpoint of a distributed static
synchronous compensator (DSTATCOM), which indirectly corresponds to the DSTATCOM's
reactive power injection.

Centralized vs. Distributed Implementation   It has to be decided whether the MPC policy will be calculated at a central control station or using an interconnected cluster of distributed computational resources. The centralized approach provides faster convergence for optimization algorithms and better controller performance, however, a disruption at the control center or in a communication link could bring the whole system down. The distributed approach is usually more resilient against disruptions in communication equipment and it is usually capable of handling larger systems. On the other hand, it usually provides less optimal performances and comes with extra design considerations. This project only focuses on centralized MPC implementations. For more information on distributed MPC refer to [84]. An example that implements a distributed MPC scheme for grid voltage control can be found under [73].

Rejecting Disturbances   An important requirement for voltage controllers is that they should reject disturbances that affect nodal voltages, namely: voltage fluctuations caused by the variation of consumption, generation, and the external high-voltage grid connection's voltage fluctuations. Unmodeled system dynamics can also be thought of as disturbances that cause the real system to behave slightly differently compared to its model, so by increasing the controller's disturbance rejection capabilities, the resilience against these unmodeled phenomena could also improve. Simple MPC already has some inherent robustness against disturbances and inaccuracies [85], however if said robustness proves insufficient, the Robust Model Predictive Control (RMPC) [18, 68, 85] and Stochastic Model Predictive Control (SMPC) [49, 85] frameworks can be used. RMPC design requires knowledge about the minimum and maximum possible disturbance, and SMPC views disturbances as a (usually independent, identically distributed) random process. In the literature, examples can be found for applying both methods to distribution grid voltage control problems. Examples of RMPC are [64, 62]. [64] uses a robust constrained model predictive control approach, and the study contains comparisons with classical MPC, which show the superiority of RMPC. In [62] Tube MPC [68] is applied which is one of the most common RMPC methods. SMPC examples for distribution grid voltage control can be found under [54, 108]. [54] applies SMPC to an IEEE 33-bus and 123-bus network, and comparisons with deterministic MPC show the better performance of SMPC. The authors of [108] create a double-layer (cascade) stochastic MPC implementation. The high-level MPC, running with a 1-hour sampling interval operates the mechanical control devices (e.g. tap-changer) and works towards minimizing their wear and tear. The low-level MPC is responsible for controlling the DG inverters and works towards minimizing active power losses with a sampling time of 5 minutes. [108] achieves improved results in an IEEE 33-bus network compared to traditional and stochastic control methods. MPC schemes designed for disturbance rejection usually result in suboptimal performance when the system operates close to its nominal dynamics, i.e. with low disturbances. For this reason, complex RMPC and SMPC schemes are not considered in this study, only the idea of simple hand-tuned voltage constraint tightening was tried as an attempt to improve voltage limit violations.

MLD Models and Hybrid MPC   Mixed Logical Dynamical (MLD) systems were introduced by Bemporad and Morari in 1999, in their paper titled "Control of systems integrating logic, dynamics and constraints" [9]. According to this paper, the MLD framework is able to model "linear hybrid systems, finite state machines, some classes of discrete event systems,

constrained linear systems, and nonlinear systems which can be approximated by piecewise linear functions", and is used to formulate MPC policies for said systems. Examples, that use the MLD framework in grid voltage MPC are [109, 36, 8, 107, 64]. [109] develops a trajectory sensitivity-based model predictive voltage control method that considers the discreteness (and the resulting hybrid dynamics) of OLTCs and load-shedding. [36] approximates the nonlinear dynamics of an example power system with the help of Piecewise Affine (PWA) functions and constructs an MLD model of the controlled power system. Additionally, the hybrid dynamics resulting from the OLTC, the switching of capacitor banks and load-shedding are also considered. [8] proposes an MLD model-based emergency voltage control scheme for a 12-bus transmission network with the following discrete inputs: load-shedding, OLTC, and capacitor banks. The controller works towards keeping the monitored bus voltages between the relaxed bounds using minimal control actions. The system is modeled in the MLD framework, incorporating a dynamic load model and a static model for synchronous generators. The power-flow equations are linearized around the nominal point of operation, and the saturation of the excitation systems in generators is considered resulting in a piecewise affine description of the system. The controller is tested during simulated trippings of transmission lines. [107] considers the presence of controlled loads (e.g. cold storage in cities, like air-conditioned buildings) in active distribution grids, through an MLD-based hybrid system model as loads can only be controlled in discrete steps. The combination of distributed generation and load control is studied, [107] focuses on the temperature fluctuations of cold storage loads instead of the voltages in active distribution grids. [64] uses the MLD framework to form robust voltage constraints for an MPC scheme. The uncertainty band around a curtailable PV plant's power production shrinks to zero in case the set power limit is lower than the minimum possible generation. Otherwise, the uncertainty band is characterized by said minimum value and the adjustable upper limit. This control action dependent uncertainty band is described using the MLD framework and is incorporated into an RMPC scheme. In this MSc project, the MLD framework will be used to describe and incorporate conditional active power curtailment logic into the designed MPC voltage controllers.

2-4 Conclusions

This chapter surveyed the state of the art in active distribution grid voltage regulation, and necessary knowledge to conduct simulation-based case studies in said field. To give a solid foundation, the first section gave an overview of power grid modeling's most relevant aspects: the power flow equations, on-load tap changers, automatic voltage control relay dynamics, and the sensitivity model which (due to its linearity) is very widely used as a prediction model in MPC based voltage control studies including this one. The second section gave an overview of voltage regulation methods in the presence of distributed generation, excluding MPC solutions as those are explained in more detail in a dedicated section, namely the third section of this chapter. The third section discussed the field of model predictive grid voltage control according to several different aspects, that form the basis of important design decisions. The discussed aspects are the states of the prediction model and their reconstruction/measurement, control inputs coordinated by MPC, different prediction models, constraints and their relaxation, direct vs. cascade structures, disturbance rejection, and the consideration of hybrid dynamics using the MLD framework. All topics are introduced and discussed with supporting work that can be found in the literature.

Chapter 3

Model Predictive Voltage Controller Designs for Active Medium Voltage Distribution Grids

This chapter presents the different Model Predictive Control (MPC) designs for active medium-voltage distribution grids that are considered in this study. The first section starts by giving a short explanation of classical model predictive control for discrete-time linear systems, which serves as the theoretical foundation for the four variations of MPC-based voltage control policies presented afterward. The section then continues by formulating a simple classical MPC-based control policy for grid voltage regulation, that coordinates the control inputs of the primary substation transformer's On-Load Tap Changer (OLTC) and the active power curtailment of large photovoltaic (PV) plants. The quadratic cost function used, the constraints (soft nodal voltage and hard control action limits), and the linear, sensitivity matrix-based prediction model are shown, with emphasis on the aspects that make this MPC-based distribution grid voltage control policy different from a general MPC scheme used for an arbitrary discrete-time linear time-invariant system. After the formulation of a simple MPC policy, the idea of conditional PV curtailment and its incorporation into the MPC policy using Mixed Integer Linear (MIL) constraints is explained in the second section. This is one of the contributions of this thesis. The third section then presents two approaches to decrease the severity of voltage limit violations: a simple and pragmatic hand-tuned voltage limit tightening and the deadband tightening of the Automatic Voltage Control (AVC) relay responsible for controlling the OLTC of the primary substation's transformer. This is followed, in the fourth section, by the introduction of an MPC policy that knows all load, generation, and external grid voltage profiles ahead throughout the prediction horizon. This idea is the second contribution of this thesis, as full exact knowledge on all these profiles hasn't been assumed in previous works, to the author's best knowledge. The intersample limit violation problems of this approach are tackled with the incorporation of midpoint voltage dynamics, formulated using MIL constraints. The resulting control policy has the potential to show the best possible performance achievable with MPC-based voltage control and the potential benefit of

accurate profile forecasting. The fifth section of this chapter focuses on the comparison and fair assessment of the designed control policies, by presenting two simple control schemes: current compounding (CC) and its combination with local active power curtailment (APC). The performance of the shown MPC policies will be compared to each other and to these simpler methods. To be able to make fair comparisons, a set of objective metrics is selected and presented in detail in this chapter's sixth section. The seventh (last) section concludes the chapter.

3-1   Classical Model Predictive Control

The basic principles of classical MPC will be presented here based on [82, 83]. After the basic concepts, the classical MPC-based optimization problem and closed-loop control policy are formulated for voltage regulation in active distribution grids.

Classical MPC is an optimal control policy for discrete-time linear time-invariant systems, with their input to state dynamic model given in the following form:

$$x(k+1) = Ax(k) + Bu(k) \tag{3-1}$$

with $x(k)$ being the vector of state variables, and $u(k)$ being the vector of inputs at time step k. A and B are the so-called system and input matrices respectively.

A series of control actions (over the course of the prediction horizon) at sampling time step k is obtained by solving the following optimization problem of cost function minimization:

$$
\begin{aligned}
\min \sum_{i=1}^{N_{\mathrm{p}}-1} & \underbrace{\left(||x(k+i) - x_{\mathrm{ref}}||_{Q_x}^2 + ||u(k+i)||_{R_u}^2 \right)}_{g(k+i)} + \underbrace{||x(k+N_{\mathrm{p}}) - x_{\mathrm{ref}}||_{P_x}^2}_{J_{\mathrm{f}}(k+N_{\mathrm{p}})} \\
\text{subject to} \quad & x(k+i+1) = Ax(k+i) + Bu(k+i) \qquad \forall i \in \{0, \ldots, N_{\mathrm{p}}-1\} \\
& x(k+i) \in \mathcal{X} \qquad \forall i \in \{1, \ldots, N_{\mathrm{p}}-1\} \\
& x(k+N_{\mathrm{p}}) \in \mathcal{X}_f \\
& u(k+i) \in \mathcal{U} \qquad \forall i \in \{0, \ldots, N_{\mathrm{p}}-1\} \\
& u(k+i) = u(k+N_{\mathrm{c}}) \qquad \forall i \in \{N_{\mathrm{c}}+1, \ldots, N_{\mathrm{p}}-1\}
\end{aligned}
\tag{3-2}
$$

The minimized cost function punishes the system states' deviation from their reference values and the usage of control actions over the prediction horizon. This is done by adding the square of weighted norm terms, for which short notations are used in order to save some space. This short notation, for example in the case of state errors expands to $||x(k+i) - x_{\mathrm{ref}}||_{Q_x}^2 = (x(k+i) - x_{\mathrm{ref}})^{\mathrm{T}} Q_x (x(k+i) - x_{\mathrm{ref}})$. In order for the optimization problem to be convex, the Q_x, R_u, and P_x matrices have to be positive semi-definite. $g(k+i)$ is the so-called stage cost term, and the $J_{\mathrm{f}}(k+N_{\mathrm{p}})$ is the so-called final cost term. It can be seen that the system's dynamic model used for state prediction is specified in the form of (linear) equality constraints. $\mathcal{X}$ is the set of allowed system states and $\mathcal{U}$ is the set of allowed control inputs, which have to be convex sets to ensure the convexity of the optimization problem. $\mathcal{X}_{\mathrm{f}} \subset \mathcal{X}$ is the final state set. The $x(k+N_{\mathrm{p}}) \in \mathcal{X}_{\mathrm{f}}$ final state constraint is used to ensure the recursive
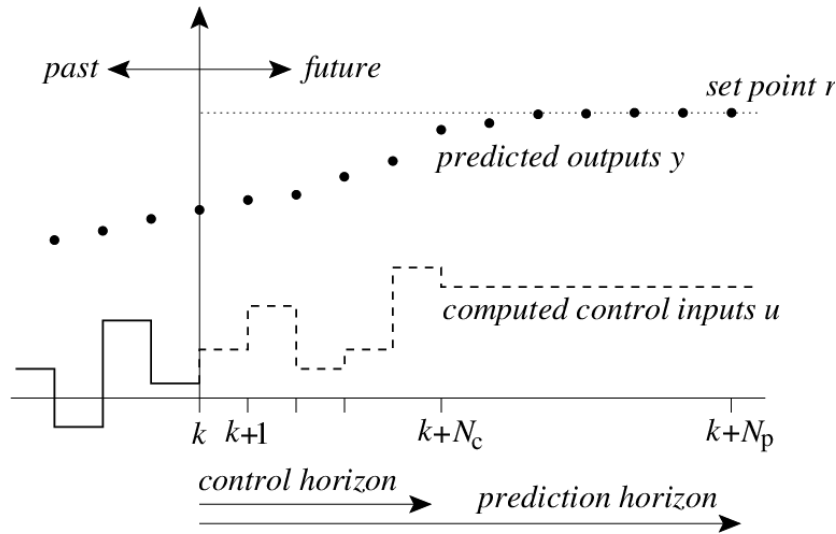
Figure 3-1: Illustration of the Basic MPC Scheme's Open-Loop Solution, Source: [74]

feasibility of the optimization problem, necessary for the stability of MPC. The last line of the optimization problem is the so-called control horizon constraint, which does not allow control inputs to change towards the prediction horizon's end, resulting in smoother control input signals.

The solution of the optimization problem given in Equation 3-2, is called the MPC policy's open-loop solution at timestep k, visualized in Figure 3-1 The y predicted output and r setpoint shown in said figure correspond to x and x_{ref} state and reference respectively. It can be seen that in order to minimize the cost function, the system state(s) converge to the reference over the course of the prediction horizon, without the excessive usage of control actions.

The closed-loop operation of MPC begins by measuring the controlled system's $x(k)$ state at time step k. After this, the optimization problem of cost function minimization is solved and the open-loop solution, i.e. a sequence of optimal inputs is obtained. The first element of the open-loop solution's calculated input sequence is applied to the system, and the digital controller then waits until the next time step, i.e. $k+1$. At timestep $k+1$ the $x(k+1)$ evolved system state is measured and the cost function minimization of Equation 3-2 is re-solved with $k := k+1$. This means that the prediction horizon has shifted from time steps $k, \ldots, k + N_{\text{p}}$ to $k + 1, \ldots, k + N_{\text{p}} + 1$, i.e. one step ahead into the future. This is called a receding horizon.

The MSc project focuses on implementing model predictive voltage controllers for Stedin medium voltage active distribution grids. The simplest MPC controller considered in this study will have the characteristics, introduced in the following paragraphs of this section.

Control Inputs   The control inputs coordinated by the MPC scheme will be the n tap positions of the primary substation transformer's OLTC and the P_{all} vector of allowed maximum active power levels for curtailable PV plants. The low-level AVC relay will remain in operation at the primary substation. To keep this control device "at rest" between the high-level MPC scheme's sampling time steps, the AVC relay's V_{set} voltage setpoint will be set to the monitored bus's 1-step ahead predicted voltage magnitude: $V_{\text{set}}(k) := V_{\text{meas}}(k + 1|k)$. Each input

of the control system is subjected to certain operational constraints, that will be described alongside other constraints of the designed MPC policy.

Cost Function   The cost function is designed with the following control goals in mind: keeping voltage magnitudes as close to the nominal 1 per unit as possible while avoiding frequent switching of the OLTC and active power curtailment of solar plants. To put these requirements in a mathematical form, a quadratic cost function is used, that punishes weighted norm squares of the V voltage magnitude vector's deviation from the V_{ref} vector of reference voltage magnitudes $||V - V_{\text{ref}}||^2_{Q_V}$, the square weighted norm of tap changes $||\Delta n||^2_{R_n}$, and the square weighted norm of PV curtailments $||P_{\text{cur}}||^2_{R_{\text{cPV}}}$ throughout the prediction horizon. The Q_V, R_n, and R_{cPV} weight matrices are tuning parameters of the MPC policy and should be positive semi-definite to keep the resulting cost function convex. Two additional terms of the policy are the terms punishing voltage limit violations, $w_{\text{low}}\varepsilon_{\text{low}}$ and $w_{\text{high}}\varepsilon_{\text{high}}$, with the w_{low} and w_{high} weights being non-negative tuning parameters. These limit violation terms will be described in more detail in the paragraph that introduces constraints. The resulting cost function is quadratic.

Constraints   The system's control inputs are subject to hard constraints, meaning that these can never be violated. Tap positions have to lie within the specified n_{min} and n_{max} values and they are only allowed to change by certain amounts, denoted Δn_{min} and Δn_{max} between adjacent time steps. The curtailments of PV plants have to lie between zero and the $P_{\text{poss}}(k)$ maximum power value resulting from solar irradiance at timestep k. Nodal voltages are subjected to soft voltage limits, to ensure the feasibility of the cost function minimization problem, during times, when the previously stated hard control input constraints, that stem from physical limitations, are unable to bring system voltages between the specified limits. This means that the limits can be expanded by introducing the ε_{low} and $\varepsilon_{\text{high}}$ non-negative decision variables, the so-called slack variables. The $V(k + i)$ vector of voltage magnitudes will be subjected to the following voltage limits at each time step of the prediction horizon: $(V_{\text{low}} - \varepsilon_{\text{low}}(k + i))\,\mathbf{1} \leq V(k + i) \leq (V_{\text{high}} + \varepsilon_{\text{high}}(k + i))\,\mathbf{1}$, with $\mathbf{1}$ being a vector of ones with the same dimension as the number of monitored buses in the studied grid. Each time step has two non-negative slack variables, that could extend the voltage limits in the lower and upper directions respectively. To only extend the limits, if necessary, high values of these slack variables are punished by adding the $w_{\text{low}}\varepsilon_{\text{low}}(k + i)$ and $w_{\text{high}}\varepsilon_{\text{high}}(k + i)$ terms to the cost function. The w_{low} and w_{high} weights have to be chosen high enough, such that the controller only violates these soft limits in case of emergency. Limit constraints on control inputs as well as nodal voltages are linear inequality constraints, from an optimization point of view.

Prediction Model   As stated in the previous chapter of this report, the sensitivity model of power grids is the most common prediction model used in model predictive grid voltage control schemes. This can be attributed to the fact that this is a linear model, that ensures linear equality constraints in the resulting optimization problems. The model is capable of describing the outcome of different control actions with reasonable accuracy, and to increase accuracy, the matrices will be re-calculated at each sampling time step of the designed MPC policies before the cost function minimization is performed. For the scheme presented in this

section, the nodal voltage magnitudes' sensitivity to tap changes at the primary substation and to changes in the active power injections of curtailable PV plants are needed. These matrices are denoted S_n and S_{PcPV} in the following respectively.

The presented ideas result in the following optimization problem that has to be solved at each sampling instant of the controller (after calculating the S_n and S_{PcPV} sensitivity matrices to tap changes and active power injections respectively):

$$\min \sum_{i=1}^{N_p} ||V(k+i) - V_{\text{ref}}||_{Q_V}^2 + ||\Delta n(k+i-1)||_{R_n}^2 + ||P_{\text{cur}}(k+i)||_{R_{\text{cPV}}}^2 +$$
$$+ w_{\text{low}}\varepsilon_{\text{low}}(k+i) + w_{\text{high}}\varepsilon_{\text{high}}(k+i)$$
$$\text{s. t. } V(k+i+1) = V(k+i) + S_n\Delta n(k+i) + S_{\text{PcPV}}\Delta P_{\text{cPV}}(k+i) \qquad \forall i \in \{0, \ldots, N_p - 1\}$$
$$(V_{\text{low}} - \varepsilon_{\text{low}}(k+i))\mathbf{1} \leq V(k+i) \leq (V_{\text{high}} + \varepsilon_{\text{high}}(k+i))\mathbf{1} \qquad \forall i \in \{1, \ldots, N_p\}$$
$$P_{\text{cPV},j}(k+i) = P_{\text{poss},j}(k) - P_{\text{cur},j}(k+i) \qquad \forall i \in \{1, \ldots, N_p\} \quad \forall j \in \mathcal{I}_{\text{cPV}}$$
$$0 \leq \varepsilon_{\text{low}}(k+i), \varepsilon_{\text{high}}(k+i) \qquad \forall i \in \{1, \ldots, N_p\}$$
$$n_{\min} \leq n(k+i) \leq n_{\max} \qquad \forall i \in \{1, \ldots, N_p\}$$
$$\Delta n_{\min} \leq \Delta n(k+i) \leq \Delta n_{\max} \qquad \forall i \in \{0, \ldots, N_p - 1\}$$
$$0 \leq P_{\text{cur},j}(k+i) \leq P_{\text{poss},j}(k) \qquad \forall i \in \{1, \ldots, N_p\} \quad \forall j \in \mathcal{I}_{\text{cPV}} \qquad (3\text{-}3)$$

where N_p is the length of the prediction horizon in sampling steps and Q_V, R_n, R_{cPV}, w_{low}, w_{high} are the tuneable weights of the cost function. V is the vector of monitored bus voltages, and V_{ref} is the vector of desired bus voltages (1 per unit for all). n is the vector of the selected tap positions and P_{cur} is the vector of active power curtailments. The letter Δ in front of a variable always refers to the change of said quantity, e.g. $\Delta n(k) = n(k+1) - n(k)$. $\varepsilon_{\text{low}}(k+i)$ and $\varepsilon_{\text{high}}(k+i)$ are the non-negative, scalar slack variables corresponding to the lower and upper voltage limit violations of the future time steps respectively. $\mathcal{I}_{\text{cPV}}$ is a set that contains the indices of the curtailable PV plants. $P_{\text{poss},j}$, $P_{\text{cPV},j}$, $P_{\text{cur},j}$ are the jth curtailable PV plant' possible active power (according to its generation profile), exported power (regarding generation profile and set limit), power loss due to curtailment respectively. The possible power production of these plants is not a decision variable, but a quantity that has to be known before solving the cost function minimization. The n tap positions and their Δn changes can only happen in certain fixed steps due to the quantized nature of tap changer mechanisms. This issue will be addressed either by considering these decision variables integers or by considering them real and rounding them after the solution of the optimization problem.

The classification of the optimization problem depends on whether the discreteness of tap positions is considered. In case the $n(k+i) \ \forall i \in \{1, \ldots, N_p\}$ tap positions are considered as continuous decision variables, and the calculated solution is rounded off to the nearest integer once the cost function minimization is finished, the optimization problem given in Equation 3-3 becomes a simple Quadratic Programming (QP) problem, due to the quadratic cost function and linear equality and inequality constraints. QP problems are one of the simplest convex optimization problems and therefore could be solved relatively fast. The main drawback of this approach is the inaccurate representation of the tap changer's behavior. In the other case, the $n(k+i)$ decision variables are integers, i.e. when the physical behavior of tap changers is represented in the optimization problem more accurately, the problem in

Equation 3-2 becomes a Mixed Integer Quadratic Programming (MIQP) problem. This results in better performance of the controller in exchange for more computational demand. From a computational point of view, MIQP problems are NP-hard, non-convex problems, and therefore take longer to solve. Integer sets are inherently non-convex, and therefore even after finding a local optimum solution, one cannot be sure, that it is also the global optimum. However, in case the continuous relaxation of the mixed-integer optimization problem is convex (like in this case), the chances of the mixed-integer optimization algorithm's convergence to the globally optimal solution are better.

It can be seen that no future knowledge is incorporated into the optimization problem about the fluctuation of the slack bus's voltage, curtailable PV plants, and the consumption and generation of low voltage areas. When predicting the effect of larger curtailable PV plants on monitored nodal voltages, it is assumed that their possible active power production stays constant during the entire prediction horizon and is equal to their $P_{\text{poss}}(k)$ production at time step k of the MPC policy.

When comparing the optimization problem formulated for grid voltage MPC (given in Equation 3-2) with the general classical MPC scheme's minimization problem given in Equation 3-2, it can be observed, that grid voltage MPC lacks three main features: a final cost, a final state constraint, and the control horizon constraint. Control horizon constraints are often omitted in practical MPC implementations to keep the optimization problem's tuning, implementation, and solution somewhat simpler. The final state cost and constraint were chosen to be omitted, as all MPC-based voltage control studies found in the literature do so. The reason behind this was not explicitly given in any of the surveyed papers, however, the author of this MSc thesis has some ideas as to why it is done this way: Firstly, regulating all voltages to exactly 1 per unit is usually not realistically possible, so the primary goal of voltage control is more to keep the monitored voltages between set limits, and ensuring the flattest possible voltage profiles are not so strictly important once those limits are kept. Secondly, the sensitivity model, resembling the state equation of a discrete-time linear time-invariant system, is only an approximation of slow grid voltage dynamics, which in reality is characterized by randomly varying load, generation, and external grid voltage profile data, and the fact that power flow equations (a set of nonlinear algebraic equations) hold at all time steps. So, the controlled system, in reality, works differently, than the discrete-time linear or linearized systems to which conventional MPC is applied. Lastly, a reason for omitting a separate final cost and final state constraint term could be simply the ease of design it brings, as this way there are fewer parameters to tune and fewer constraints to keep, making the MPC design simpler.

The closed loop operation at sampling time step k of this MPC-based voltage control policy begins by obtaining the state of the controlled power grid. Nodal voltage magnitudes, the position of the tap changer, possible and allowed power productions of curtailable PV plants, and the additional information necessary for sensitivity calculations (e.g. power exchange through the transformers of secondary substations) are measured, and transmitted to a centralized controller. Once the grid's state is known the S_n and S_{PcPV} sensitivity matrices are calculated, based on state measurements and knowledge about the grid's physical structure. Then the problem of cost function minimization given in Equation 3-3 is solved. After solving the optimization problem, the calculated control actions are applied, namely the newly calculated tap position is changed to $n(k + 1|k)$ (the next time step's predicted quantity based on current knowledge, i.e. the solutions of the cost function minimization, will be denoted this
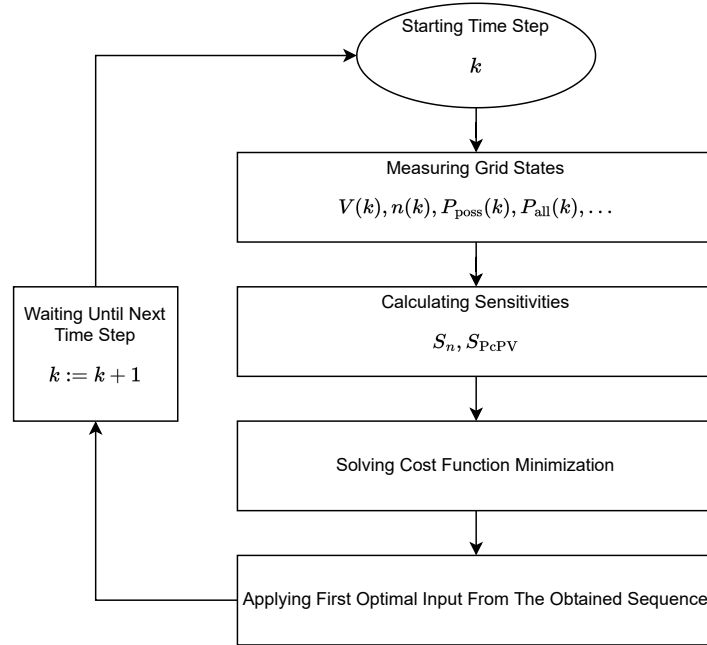
Figure 3-2: Flowchart of the Grid Voltage MPC's Closed Loop Operation

way in the following). P_{all} power limits for the curtailable PV plants are set to $P_{\mathrm{cPV}}(k+1|k)$. The setpoint of the AVC relay at the primary substation is set to be $V_{\mathrm{meas}}(k+1|k)$, and its inner integrator's state is reset to zero, to keep the relay at rest until the next sampling time of the MPC policy. Once the MPC's calculated inputs have been applied to the system, the controller waits until the policy's next $(k+1)$ sampling time step, and the whole process is repeated, with updated grid state measurements, re-calculated sensitivity values, and with the prediction horizon shifted 1-step ahead into the future. In other words, the designed MPC policy is operated in a receding horizon, closed-loop manner. This operation algorithm is also visualized in Figure 3-2.

While selecting the $T_{\mathrm{s,MPC}}$ sampling time for this MPC policy, one has to pay attention to having it large enough, to have enough time to solve the cost function minimization and let the grid state settle between the controller's actions. In the case study, the chosen sampling time for this MPC policy will be above the sampling time of the profiles with the highest temporal resolution, to show the effect of intersample disturbances and thus make the simulations more realistic.

The tuning of the MPC policy, i.e. the selection of the sampling time, different weight parameters, and limits is not a self-explanatory process. In this study, it was done iteratively relying on physical intuition and many simulations. The parameter values selected to be used are presented in Section C-1 of Appendix C. There is also a more detailed explanation of the iterative tuning process alongside a detailed interpretation of the different tuning parameters in said appendix.

3-2   Conditional Curtailment with Mixed-Integer Linear Constraints

Conditional active power curtailment is a common approach used in local voltage controllers of PV plants [78, 101], as this ensures that active power output (i.e. energy export) is only limited when said expensive action is justifiable. The condition on which it depends whether power can be limited is usually based on the PV plant's connection point's voltage magnitude, more specifically curtailment is only allowed in case the local $V_{\mathrm{cPV},j}$ voltage of the $j^{\mathbf{th}}$ plant is above a V_{crit} threshold.

The same logic can be incorporated into an MPC policy's optimization problem by using binary variables and MIL constraints [9]. To this MSc project's author's best knowledge, this is the first time this conditional curtailment logic is used this way in an MPC-based voltage control policy to avoid unnecessary curtailment and thus save otherwise usable energy. This idea is the first contribution of this MSc project, also listed in the introductory chapter of this report. Firstly the $b_{\mathrm{cur},j}(k+i)$ binary variables have to be defined for each $j \in \mathcal{I}_{\mathrm{cPV}}$ PV plant and for each $i = 1, \ldots, N_{\mathrm{p}}$ time step of the prediction horizon. The value of these binary variables is 1 if and only if said PV plant's local voltage is above a tuneable V_{crit} threshold voltage at time step $k + i$:

$$b_{\mathrm{cur},j}(k+i) = \begin{cases} 1 & \text{if} \quad V_{\mathrm{cPV},j}(k+i) \geq V_{\mathrm{crit}} \\ 0 & \text{if} \quad \text{otherwise} \end{cases} \tag{3-4}$$

This logic can be converted to the following set of MIL constraints based on the rules in [9], and assuming that all nodal voltages lie between the minimum and maximum value of 0 pu and 2 pu respectively. The assumption on voltage bounds is needed as the following MIL constraints require bounded state variables, and these chosen values would be quite unrealistic to occur from a physical point of view.

$$V_{\mathrm{crit}} - V_{\mathrm{cPV},j}(k+i) \leq V_{\mathrm{crit}}\,(1 - b_{\mathrm{cur},j}(k+i)) \qquad \forall i \in \{1, \ldots, N_{\mathrm{p}}\} \quad \forall j \in \mathcal{I}_{\mathrm{cPV}}$$
$$V_{\mathrm{crit}} - V_{\mathrm{cPV},j}(k+i) \geq \varepsilon + (-2 - \varepsilon)\,b_{\mathrm{cur},j}(k+i) \qquad \forall i \in \{1, \ldots, N_{\mathrm{p}}\} \quad \forall j \in \mathcal{I}_{\mathrm{cPV}} \tag{3-5}$$

where ε is the machine precision (smallest number that is possible to be stored on the computer used for solving the optimization problem), necessary for the numerical formulation of strict inequalities. Now that we have a binary variable, that can indicate if the local $V_{\mathrm{PV},j}$ voltage magnitude at the jth PV plant's connection point is above a tuneable V_{crit} threshold, we have to ensure that the $P_{\mathrm{cur},j}(k+i)$ decision variables in the MPC policy's optimization can only be non zero in case the $b_{\mathrm{cur},j}(k+i)$ values are 1. In case $b_{\mathrm{cur},j}(k+i)$ is 0, then its corresponding $P_{\mathrm{cur},j}(k+i)$ curtailment value will also have to be equal to 0. This can be done by modifying the bounds of the $P_{\mathrm{cur},j}(k+i)$ decision variables to the following MIL constraints:

$$0 \leq P_{\mathrm{cur},j}(k+i) \leq P_{\mathrm{poss},j}(k)b_{\mathrm{cur},j}(k+i) \qquad \forall i \in \{1, \ldots, N_{\mathrm{p}}\} \quad \forall j \in \mathcal{I}_{\mathrm{cPV}} \tag{3-6}$$

which is linear because $P_{\mathrm{poss},j}(k)$ is not a decision variable of the cost function minimization problem, but a quantity that is known before solving said optimization problem.

The derivation of MIL constraints describing logic is in general not a straightforward process. Still, it could be easily verified, that the inequalities given in Equation 3-5 and Equation 3-6 indeed describe the desired logic. For more information about MIL constraints and the framework of Mixed Logical Dynamical (MLD) systems [9] should be referred to.

The addition of the MIL constraints modifies the optimization problem of the MPC policy in the following way:

$$
\begin{aligned}
\min \sum_{i=1}^{N_\mathrm{p}} & ||V(k+i) - V_\mathrm{ref}||^2_{Q_V} + ||\Delta n(k+i-1)||^2_{R_n} + ||P_\mathrm{cur}(k+i)||^2_{R'_\mathrm{cPV}} + \\
& + w_\mathrm{low}\varepsilon_\mathrm{low}(k+i) + w_\mathrm{high}\varepsilon_\mathrm{high}(k+i) \\
\text{s. t. } V(k+i+1) &= V(k+i) + S_n\Delta n(k+i) + S_\mathrm{PcPV}\Delta P_\mathrm{cPV}(k+i) \qquad \forall i \in \{0, \ldots, N_\mathrm{p}-1\} \\
(V_\mathrm{low} - \varepsilon_\mathrm{low}(k+i))\,\mathbf{1} &\leq V(k+i) \leq (V_\mathrm{high} + \varepsilon_\mathrm{high}(k+i))\,\mathbf{1} \qquad \forall i \in \{1, \ldots, N_\mathrm{p}\} \\
P_\mathrm{cPV,\it j}(k+i) &= P_\mathrm{poss,\it j}(k) - P_\mathrm{cur,\it j}(k+i) \qquad \forall i \in \{1, \ldots, N_\mathrm{p}\} \quad \forall j \in \mathcal{I}_\mathrm{cPV} \\
0 &\leq \varepsilon_\mathrm{low}(k+i), \varepsilon_\mathrm{high}(k+i) \qquad \forall i \in \{1, \ldots, N_\mathrm{p}\} \\
n_\mathrm{min} &\leq n(k+i) \leq n_\mathrm{max} \qquad \forall i \in \{1, \ldots, N_\mathrm{p}\} \\
\Delta n_\mathrm{min} &\leq \Delta n(k+i) \leq \Delta n_\mathrm{max} \qquad \forall i \in \{0, \ldots, N_\mathrm{p}-1\} \\
V_\mathrm{crit} - V_\mathrm{cPV,\it j}(k+i) &\leq V_\mathrm{crit}\,(1 - b_\mathrm{cur,\it j}(k+i)) \qquad \forall i \in \{1, \ldots, N_\mathrm{p}\} \quad \forall j \in \mathcal{I}_\mathrm{cPV} \\
V_\mathrm{crit} - V_\mathrm{cPV,\it j}(k+i) &\geq \varepsilon + (-2 - \varepsilon)\,b_\mathrm{cur,\it j}(k+i) \qquad \forall i \in \{1, \ldots, N_\mathrm{p}\} \quad \forall j \in \mathcal{I}_\mathrm{cPV} \\
0 &\leq P_\mathrm{cur,\it j}(k+i) \leq P_\mathrm{poss,\it j}(k)b_\mathrm{cur,\it j}(k+i) \qquad \forall i \in \{1, \ldots, N_\mathrm{p}\} \quad \forall j \in \mathcal{I}_\mathrm{cPV}
\end{aligned}
\tag{3-7}
$$

It can be seen, that this is a MIQP problem regardless of whether the discreteness of the OLTC mechanism is considered or not, due to the newly introduced binary variables. For this reason, it can be stated, that this way of avoiding energy waste comes at an increased computational cost.

With this conditional curtailment logic, the $P_\mathrm{all,\it j}$ allowed maximum power exports are adjusted differently after the optimization problem is solved. $P_\mathrm{cPV,\it j}(k+1|k)$ is the set limit for curtailable plant j in case $b_\mathrm{cur,\it j}(k+1|k)$ is 1. Otherwise, the set limit is the $P_\mathrm{nom,\it j}$ nominal power of plant j.

Conditional curtailment allows the modifications of the tuned parameter values given in Table C-1, more specifically the R_cPV weight matrix in the cost term on PV curtailments is changed to R'_cPV. The originally tuned curtailment cost could be reduced (e.g. cut in half), as this way during the justified (one could say emergency) conditions, the controller will limit PV plants more strictly, eliminating voltage disturbances more effectively, without wasting significantly more energy in the long run. This shows that with conditional curtailment it is easier to come up with a "one size fits all" tuning for the MPC policy, i.e. one that performs well both during winter and summer days as well as in case of emergencies. On the other hand, tuning gets complicated by the fact that the V_{crit} critical voltage - above which PV curtailment will be allowed - will also have to be chosen. Similarly to the simple MPC scheme, these parameters were also tuned iteratively during the case study with the help of simulations, and their values are given in Section C-2 of Appendix C. Besides the extra tuning parameters and the modifications of curtailment weights, this policy can be applied with the same $T_\mathrm{s,MPC}$ sampling time and other parameters that were chosen for the simple MPC policy described in the previous section.

3-3 Constraint and Automatic Voltage Control Relay Deadband Tightening

While simple MPC has some inherent robustness against exogenous disturbances, there are methods to increase the resilience of MPC schemes against said unwanted phenomena. The most common approaches are the Robust Model Predictive Control (RMPC) and Stochastic Model Predictive Control (SMPC) frameworks. These methods, however, require extra design considerations and usually also have a higher computational demand. For this reason, this study does not deal with such solutions, instead, this section presents, two simple and pragmatic approaches as a way to increase resilience against disturbances and ease the severity of voltage limit violations. These two ideas are a simple voltage constraint tightening scheme and the deadband tightening of the primary substation's AVC relay.

3-3-1 Voltage Constraint Tightening

Constraint tightening is a common approach to increase the robustness of MPC against state limit violations caused by unknown exogenous disturbances. In the simplest case, it is assumed that an unknown bounded additive disturbance acts on the system states at all time steps of the prediction horizon, making the predicted system's states more and more uncertain, the further the MPC policy looks into the future. This means, that the state constraints, that are towards the end of the prediction horizon have to be tightened more, compared to the ones acting on the states closer in time to the present system state. More advanced robust MPC schemes optimize feedback policies instead of simple inputs throughout the control horizon, which reduces the uncertainty of state predictions. For more information on these advanced MPC schemes [85] should be referred. All these approaches are considered quite conservative and come with extra design considerations and higher computational costs. For these reasons, in this thesis, a simpler, pragmatic approach is used, where the V_{low} and V_{high} limits are modified to be V'_{low} and V'_{high} respectively, for all time steps of the prediction horizon ahead, the following way:

$$V'_{\text{low}} = V_{\text{low}} + V_{\text{tighten}} \qquad V'_{\text{high}} = V_{\text{high}} - V_{\text{tighten}} \qquad (3\text{-}8)$$

where V_{tighten} is the amount with which both lower and upper limits are shrunk, throughout the whole prediction horizon. In addition to voltage constraint tightening, the weights on voltage limit violations were increased to w'_{low} and w'_{high}, as tightening too soft limits would practically not affect the controller's performance at all. The chosen values for these parameters used in the case study were hand-tuned iteratively using many simulations and are given in Section C-3 of Appendix C. The used sampling time can be the same $T_{\text{s,MPC}}$ and the other tuning parameters can be also the same as the ones used with the previously presented conditional curtailment MPC.

3-3-2 AVC Relay Deadband Tightening

Another idea to reduce voltage limit violations in the controlled grid is to tighten the V_{db} deadband of the AVC relay fitted to the primary substation's transformer to be V'_{db}. This

approach however only protects from disturbances that are felt at said relay's monitored bus, e.g. disturbances coming from the external high voltage grid connection's voltage fluctuations. Localized voltage issues by e.g. the ones caused by distributed generator units located far from the primary substation cannot be reduced this way. The deadband cannot be tightened arbitrarily small, since too small values could lead to "tap hunting", a phenomenon when the AVC relay gets stuck periodically switching between two adjacent tap positions. To avoid this, the V'_db deadband has to be larger than half of the voltage with which the AVC relay's V_meas measured voltage changes after a corrective tap change action. The chosen V'_db used in the case study is given in Section C-4 of Appendix C. Besides this modified parameter, the same tuning parameters can be used as with a conditional curtailment MPC presented in the previous section.

3-4 Incorporation of Future Knowledge

Previously it was discussed how the MPC's robustness can increase against voltage limit violations with the tightening of voltage constraints. In this section, a different approach will be explored, namely the idea to incorporate exact knowledge about future disturbances, that affect voltages. The incorporation of exact future knowledge and the tackling of resulting intersample phenomena through modeling midpoint voltages is the second contribution of this MSc thesis, which was also listed in Chapter 1 of this report.

The $\Delta V_\mathrm{dist}(k+i)$ voltage disturbances (changes in voltage magnitudes) resulting from changes in the load and generation profiles of low-voltage customers and the external high voltage grid's voltage magnitude profile, between time step $k+i$ and $k+i+1$ of the MPC policy, could be expressed with the following linear sensitivity matrix-based expression:

$$\Delta V_\mathrm{dist}(k+i) = S_\mathrm{PLV}\Delta P_\mathrm{LV}(k+i) + S_\mathrm{sl}\Delta V_\mathrm{sl}(k+i) \qquad \forall i \in \{0, \ldots, N_\mathrm{p}-1\} \tag{3-9}$$

where S_PLV and S_sl are the voltage magnitudes' sensitivity matrices to the power injections of low-voltage customers and the external grid's (slack bus's) voltage magnitude fluctuations respectively. $\Delta P_\mathrm{LV}(k+i) = P_\mathrm{LV,gen}(k+i+1) - P_\mathrm{LV,con}(k+i+1) - P_\mathrm{LV,gen}(k+i) + P_\mathrm{LV,con}(k+i)$ is the vector of changes in the low voltage customers' active power injection with $P_\mathrm{LV,gen}$ containing the generated and $P_\mathrm{LV,con}$ the consumed active power of said customers. $\Delta V_\mathrm{sl}(k+i) = V_\mathrm{sl}(k+i+1) - V_\mathrm{sl}(k+i)$ is the change in the external grid's voltage magnitude. The effect of the low-voltage customers' reactive power injection is neglected, as the grid's voltage magnitudes are relatively insensitive to reactive power flow with high R/X ratios. In addition, the small household PV plants generate power at a unity power factor and households consume at a power factor close to 1. The latter statement holds, as most modern household appliances are required to be fitted with power factor correction. For this reason, the power factor of low-voltage customers is relatively close to unity.

The MPC-based voltage control scheme's prediction model is therefore modified the following way:

$$V(k+i+1) = V(k+i) + S_n\Delta n(k+i) + S_\mathrm{PcPV}\Delta P_\mathrm{cPV}(k+i) + \Delta V_{dist}(k+i) \qquad \forall i \in \{0, \ldots, N_\mathrm{p}-1\} \tag{3-10}$$

where contrary to the previously presented MPC schemes, the $\Delta P_{\mathrm{cPV}}(k+i)$ vector of curtailable PV power changes also has to incorporate future knowledge. More specifically, knowledge will be assumed on how the $P_{\mathrm{poss},j}(k+i)$ possibly injectable power of plant j changes throughout the prediction horizon. The $P_{\mathrm{cPV}}(k+i)$ injected power of curtailable PV plant j therefore takes the following form:

$$P_{\mathrm{cPV},j}(k+i) = P_{\mathrm{poss},j}(k+i) - P_{\mathrm{cur},j}(k+i) \qquad \forall i \in \{1,\ldots,N_{\mathrm{p}}\} \quad \forall j \in \mathcal{I}_{\mathrm{cPV}} \qquad (3\text{-}11)$$

where the $P_{\mathrm{cur},j}(k+i)$ curtailments i steps ahead the prediction horizon are continuous decision variables of the resulting optimization problem.

Knowledge of large disturbances could result in unwanted intersample phenomena, as the calculated control actions take effect at the beginning of the sampling time interval while the change in disturbances only happens at the end of the said time interval. For this reason, the MPC policy could cause intersample voltage limit violations, which were addressed by the introduction of the $V_{\mathrm{mid}}(k+i)$ midpoint voltages (that could be observed between time step $k+i$ and $k+i+1$) and their subjection to the same voltage limit constraints as the $V(k+i)$ monitored voltage magnitude vector.

In Equation 3-10 the $S_n\Delta n(k+i)$ effect of tap change action could be felt right at the beginning of time interval $k+i$, and the $\Delta V_{dist}(k+i)$ change in low-voltage customer and external grid disturbances only takes effect at the end of interval $k+i$ (right before the voltage measurements of interval $k+i+1$ are taken). Whether the change in curtailable PV plants curtailment is felt at the beginning of the interval depends on both the changes in the $P_{\mathrm{poss},j}$ possible injectable power and the modification of the $P_{\mathrm{all},j}$ allowed power level for plant j; $\forall j \in \mathcal{I}_{\mathrm{cPV}}$. This is illustrated in Figure 3-3. In the following equation for $V_{\mathrm{mid}}(k+i+1)$ midpoint voltages, the vector that contains the changes in the power injections of curtailable PV plants will be denoted $\Delta P_{\mathrm{cPV,mid}}(k+i)$:

$$V_{\mathrm{mid}}(k+i) = V(k+i) + S_n\Delta n(k+i) + S_{\mathrm{PcPV}}\Delta P_{\mathrm{cPV,mid}}(k+i) \qquad \forall i \in \{0,\ldots,N_{\mathrm{p}}-1\} \quad (3\text{-}12)$$

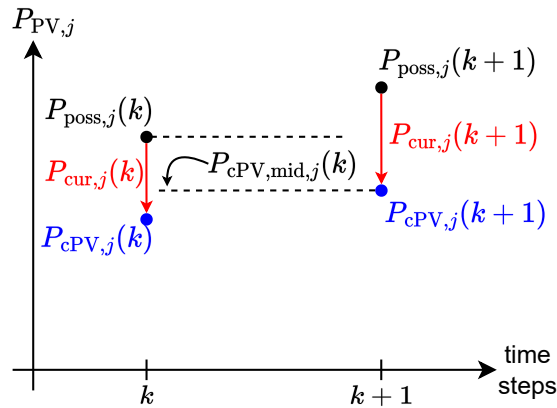**Figure 3-3:** $P_{\mathrm{cPV,mid},j}(k)$ Midpoint Power Injection of Curtailable PV Plant j

$\Delta P_{\text{cPV,mid},j}(k+i)$ can be expressed the following way, using Figure 3-3:

$$\Delta P_{\text{mid},j}(k+i) = \underbrace{\min\left(P_{\text{poss},j}(k+i), P_{\text{cPV},j}(k+i+1)\right)}_{P_{\text{mid},j}(k+i)} - P_{\text{cPV},j}(k+i) \tag{3-13}$$

$$\Delta P_{\text{cPV,mid},j}(k+i) = \begin{cases} P_{\text{cPV},j}(k+i+1) - P_{\text{cPV},j}(k+i) & \text{if} \quad P_{\text{cPV},j}(k+i+1) \leq P_{\text{poss},j}(k+i) \\ P_{\text{poss},j}(k+i) - P_{\text{cPV},j}(k+i) & \text{if} \quad P_{\text{cPV},j}(k+i+1) > P_{\text{poss},j}(k+i) \end{cases} \tag{3-14}$$

$$\Delta P_{\text{cPV,mid},j}(k+i) = \begin{cases} \Delta P_{\text{cPV},j}(k+i) & \text{if} \quad P_{\text{cPV},j}(k+i+1) \leq P_{\text{poss},j}(k+i) \\ P_{\text{cur},j}(k+i) & \text{if} \quad P_{\text{cPV},j}(k+i+1) > P_{\text{poss},j}(k+i) \end{cases} \tag{3-15}$$

To implement this logic, the $b_{\text{mid},j}(k+i)$ binary variables are introduced, which are 1 if and only if $P_{\text{cPV},j}(k+i+1) \leq P_{\text{poss},j}(k+i) \ \forall j \in \mathcal{I}_{\text{cPV}}$. Knowing that $\min P_{\text{cPV},j}(k+i+1) \leq P_{\text{poss},j}(k+i) = -P_{\text{nom},j}$ and $\max P_{\text{cPV},j}(k+i+1) \leq P_{\text{poss},j}(k+i) = P_{\text{nom},j}$ with $P_{\text{nom},j}$ being the nominal (maximum) power of curtailable PV plant j, $\forall j \in \mathcal{I}_{\text{cPV}}$. Using [9], this can be done with the following MIL constraints (assuming the biggest difference between a plant j's curtailed and possible power export is its $P_{\text{nom},j}$ nominal power):

$$P_{\text{cPV},j}(k+i+1) - P_{\text{poss},j}(k+i) \leq P_{\text{nom},j}\left(1 - b_{\text{mid},j}(k+i)\right) \quad \forall i \in \{1,\dots,N_{\text{p}}\} \quad \forall j \in \mathcal{I}_{\text{cPV}}$$
$$P_{\text{cPV},j}(k+i+1) - P_{\text{poss},j}(k+i) \geq \varepsilon + \left(-P_{\text{nom},j} - \varepsilon\right)b_{\text{mid},j}(k+i) \quad \forall i \in \{1,\dots,N_{\text{p}}\} \quad \forall j \in \mathcal{I}_{\text{cPV}} \tag{3-16}$$

The midpoint change in power injection becomes:

$$\Delta P_{\text{cPV,mid},j}(k+i) = b_{\text{mid},j}(k+i)\Delta P_{\text{cPV},j}(k+i) + \left(1 - b_{\text{mid},j}(k+i)\right)P_{\text{cur},j}(k+i) \tag{3-17}$$

Introducing the $z_{\text{cPV},j}(k+i)$ and $z_{\text{cur},j}(k+i)$ auxiliary decision variables:

$$\Delta P_{\text{cPV,mid},j}(k+i) = \underbrace{b_{\text{mid},j}(k+i)\Delta P_{\text{cPV},j}(k+i)}_{z_{\text{cPV},j}(k+i)} + P_{\text{cur},j}(k+i) - \underbrace{b_{\text{mid},j}(k+i)P_{\text{cur},j}(k+i)}_{z_{\text{cur},j}(k+i)} \tag{3-18}$$

Using [9], MIL constraints can be derived that ensure the values of these auxiliary variables, i.e. the binary-continuous multiplication.

For $z_{\text{cPV},j}(k+i) = b_{\text{mid},j}(k+i)\Delta P_{\text{cPV},j}(k+i)$, knowing that $\min \Delta P_{\text{cPV},j}(k+i) = -P_{\text{nom},j}$ and $\max \Delta P_{\text{cPV},j}(k+i) = P_{\text{nom},j}$:

$$z_{\text{cPV},j}(k+i) \leq P_{\text{nom},j}b_{\text{mid},j}(k+i) \quad \forall i \in \{1,\dots,N_{\text{p}}\} \quad \forall j \in \mathcal{I}_{\text{cPV}}$$
$$z_{\text{cPV},j}(k+i) \geq -P_{\text{nom},j}b_{\text{mid},j}(k+i) \quad \forall i \in \{1,\dots,N_{\text{p}}\} \quad \forall j \in \mathcal{I}_{\text{cPV}}$$
$$z_{\text{cPV},j}(k+i) \leq \Delta P_{\text{cPV},j}(k+i) + P_{\text{nom},j} - P_{\text{nom},j}b_{\text{mid},j}(k+i) \quad \forall i \in \{1,\dots,N_{\text{p}}\} \quad \forall j \in \mathcal{I}_{\text{cPV}}$$
$$z_{\text{cPV},j}(k+i) \geq \Delta P_{\text{cPV},j}(k+i) - P_{\text{nom},j} + P_{\text{nom},j}b_{\text{mid},j}(k+i) \quad \forall i \in \{1,\dots,N_{\text{p}}\} \quad \forall j \in \mathcal{I}_{\text{cPV}} \tag{3-19}$$

For $z_{\text{cur},j}(k+i)$, knowing that $\min P_{\text{cur},j}(k+i) = 0$ and $\max P_{\text{cur},j}(k+i) = P_{\text{nom},j}$

$$z_{\text{cur},j}(k+i) \leq P_{\text{nom},j} b_{\text{mid},j}(k+i) \quad \forall i \in \{1,\ldots,N_{\text{p}}\} \quad \forall j \in \mathcal{I}_{\text{cPV}}$$
$$z_{\text{cur},j}(k+i) \geq 0 \quad \forall i \in \{1,\ldots,N_{\text{p}}\} \quad \forall j \in \mathcal{I}_{\text{cPV}}$$
$$z_{\text{cur},j}(k+i) \leq P_{\text{cur},j}(k+i) \quad \forall i \in \{1,\ldots,N_{\text{p}}\} \quad \forall j \in \mathcal{I}_{\text{cPV}}$$
$$z_{\text{cur},j}(k+i) \geq P_{\text{cur},j}(k+i) - P_{\text{nom},j} + P_{\text{nom},j} b_{\text{mid},j}(k+i) \quad \forall i \in \{1,\ldots,N_{\text{p}}\} \quad \forall j \in \mathcal{I}_{\text{cPV}}$$
$$(3\text{-}20)$$

The MPC policy's optimization problem that incorporates exact knowledge about the future profiles (disturbances), the midpoint voltage dynamics with the necessary MIL constraints, and conditional curtailment logic is given in Equation 3-21.

$$\min \sum_{i=1}^{N_{\text{p}}} \|V(k+i) - V_{\text{ref}}\|_{Q_V}^2 + \|\Delta n(k+i-1)\|_{R_n}^2 + \|P_{\text{cur}}(k+i)\|_{R'_{\text{cPV}}}^2 +$$
$$+ w'_{\text{low}} \varepsilon_{\text{low}}(k+i) + w'_{\text{high}} \varepsilon_{\text{high}}(k+i)$$
$$\text{s. t. } V(k+i+1) = V(k+i) + S_n \Delta n(k+i) + S_{\text{PcPV}} \Delta P_{\text{cPV}}(k+i) +$$
$$+ \Delta V_{dist}(k+i) \qquad \forall i \in \{0,\ldots,N_{\text{p}}-1\}$$
$$V_{\text{mid}}(k+i) = V(k+i) + S_n \Delta n(k+i) + S_{\text{PcPV}} \Delta P_{\text{cPV,mid}}(k+i) \qquad \forall i \in \{0,\ldots,N_{\text{p}}-1\}$$
$$(V_{\text{low}} - \varepsilon_{\text{low}}(k+i))\,\mathbf{1} \leq V(k+i), V_{\text{mid}}(k+i-1) \leq (V_{\text{high}} + \varepsilon_{\text{high}}(k+i))\,\mathbf{1} \qquad \forall i \in \{1,\ldots,N_{\text{p}}\}$$
$$P_{\text{cPV},j}(k+i) = P_{\text{poss},j}(k+i) - P_{\text{cur},j}(k+i) \qquad \forall i \in \{1,\ldots,N_{\text{p}}\} \quad \forall j \in \mathcal{I}_{\text{cPV}}$$
$$0 \leq \varepsilon_{\text{low}}(k+i), \varepsilon_{\text{high}}(k+i) \qquad \forall i \in \{1,\ldots,N_{\text{p}}\}$$
$$n_{\min} \leq n(k+i) \leq n_{\max} \qquad \forall i \in \{1,\ldots,N_{\text{p}}\}$$
$$\Delta n_{\min} \leq \Delta n(k+i) \leq \Delta n_{\max} \qquad \forall i \in \{0,\ldots,N_{\text{p}}-1\}$$
$$V_{\text{crit}} - V_{\text{cPV},j}(k+i) \leq V_{\text{crit}} \left(1 - b_{\text{cur},j}(k+i)\right) \qquad \forall i \in \{1,\ldots,N_{\text{p}}\} \quad \forall j \in \mathcal{I}_{\text{cPV}}$$
$$V_{\text{crit}} - V_{\text{cPV},j}(k+i) \geq \varepsilon + (-2 - \varepsilon)\,b_{\text{cur},j}(k+i) \qquad \forall i \in \{1,\ldots,N_{\text{p}}\} \quad \forall j \in \mathcal{I}_{\text{cPV}}$$
$$0 \leq P_{\text{cur},j}(k+i) \leq P_{\text{poss},j}(k+i) b_{\text{cur},j}(k) \qquad \forall i \in \{1,\ldots,N_{\text{p}}\} \quad \forall j \in \mathcal{I}_{\text{cPV}}$$
$$\Delta P_{\text{cPV,mid},j}(k+i) = z_{\text{cPV},j}(k+i) + P_{\text{cur},j}(k+i) - z_{\text{cur},j}(k+i)$$
$$P_{\text{cPV},j}(k+i+1) - P_{\text{poss},j}(k+i) \leq P_{\text{nom},j}\left(1 - b_{\text{mid},j}(k+i)\right) \quad \forall i \in \{1,\ldots,N_{\text{p}}\} \quad \forall j \in \mathcal{I}_{\text{cPV}}$$
$$P_{\text{cPV},j}(k+i+1) - P_{\text{poss},j}(k+i) \geq \varepsilon + (-P_{\text{nom},j} - \varepsilon)\,b_{\text{mid},j}(k+i) \quad \forall i \in \{1,\ldots,N_{\text{p}}\} \quad \forall j \in \mathcal{I}_{\text{cPV}}$$
$$z_{\text{cPV},j}(k+i) \leq P_{\text{nom},j} b_{\text{mid},j}(k+i) \quad \forall i \in \{1,\ldots,N_{\text{p}}\} \quad \forall j \in \mathcal{I}_{\text{cPV}}$$
$$z_{\text{cPV},j}(k+i) \geq -P_{\text{nom},j} b_{\text{mid},j}(k+i) \quad \forall i \in \{1,\ldots,N_{\text{p}}\} \quad \forall j \in \mathcal{I}_{\text{cPV}}$$
$$z_{\text{cPV},j}(k+i) \leq \Delta P_{\text{cPV},j}(k+i) + P_{\text{nom},j} - P_{\text{nom},j} b_{\text{mid},j}(k+i) \quad \forall i \in \{1,\ldots,N_{\text{p}}\} \quad \forall j \in \mathcal{I}_{\text{cPV}}$$
$$z_{\text{cPV},j}(k+i) \geq \Delta P_{\text{cPV},j}(k+i) - P_{\text{nom},j} + P_{\text{nom},j} b_{\text{mid},j}(k+i) \quad \forall i \in \{1,\ldots,N_{\text{p}}\} \quad \forall j \in \mathcal{I}_{\text{cPV}}$$
$$z_{\text{cur},j}(k+i) \leq P_{\text{nom},j} b_{\text{mid},j}(k+i) \quad \forall i \in \{1,\ldots,N_{\text{p}}\} \quad \forall j \in \mathcal{I}_{\text{cPV}}$$
$$z_{\text{cur},j}(k+i) \geq 0 \quad \forall i \in \{1,\ldots,N_{\text{p}}\} \quad \forall j \in \mathcal{I}_{\text{cPV}}$$
$$z_{\text{cur},j}(k+i) \leq P_{\text{cur},j}(k+i) \quad \forall i \in \{1,\ldots,N_{\text{p}}\} \quad \forall j \in \mathcal{I}_{\text{cPV}}$$
$$z_{\text{cur},j}(k+i) \geq P_{\text{cur},j}(k+i) - P_{\text{nom},j} + P_{\text{nom},j} b_{\text{mid},j}(k+i) \quad \forall i \in \{1,\ldots,N_{\text{p}}\} \quad \forall j \in \mathcal{I}_{\text{cPV}}$$
$$(3\text{-}21)$$

Similarly to the optimization problem in Equation 3-7, that introduced conditional curtailment, this is also an MIQP problem, regardless of whether the discreteness of tap positions is considered or not. Besides the binary variables of the conditional curtailment logic, the midpoint voltage prediction model requires the usage of extra binary and continuous decision variables, which makes solving the optimization problem harder (longer computation times) than the previously presented ones. The $\Delta V_{\mathrm{dist}}(k+i)$ voltage disturbance terms have to be calculated before solving the cost function minimization. As it was shown in Equation 3-9, this requires the calculation of the S_{PLV} and S_{sl} sensitivity matrices beside knowing the future values of $\Delta P_{\mathrm{LV}}(k+i)$ and $\Delta V_{\mathrm{sl}}(k+i) \ \forall i \in \{0, \ldots, N_{\mathrm{p}}-1\}$. These extra sensitivity calculations also add to the increased computational demand of this policy.

Besides modeling the midpoint dynamics, there is still a chance for unwanted intersample phenomena caused by the AVC relay. The reason behind this is the fact that the relay's V_{set} setpoint is adjusted to be $V_{\mathrm{meas}}(k+1|k)$ prediction at time step k which already contains knowledge about future disturbances that haven't happened yet. This could cause mismatches between the relay's setpoint and measured value, causing tap changes, which could lead to limit violations when the disturbances right before time step $k+1$ take effect. To counteract this, the AVC relay is deactivated whilst testing this MPC policy with future knowledge. This is a reason why this policy should operate with a higher sampling time than the other MPC-based voltage control policies presented previously.

Knowing how loading, generation, and external grid voltage change over the course of the considered prediction horizon could seem slightly unrealistic and impractical at first. However, the simulations that are conducted using this control policy, show the best possible performance one could get with an MPC-based voltage controller. To further embrace this direction, this policy's $T_{\mathrm{s,idMPC}}$ sampling time will be chosen the same as the sampling time of the profile with the highest temporal resolution in the simulations of the case study. This way, the control policy will be able to react to disturbances right as they take effect, in addition to knowing them in advance. In case said ideal results are not satisfactory, as maybe a much simpler or cheaper control scheme could produce similar or only slightly worse results, the value behind this idea is the insight it provides to distribution system operators (Stedin in this case) that there is no benefit to be gained from the further investigation of MPC in their medium-voltage grids. In case the ideal MPC policy with future knowledge and midpoint dynamics gives convincing results, i.e. considerably better performance when compared with other MPC schemes or simpler controllers, the added insight of this idea is the fact that the distribution system operator should research forecasting methods for the quantities on which future knowledge was assumed. Examples of such works in the literature are: [29, 37, 106, 20, 39, 56].

3-5 Other Control Schemes For Comparison

In order to assess, the MPC-based voltage control schemes, presented in the previous section, a comparative study needs to be conducted. In addition to being compared to each other, the MPC schemes will be compared, with two different control schemes. Since MPC is quite demanding, from a computational and infrastructural point of view, two simple schemes were selected, namely current compounding, and current compounding with local active power curtailment. These are simple localized control schemes, that are considerably easier to

implement in contrast to MPC. In case MPC does not perform considerably better than these schemes, it is not worth implementing.

3-5-1   Current Compounding

This control scheme modifies the behavior of the AVC relay at its controlled grid's primary substation. With this simple method, in addition to the voltage at the primary substation's medium voltage busbar, the transformer's supplied (load) current is also measured, hence the name Current Compounding (CC). Using the voltage and current measurements of the substation, the power supplied by the transformer can be calculated and the V_{set} setpoint of the AVC relay can be compensated accordingly. The AVC setpoint is adjusted based on the $P_{prim,supp}$ active power supplied by the primary distribution transformer (flowing from the external high-voltage grid towards the supplied medium-voltage grid). When a lot of power is flowing back to the high-voltage grid through the transformer, the voltage setpoint is lowered to compensate for the voltage rise in the MV grid. In the other case, when a lot of power is being supplied from the high-voltage grid through the transformer, the voltage setpoint is raised to compensate for the voltage drops.

As already mentioned in Section 2-2 of Chapter 2, the CC scheme needs to be tuned exactly to the grid it is applied to, as each different distribution grid comes with unique customers that have their unique load and generation profiles, and different grid parameters (e.g. cable parameters) result in different nodal voltages even with the same consumption and generation values. The shaping of the $V_{set}(P_{prim,supp})$ function is a non-trivial task, and to the author's best knowledge, no uniformly accepted systematic method exists in the literature to do this. In this MSc project, a "stairstep" function will be used, formulated by equally dividing 5 voltage setpoints between the minimum and maximum active power values supplied by the transformer. This function is shown in Figure 3-4. This even distribution of setpoints is straightforward to tune and was chosen for easier reproducibility. It could happen that a different setpoint adjustment function better tailored to the specific controlled grid could result in slightly better performance. It also has to be noted, that the chosen setpoints should be at least V_{db} away from the minimum and maximum voltage limits (where V_{db} is the deadband of the AVC relay) to ensure that the relay always acts in case its V_{meas} local measurement violates said limits.

The CC-based adjustment of the V_{set} setpoint is implemented with the same sampling time as the MPC policies without future knowledge to ensure fair comparability: $T_{s,CC} = T_{s,MPC}$. Similarly to the ideal MPC, the sampling time of this policy was also lowered but contrary to MPC-based schemes, the performance of CC is not so heavily dependent on the chosen sampling time.

At the time of writing this thesis, Stedin is using a similar control policy to mitigate voltage violation problems in the large distribution grid from which the grid segment simulated in the case study was taken. Initial tests have shown promising results with this method, that is why this controller and its combination with active power curtailment are selected to be compared with MPC-based schemes. The exact tuning of this policy that was used in the case study is given in Section C-6-1 of Appendix C.
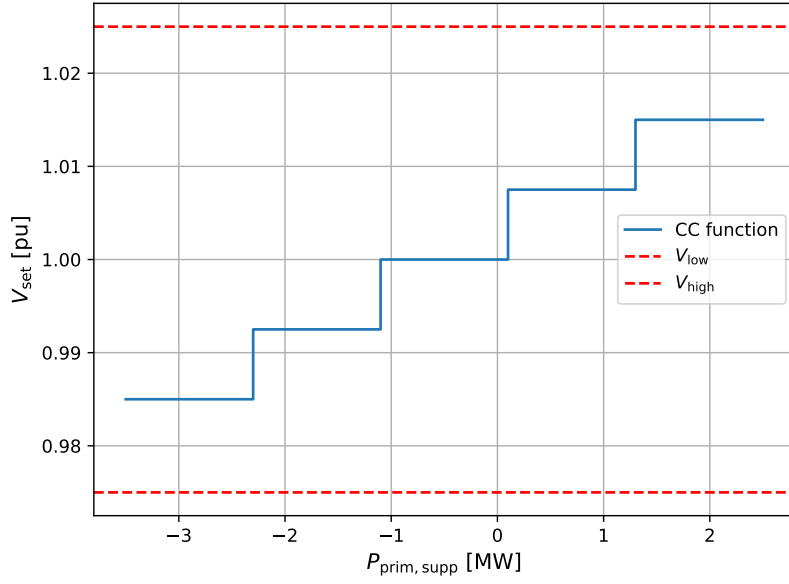
Figure 3-4: Illustration of the Current Compounding Voltage Control Scheme

3-5-2 Current Compounding with Active Power Curtailment

The MPC policies in this study use two control actions: the OLTC of the primary substation's transformer and the active power curtailment of PV plants. The CC scheme presented in the previous section only uses the primary substation transformer's OLTC (indirectly, by adjusting the setpoint of its AVC relay), so in order to also compare MPC with a control method that uses the same actions, the large curtailable PV plants are fitted with local Active Power Curtailment (APC) controllers. These work alongside the previously shown CC scheme.

The $P_{\mathrm{all},j}$ active power limit of the jth curtailable PV plant is adjusted based on its local $V_{\mathrm{cPV},j}$ voltage magnitude measurement. Below a certain $V_{\mathrm{crit},j}$ voltage, the plant is allowed to export its $P_{\mathrm{max},j}$ maximum possible active power, which is equal to its $P_{\mathrm{nom},j}$ nominal power. Above the $V_{\mathrm{max},j}$ the PV plant is not allowed to export any power at all. If the locally measured $V_{\mathrm{cPV},j}$ voltage is in between $V_{\mathrm{crit},j}$ and $V_{\mathrm{max},j}$, the active power limit decreases linearly as the $V_{\mathrm{cPV},j}$ voltage magnitude gets higher. Knowing this the $P_{\mathrm{all,r},j}$ allowed power export reference for the jth power plant can be expressed the following way (also illustrated in the first block of Figure 3-5):

$$
P_{\mathrm{all,r},j} = \begin{cases} P_{\mathrm{max},j} & \text{if} \quad V_{\mathrm{cPV},j} < V_{\mathrm{crit},j} \\ P_{\mathrm{max},j}\left(1 - \frac{V_{\mathrm{cPV},j}-V_{\mathrm{crit},j}}{V_{\mathrm{max},j}-V_{\mathrm{crit},j}}\right) & \text{if} \quad V_{\mathrm{crit},j} \leq V_{\mathrm{cPV},j} < V_{\mathrm{max},j} \\ 0 & \text{if} \quad V_{\mathrm{max},j} \leq V_{\mathrm{cPV},j} \end{cases} \tag{3-22}
$$

During the initial simulations of this policy, it was found that it is quite prone to chattering, i.e. the curtailment policy was constantly overcorrecting its actions at the previous sampling time step. In order to get rid of this behavior, an integrator was added to the system, to slow

down, the response of curtailable PV plants to new power limit settings. The addition of said integrator, and the block diagram of the resulting APC scheme is shown in Figure 3-5.
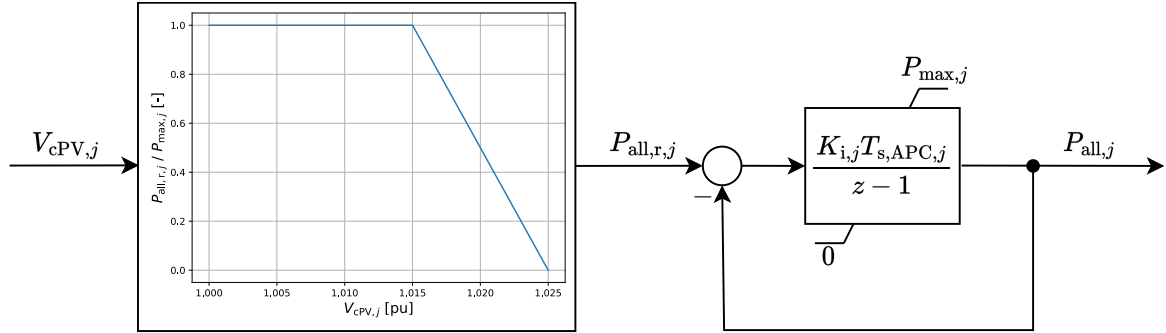

Figure 3-5: Block Diagram of the Local Active Power Curtailment Controller

It can be seen that the local APC controller first takes a measurement of the jth curtailable PV plant's voltage magnitude, then selects a $P_{\text{all,r},j}$ reference power level based on the piecewise linear function described in Equation 3-22. The PV plants $P_{\text{all},j}$ allowed power level then converges to this reference value, while the grid also responds to the action of active power curtailment. Equilibrium is reached, until due to changes in the jth PV plant's production or some other external factor, the $V_{\text{cPV},j}$ voltage changes, and the APC scheme has to respond again.

The CC scheme used alongside the local APC controllers could result in uncoordinated behavior, and it could happen that the controllers start "fighting" with each other. The reason behind this is the fact, that the local APC controllers interfere with the grid's active power flow and consequently modify the $P_{\text{prim,supp}}$ power that is supplied through the transformer of the primary substations. This way, the APC controllers, indirectly have an effect on the behavior of the CC scheme. The OLTC actions, which are governed by CC modify all voltage magnitudes in the grid to some extent, including $V_{\text{cPV},j}$ so CC could also have an effect on the behavior of local APC. In order to avoid any unwanted phenomena caused by the interaction of CC and local APC controllers, the schemes have to be implemented with considerably different sampling times: CC acts slower as it has an effect on all nodal voltages, while the local APC's effect on the nodal voltages is more localized, and for this reason, this scheme was chosen to operate faster. In addition to different sampling times, the stairstep function of the CC policy needs to be "crude enough", i.e. only a few setpoints should be used and active power ranges for different setpoints should be sufficiently large, such that smaller quick changes in the transformer's active power delivery are less likely to cause changes in the AVC relay's setpoint. The tuning parameters for the APC controllers in the case study are given in Section C-6-2 of Appendix C.

3-6   Selection of Metrics

In order to make a fair comparison between the different voltage controllers, objective metrics are needed that show different aspects of the controllers' performance. The selected metrics, their short description, and calculation method are presented in this section. More specifically, the root mean square error (RMSE) of monitored nodal voltages, the total area of voltage

limit violations, the relative amount of curtailed PV energy, and the total number of tap changes over the course of the simulated time interval. In addition, for MPC based schemes, the CPU time necessary for computation will also be analyzed.

RMSE of Monitored Nodal Voltages

The $V_{\mathrm{RMSE}}(t)$ root mean square error (RMSE) at time t is calculated for all the monitored nodal voltages in the grid, and can be expressed the following way:

$$V_{\mathrm{RMSE}}(t) = \sqrt{\frac{1}{N_{\mathrm{mon}}} \left(V(t) - V_{\mathrm{ref}}\right)^{\mathrm{T}} \left(V(t) - V_{\mathrm{ref}}\right)} \tag{3-23}$$

where N_{mon} is the number of monitored buses, $V(t)$ is the vector of monitored nodal voltage magnitudes at time t, and V_{ref} is a vector with the reference voltage magnitudes, which in this case contains N_{mon} 1 entries. The average of this metric is calculated for the $t \in [0, t_{\mathrm{sim}}]$ simulated time interval the following way (with t_{sim} being the length of the simulated interval):

$$V_{\mathrm{RMSE}} = \sqrt{\frac{1}{t_{\mathrm{sim}} N_{\mathrm{mon}}} \int_{0}^{t_{\mathrm{sim}}} \left(V(t) - V_{\mathrm{ref}}\right)^{\mathrm{T}} \left(V(t) - V_{\mathrm{ref}}\right) \mathrm{d}t} \tag{3-24}$$

In practice (in case of a numerical simulation), the integral above has to be approximated numerically. V_{RMSE} is a metric that shows how different monitored nodal voltages deviate from their nominal value, in the entire grid over the course of the simulated time interval. The lower this metric, the better, as low V_{RMSE} values indicate flat voltage profiles close to the nominal value for the majority of the nodes. The ideal value for this metric would be 0, however achieving that goal is highly unlikely in reality, so the goal during the simulated test cases is to have this number as low as possible. Similarly to nodal voltages, $V_{\mathrm{RMSE}}(t)$ and V_{RMSE} are measured in per unit (pu).

Total Area of Voltage Limit Violations

The total area of voltage limit violation is a metric that indicates how seriously the V_{low} and V_{high} limits are violated. The total $A_{\mathrm{viol,low}}$ area of violation for the V_{low} voltage limit during the studied $[0, t_{\mathrm{sim}}]$ time interval is the following:

$$A_{\mathrm{viol,low}} = \sum_{i \in \mathcal{I}_{\mathrm{mon}}} \int_{0}^{t_{\mathrm{sim}}} \max\left(V_{\mathrm{low}} - V_i(t), 0\right) \mathrm{d}t \tag{3-25}$$

where $\mathcal{I}_{\mathrm{mon}}$ is a set that contains all the indices of the monitored buses, and $V_i(t)$ is the voltage magnitude of the monitored bus indexed i. The max function in the integral ensures that the $A_{\mathrm{viol,low}}$ metric is only incremented if (one or more) voltage magnitude is below the limit, and the incrementation is proportional to the amount and length of violation. The total $A_{\mathrm{viol,high}}$ area of the V_{high} upper limit's violation can be expressed similarly:

$$A_{\text{viol,high}} = \sum_{i \in \mathcal{I}_{\text{mon}}} \int_0^{t_{\text{sim}}} \max\left(V_i(t) - V_{\text{high}}, 0\right) \mathrm{d}t \tag{3-26}$$

The A_{viol} area of total limit violation is the sum of the $A_{\text{viol,low}}$ and $A_{\text{viol,high}}$ areas:

$$A_{\text{viol}} = A_{\text{viol,low}} + A_{\text{viol,high}} \tag{3-27}$$

This metric incorporates the three problematic aspects of limit violation, as it is proportional to how large violations are, how long they last, and how spread out the problem is (i.e. how many nodes are affected). The ideal value for A_{viol} and its lower and upper components is 0, as that means that no voltage limits were violated during the studied time interval. For this reason, keeping A_{viol} as low as possible is also an important goal of the voltage control designs of this study. $A_{\text{viol,low}}$, $A_{\text{viol,high}}$ and A_{viol} are all measured in per unit times seconds $(\text{pu} \cdot \text{s})$ in the conducted simulations. Similarly to other metrics, the necessary integrals were computed with numerical approximation.

PV curtailment

The energy produced by PV plants is quite valuable as distribution system operator companies (including Stedin) are required to pay compensation for the energy they forbid Distributed Generation (DG) unit operators from exporting. This makes PV curtailment an expensive control input, and there should be a metric to indicate how much PV energy is lost by each control scheme due to this action. One of such metrics, is the $E_{\text{cur},j}$ amount of energy lost due to curtailment at PV plant j during the studied $[0, t_{\text{sim}}]$ time interval:

$$E_{\text{cur},j} = \int_0^{t_{\text{sim}}} \max\left(P_{\text{poss},j}(t) - P_{\text{all},j}(t), 0\right) \mathrm{d}t \tag{3-28}$$

where $P_{\text{poss},j}(t)$ is the possible, and $P_{\text{all},j}(t)$ is the allowed power export of PV plant j at time t respectively. The maximum function is necessary, as power is only lost due to curtailment when the possible export is higher than the set upper limit. The E_{cur} total loss due to PV curtailment will take the following form (summing curtailment losses for all curtailable PV plants):

$$E_{\text{cur}} = \sum_{j \in \mathcal{I}_{\text{cPV}}} \int_0^{t_{\text{sim}}} \max\left(P_{\text{poss},j}(t) - P_{\text{all},j}(t), 0\right) \mathrm{d}t \tag{3-29}$$

where $\mathcal{I}_{\text{cPV}}$ is a set that contains the indices of curtailable PV plants. These losses during the studied time interval are measured in megawatt hours (MWh). For simulated quantities, the integrals are approximated numerically. The lower these losses the better.

The previously shown curtailment loss quantities only focus on the absolute amount of PV energy lost. This might be misleading as produced energy is worth more on the market during days when generation is low (e.g. in the winter) and less during days when there is a lot of distributed generation (e.g. on sunny summer days). To indicate this, the relative PV curtailment will be used as a metric to indicate how much power is wasted by the controller. This $p_{\text{cur},j}$ relative curtailment for curtailable PV plant j during the studied $[0, t_{\text{sim}}]$ time interval is:

$$p_{\mathrm{cur},j} = \frac{E_{\mathrm{cur},j}}{E_{\mathrm{poss},j}} \cdot 100 = \frac{\int_0^{t_{\mathrm{sim}}} \max\left(P_{\mathrm{poss},j}(t) - P_{\mathrm{all},j}(t), 0\right) \mathrm{d}t}{\int_0^{t_{\mathrm{sim}}} P_{\mathrm{poss},j}(t)\mathrm{d}t} \cdot 100 \qquad (3\text{-}30)$$

it can be seen that it is a fraction of the energy lost due to curtailment and the possible energy production. This quantity can be aggregated $\forall j \in \mathcal{I}_{\mathrm{cPV}}$ plants the following way, resulting in the p_{cur} relative curtailment for the whole studied network during the whole studied time interval:

$$p_{\mathrm{cur}} = \frac{\sum_{j \in \mathcal{I}_{\mathrm{cPV}}} E_{\mathrm{cur},j}}{\sum_{j \in \mathcal{I}_{\mathrm{cPV}}} E_{\mathrm{poss},j}} \cdot 100 = \frac{\sum_{j \in \mathcal{I}_{\mathrm{cPV}}} \int_0^{t_{\mathrm{sim}}} \max\left(P_{\mathrm{poss},j}(t) - P_{\mathrm{all},j}(t), 0\right) \mathrm{d}t}{\sum_{j \in \mathcal{I}_{\mathrm{cPV}}} \int_0^{t_{\mathrm{sim}}} P_{\mathrm{poss},j}(t)\mathrm{d}t} \cdot 100 \qquad (3\text{-}31)$$

$p_{\mathrm{cur},j}$ and p_{cur} will be given as percentages, and the integrals necessary for their calculations will be obtained numerically. Ideally, these metrics should be kept as low as possible.

Tap Changes During the Studied Time Interval

Besides evaluating the usage of PV curtailment another metric will be used that quantifies the usage of the other control action, more specifically the OLTC of the primary substation's transformer. The metric to indicate this will be N_{tc} which will show how many taps the OLTC has moved in total during the studied (simulated) $[0, t_{\mathrm{sim}}]$ time interval. N_{tc} is expressed the following way:

$$N_{\mathrm{tc}} = \sum_{l=0}^{N_{\mathrm{sim}}-1} |\Delta n(l)| \qquad (3\text{-}32)$$

where $N_{\mathrm{sim}} = \mathrm{floor}\left(t_{\mathrm{sim}}/\tau_{\mathrm{sim}}\right)$ is the number of time steps in the numerical simulation conducted for studying the $[0, t_{\mathrm{sim}}]$ time interval. τ_{sim} is the (fixed) time step of this numerical simulation and the l running index iterates over these steps during summation. $\Delta n(l) = n(l+1) - n(l)$ is the change in tap position at time step l. N_{tc} will be measured in taps.

A high N_{tc} value indicates a heavy usage of the OLTC. Many switchings lead to faster degradation of the whole mechanism, especially the contact points. For this reason, N_{tc} should be kept low if possible. On the other hand, the OLTC's wear and tear is less of a problem than voltage limit violations, high fluctuations, or excessive PV curtailment. Knowing this, it can be stated, that N_{tc} is somewhat of a less important metric, compared to the ones listed above; and a slightly higher N_{tc} could be tolerated when it results in lower V_{RMSE}, A_{viol} and p_{cur} values.

Computation Time

MPC in general has a high computational demand, due to the necessity of solving an optimization problem at each sampling time step of the controller. With MPC-based grid voltage

control, the sensitivity computation also takes some time, and therefore increases the computational cost of the control policy. To quantify, the computational demand, the $T_{\text{sens}}(k)$ CPU time necessary for sensitivity calculation at time step k and the $T_{\text{opt}}(k)$ CPU time necessary for solving the optimization problem at time step k will be measured during the simulations. The total $T_{\text{MPC}}(k)$ computation time is the sum of these two quantities:

$$T_{\text{MPC}}(k) = T_{\text{sens}}(k) + T_{\text{opt}}(k) \tag{3-33}$$

This computation time is only measured in case of MPC-based policies, and for the other two control schemes used for comparison, it will be considered negligibly small. In order to be implementable, the T_{MPC} time needs to be smaller than the control policy's sampling time. In case a good performance is desired, $T_{\text{MPC}}(k)$ values should be as small as possible, since the policy's computation time introduces a delay in the control loop, which when too large, could negatively affect performance. When comparing controllers, the $T_{\text{MPC,max}}$ maximum of MPC computation times will be used:

$$T_{\text{MPC,max}} = \max_k T_{\text{MPC}}(k) \tag{3-34}$$

3-7 Conclusions

The content of this chapter was divided into two main parts: firstly the different MPC policies used in this MSc project were shown, and secondly, the chapter presented alternative controllers with which MPC policies will compared alongside the objective metrics which will be used for comparison. The first section began by giving a short explanation of MPC in general, and after that formulated a simple MPC-based voltage control policy. Then the idea of conditional PV curtailment was introduced in the second section which is one of the contributions of this work. Afterward, in Section 3, two pragmatic approaches were given, that could potentially lessen the severity of voltage limit violations: voltage limit and AVC relay deadband tightening. The idea of including exact knowledge on load, generation, and slack voltage profiles into the MPC policy was presented in this chapter's fourth section. This idea is the second contribution of this MSc project. In order to solve intersample limit violations, commonly happening with this approach, midpoint voltage limits were incorporated into the MPC policy, where the midpoint voltage dynamics were formulated using MIL constraints. The fifth section of this chapter presented two alternative control schemes: current compounding and current compounding in combination with local active power curtailment for large PV plants. These controllers are considerably simpler to implement and come at a negligible computational cost as opposed to MPC, so comparing their performance in a comparative study will give valuable insight for Stedin whether the usage of an MPC-based voltage control policy is worth considering in their medium voltage distribution grids. In order to make a fair and objective comparison, the sixth section of this chapter introduced certain metrics, that quantify the performance of different controllers. The smoothness of voltage profiles will be quantified by the root mean square error (RMSE) of nodal voltages, and the severity of voltage limit violations will be measured by the total voltage limit violation area. The usage (and possible over usage) of control actions will be quantified by relative PV curtailment and the total number of tap changes. The computational cost of MPC policies is quantified by the CPU time necessary for their computations.

Chapter 4

Case Study and Simulation Results

This chapter focuses on presenting the case study that was conducted as part of this MSc project. The first three sections focus on the building blocks of said study, namely the studied grid, the simulation framework created to examine slow voltage dynamics, the profile data used, and the four constructed test cases. Sections 4 to 7 present numerical results for different controllers, and the eighth section compares the performance of three different controllers: an uncoordinated scheme (current compounding with local active power curtailment) and two Model Predictive Control (MPC) schemes (realistic and ideal). The ninth section summarizes and concludes the chapter.

4-1 Studied Grid

In the literature, many different benchmark grids exist, each constructed for different fields of research on power grid operation, dynamics, and control. These grids - while often based on real grids - have artificially constructed structures and parameters that have been adjusted, such that the network is best at reproducing certain phenomena of interest. Examples of such benchmark grids are: The CIGRÉ benchmark grids [10, 87] constructed to study the effect of distributed generation in European and North American networks. The IEEE grids, which are mainly medium voltage grids [94] originally constructed to test power flow solution software, but nowadays also commonly used in distributed generation and renewable energy research. Other, less widespread benchmark grids are: SimBench [71], the European Representative Networks [67], and ATLANTIDE [79] which all are based on European grids. [91] gives an overview of benchmark grids, also including other regions, e.g. Australia (Ausgrid) or the USA (PNNL, EPRI Feeders).

This case study, however, does not use a benchmark grid. Instead, the voltage controller designs, presented in Chapter 3, will be tested on a section of a Stedin medium voltage grid, in order to specifically demonstrate, how the considered control policies act in the company's network. The reason only a smaller section of the grid is considered is the fact that the actual
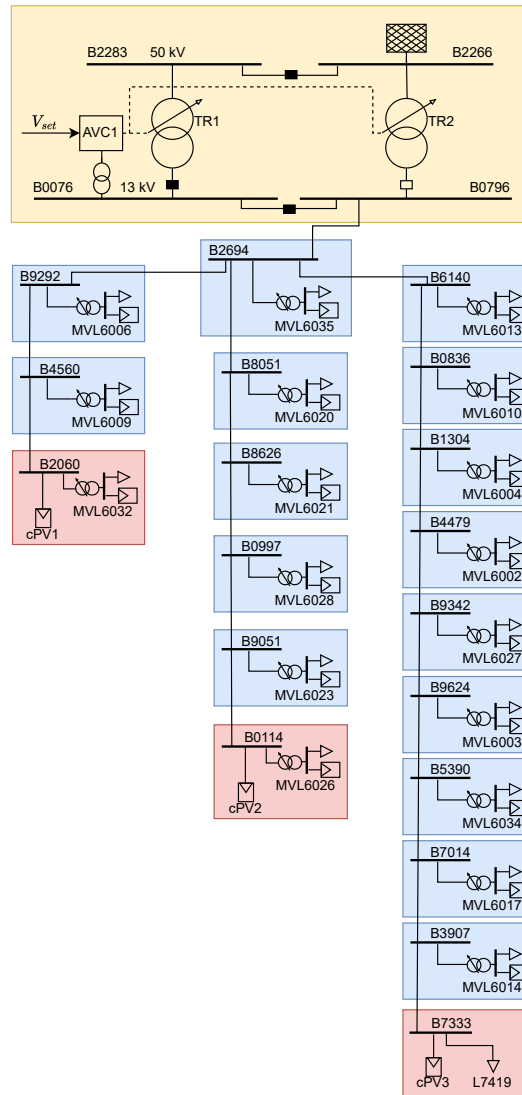
Figure 4-1: Single Line Diagram of the Studied Grid

grid is quite large (315 medium voltage nodes), which would make the initial debugging, tuning, and evaluation of control policies much harder and more complex.

The single-line diagram of the studied grid is shown in Figure 4-1. It is a balanced three-phase grid with a nominal frequency of 50 Hz. All generators and consumers are assumed to be balanced, and the grid frequency is assumed to be nominal during all simulations. It can be seen that 19 secondary substations connect to the primary substation in a radial pattern, which reflects the real meshed network's radial operation. The primary substation features two high-voltage (50 kV line-to-line) and two medium-voltage (13 kV line-to-line) buses. The 50 kV buses are connected to an external high-voltage transmission grid. This station is fitted with two transformers, out of which only one supplies power at a time, the other is kept on a hot standby with its primary energized, as the diagram's breaker configuration shows. In case the actively used transformer fails, the other could take over right away, however, these situations are not considered in this study. Both transformers are equipped with On-Load

Tap Changer (OLTC) mechanisms which are controlled with the same Automatic Voltage Control (AVC) relay, that intends to keep the voltage magnitude of B0076 (V_{meas}) as close to its V_{set} setpoint as possible. The secondary substations feature connections to low-voltage customers, which have a lumped representation consisting of a transformer with an off-load tap changer, and lumped load and photovoltaic (PV) elements, which can be modeled as single medium-voltage load (MV-load) elements in simulation software for simplicity. These represent the consumers and household solar generation, connected at the low-voltage, more specifically 400 V line-to-line voltage level. The low-voltage nominal consumption values lie in a range of 0.086 to 0.576 MW and nominal household generation values are between 0 and 0.1 MW. These low-voltage connections are assumed to be entirely uncontrollable, the household PV plants all feed in at a unity power factor, and the households consume at a fixed power factor (close to unity) according to the corresponding generation and load profiles. Three secondary substations, with B2061, B0114, and B7333 also feature connections to larger curtailable PV plants, named cPV1, cPV2, and cPV3 respectively. These all have a nominal power of 0.7 MW and feed directly into the medium voltage grid at a unity power factor. Originally the selected grid section did not contain such plants, but other parts of the large grid did, so these were added here to better illustrate problems caused by the presence of excessive solar generation. The nominal power of these plants was selected such that their presence still does not cause any cable overloads, i.e. all cable loadings stayed below 60% during normal operation, as they should according to company policies. At the time of writing this thesis, Stedin does not have centralized remote control capability over these large PV plants but plans to install it in the near future. The buses are interconnected with underground cables, that have high R/X ratios, making nodal voltage magnitudes insensitive to reactive power flow. All 19 of medium-voltage buses will be monitored during the voltage control studies. The voltage of the 50 kV buses is excluded from the set of monitored voltages, as they cannot be influenced from this grid section, due to the stiffness of the external high voltage grid. The control actions to influence voltage in this studied grid are the switching of the OLTC on TR1, the adjustment of V_{set} and the curtailment of cPV1, cPV2, and cPV3. Details of the studied grid, including nominal voltages, nominal powers, power factors, transformer, cable, and external grid data can all be found in Appendix A of this report.

4-2   Simulation Framework Used

The case study conducted in this MSc project is based on numerical simulations. In order to obtain results, i.e. test the proposed controllers' effect on the studied grid's slow voltage dynamics, a co-simulation framework was created using Python and DIgSILENT PowerFactory. This section first gives a brief description of the necessary software tools, namely DIgSILENT PowerFactory, Python, and the Pyomo package. After the necessary software is described, their interconnection, data exchange, and the working principle of the main simulation script are presented here.

DIgSILENT PowerFactory (in the following "PowerFactory") is an all-purpose power system simulation and analysis software that is widely used in both research and industrial projects. This is a commercial software developed by DIgSILENT GmbH. in Gomaringen Germany, and is currently used in 170+ countries all around the world [28]. PowerFactory is popular in simulation-based model predictive voltage control studies [64, 6, 78, 38] as the software of-

fers a wide range of different time-domain simulation tools (electromagnetic transients, RMS simulations, quasi-dynamic simulations) and interfaces towards other software. Power Factory features its own dynamic modeling framework [23] and a scripting language called the DIgSILENT Programming Language (DPL) [24, 22]. Besides time domain simulations PowerFactory also offers other functions such as short circuit and optimal power flow calculation, economic dispatch, contingency analysis, etc. Many interfaces exist towards other software [58, 97], however the most important of these is the application programming interface (API) to the Python programming language [90, 25, 27, 22]. This API makes changing grid parameters, starting calculations, and retrieving their results very easy, which are all necessary for the MPC-based voltage control simulations. The features of PowerFactory which will be utilized in this study are, power-flow equation solution using the Newton-Raphson method, sensitivity matrix calculation, and the software's Python API.

Python is a general-purpose programming language, which is used to construct the main simulation script. This handles all other software, namely PowerFactory, and the optimization solvers necessary to perform the cost function minimization of the MPC policies. Pyomo [1] is an open-source optimization modeling package for Python, with well-documented usage in the academic literature under [47, 16]. Many projects that need optimization problem modeling in energy/power engineering use Pyomo, examples according to the package's website [1] are: the Dispa-SET model [55], the Open Energy Modelling Framework [50], the Minpower toolkit [44], PowerGAMA [99], etc. Pyomo in itself only acts as a solver-agnostic interface between Python and low-level optimization solvers (e.g. GLPK, Ipopt, Gurobi, Baron, etc.), which have to be installed separately. The MPC policies in this study require the solution of Mixed Integer Quadratic Programming (MIQP) problems, for which Pyomo's mixed-integer nonlinear decomposition toolbox, MindtPy [11] will be used. This toolbox is able to decompose Mixed Integer Nonlinear Programming (MINLP) problem into Mixed Integer Linear Programming (MILP) and Nonlinear Programming (NLP) subproblems, which are solved by the low-level solvers GLPK [65] and Ipopt [105] respectively. The Quadratic Programming (QP) problems are solved using Ipopt only.

In order to simulate the studied grid's slow voltage dynamics, the simulation model has to capture the network's reaction to changes in load and generation profiles, the external grid connection's voltage fluctuation, and the dynamic behavior of the slowest voltage control device in the network: the AVC relay of TR1. The simulation is similar to a quasi-dynamic simulation in the sense that the grid is always assumed to be at a steady state, and its response to control actions (OLTC switching and PV curtailment) and changes in profile data are calculated by solving the (three phase balanced) power flow equations. The simulation is different from a quasi-dynamic study in the sense, that the dynamic behavior of the AVC relay is captured with the help of the differential equations previously given in Equation 2-11 and Equation 2-12 in Chapter 2. This way, the simulations capture slow voltage dynamics more accurately compared to a simple quasi-dynamic study, without the necessity to model and capture faster phenomena (e.g. electromagnetic transients, or the relatively fast dynamic response of inverters) which would not add extra insight but would increase the computational demands of the simulation.

The designed co-simulation framework is based on the interaction of different software tools. The data exchange between PowerFactory and Python is visualized in Figure 4-2, and it can be seen, that data is exchanged between the programs with the help of the DIgSILENT Python API. PowerFactory is responsible for storing the structure of the studied grid, and it also
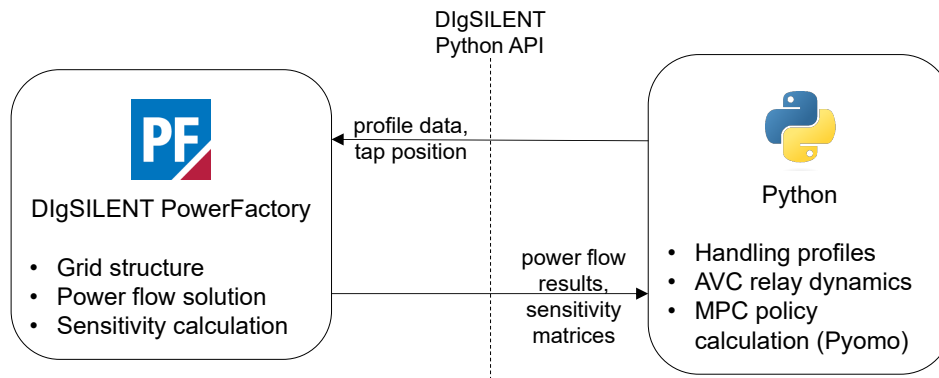
Figure 4-2: Illustration of the PowerFactory-Python Co-Simulation Framework

acts as a calculation engine responsible for solving the power flow equations and calculating sensitivity matrices. The Python scripts are responsible for handling (load, generation, slack bus voltage magnitude) profile data, they simulate the inner dynamics of the AVC relay, and they perform the cost function minimization. This last task requires the solution of a MIQP problem, which is formulated in Pyomo, decomposed with Mindtyp, and solved using two low-level solvers: GLPK and Ipopt. As far as the exchanged data is concerned, the Python scripts send profile data and the set tap positions to PowerFactory. The power injection of curtailable PV plants is sent to PowerFactory based on their possible generation profile and the allowed maximum power set by controllers. The results of power flow calculations, and the obtained sensitivity matrices are sent back to the Python scripts. The data transfer is always initiated by the simulation's main Python script, as well as power flow and sensitivity calculations.

The whole simulation framework is governed by one main Python script, for which a flowchart is shown in Figure 4-3. The program simulates the studied grid's behavior with a fixed time step of 1 second. At the beginning of each time step, the script checks whether profile data has changed or a controller has adjusted something at the previous step. If yes, the re-calculation of the power flow equations is requested from PowerFactory. Once this is done, the relevant signals of the current time step are stored, and if in use, the AVC relay's state is advanced (with the help of numerically integrating, the corresponding differential equations using the Forward Euler method with the fixed 1 second time step). If the AVC relay triggered a tap change after its state update, the new tap position is sent to PowerFactory, and the Control Event flag is set, to initiate a power-flow re-calculation at the next time step. If the current simulation time step is a sampling time of a voltage control policy (MPC-based, Current Compounding (CC), or CC with Active Power Curtailment (APC)), then the relevant control actions are calculated. For CC and the CCAPC, schemes the actions can be calculated right away knowing the previously stored grid state signals. In case of MPC-based policies, PowerFactory is firstly requested to calculate the relevant sensitivity matrices in the current grid state. After that, the cost function minimization is done with the help of Pyomo. In case a high-level voltage control scheme has acted on the grid, the Control Event flag is set, to trigger a power-flow re-calculation at the beginning of the next time step. The simulation script then moves on to the next simulated time step. The set Control Event flag is cleared in the next time step after solving the power flow equations and updating the relevant signals.
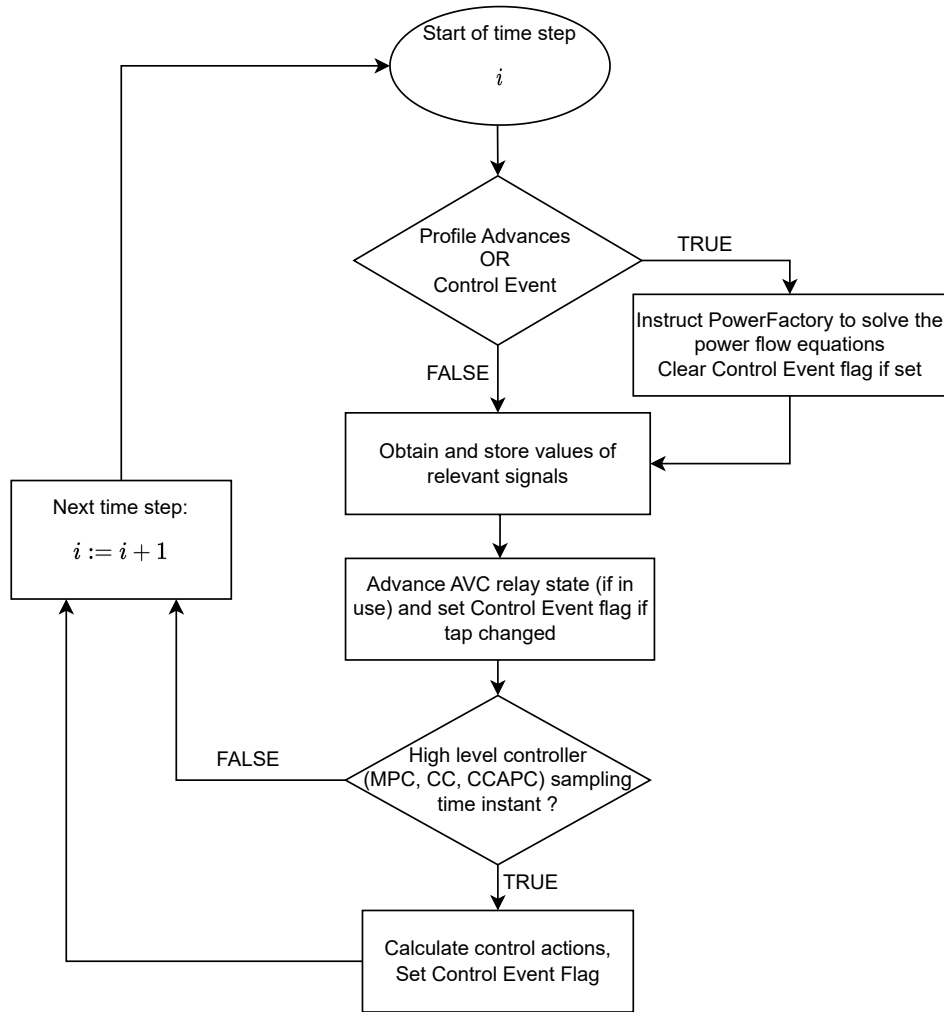
Figure 4-3: Flowchart of the Simulation's Main Python Script

The simulations were conducted using PowerFactory version 2022 SP1 (x64), Python 3.10.9, Pyomo 6.5.0, GLPK 5.0, and Ipopt 3.11.1. The scripts were run on a standard Stedin company laptop with a 1.90 GHz Intel Core i5 CPU and 16GB of RAM.

4-3   Profile Data and Test Cases

This section presents how the load, generation, and external grid voltage magnitude profile data was obtained for the simulations and what type of test cases were constructed from it. Firstly it is shown, how profiles available with low (hourly) temporal resolution were interpolated using a method found in the literature. Then, the four test cases are presented, in which the performance of different voltage controllers is evaluated and compared.

4-3-1 Enhancing Profile Data with Super Resolution General Adversarial Networks

Load and PV generation profiles of low-voltage customers were only available in the form of hourly samples. To make the simulated test cases more realistic, the temporal resolution of this data had to be increased. Many works in the literature only use simple linear or spline interpolation to perform this task [4], however, this study will use a more sophisticated method found under [100]. The authors of [100] use a Super Resolution General Adversarial Network (SRGAN) to increase the temporal resolution of load and generation profiles to 5 minutes. The sampling time of the input data can either be 1 hour or 30, minutes, which makes this method very suitable for this study, as the low-resolution data, in this case, is also available with 1 hour sampling time.

SRGAN is a machine learning tool in which two neural networks are used: the generator is a network used for increasing the resolution (interpolation) of low-resolution data, and the discriminator is a network that tells whether a data set is originally a high resolution or was interpolated. The authors of [100] trained their SRGAN PV and load data collected from 2925 Australian households during the whole year of 2017. They implemented their SRGAN framework in Python 3.6.10 using TensorFlow 1.9.0 and Keras 2.2.4. The trained models were freely published with encouragement for usage in further research works. For this reason, the trained generators found in this publication were used in this MSc project to increase the temporal resolution of low voltage PV and load profiles. Test results with Stedin measurements are visualized in Figure 4-4.
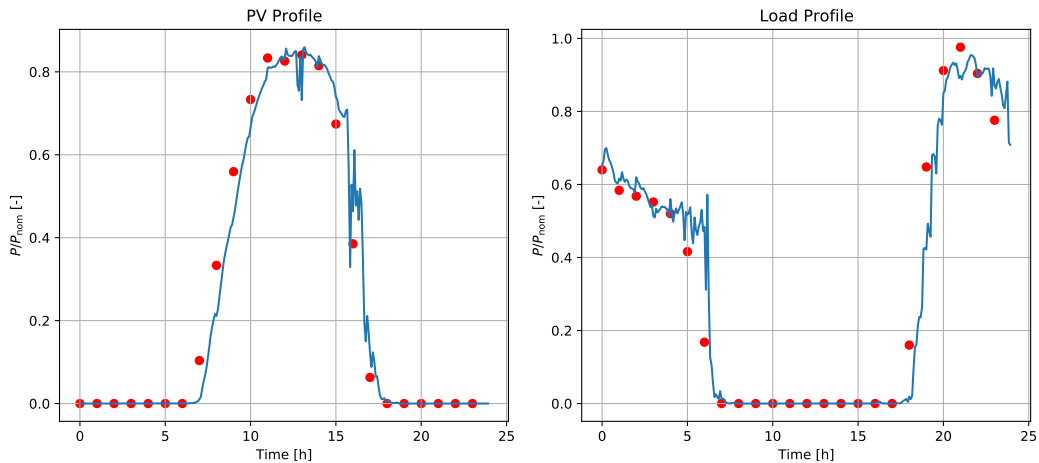
Figure 4-4: Testing the SRGAN Profile Interpolation on Normalized Stedin Measurements

Figure 4-4 shows the results of the SRGAN interpolation method of [100] applied to hourly PV and load profiles of low-voltage Stedin customers. The hourly measurements are shown with red dots and the interpolated data is visualized with blue lines. Both profiles were captured during different summer days. The generator of the SRGAN only takes normalized measurements, so before interpolation, the profile data was divided with the nominal (maximum) values of said profiles. This normalized data is shown in the figure, and to be used in the simulation, the interpolated profiles have to be multiplied by the nominal powers again. It can be seen, that the interpolated data matches with the red points quite well, and produces

realistic intersample fluctuations. The reason for the red dots not exactly matching the blue lines is the fact that the SRGAN-based interpolation method treats incoming profile data as hourly averages, not as measurements captured at the exact data point. To the best knowledge of this MSc project's author, this is the first time the work in [100] is applied in order to increase the temporal resolution of profile data in an MPC-based voltage control study. The case study presented in this chapter alongside the added novelty of this interpolation method is the third contribution of this MSc project, as it was also listed in Chapter 1 of this report.

4-3-2   The Test Cases

This study simulated all considered voltage control policies in 4 test cases. Each test case is a different 24-hour time interval, in which the controllers are subjected to different operational conditions. The test cases are listed in the following:

- **Summer:** A typical summer day with extensive solar generation and light loading (low consumption), especially in the hours around noon. The grid is likely to experience overvoltage problems, and power flow reversals (supplying back to the high-voltage external grid). Due to a lot of production, PV energy is not that expensive, therefore curtailment of solar plants is acceptable to some reasonable extent.

- **Winter:** A typical winter day with low solar generation and heavier loading. Remote regions of the grid are more likely to experience undervoltage events. Only a small amount of PV energy is produced during a short period of the day, and these small active power injections actually help with keeping smooth voltage profiles in the network. PV energy is worth a lot at the market due to scarcity, so active power curtailment of PV plants should be avoided if possible.

- **Summer Slovervolt:** The same profile data is used as with the Summer test case, except for the external grid's voltage magnitudes. Voltages at all time points in this profile were increased by 0.03 pu, causing overvoltage events, which cause the primary substation transformer's OLTC mechanism to hit its limit position. During these times, the only control action against overvoltage events is the curtailment of PV plants, which means that mitigation of said events is a harder challenge for the controllers.

- **Summer Cpvout:** The same profile data is used as with the Summer test case, except for curtailable PV plants cPV1 and cPV2. In this test case, these plants don't export any power at all, due to e.g. maintenance. This test case shows how the CC and CC with APC schemes might get confused as the voltage setpoint adjustment and therefore indirectly TR1's OLTC position were tuned to the power flows of normal operation.

It can be seen that the Summer and Winter test cases correspond to normal operation, and Summer Slovervolt and Summer Cpvout correspond to unusual operation of the grid. The summer and winter profile data is based on real Stedin measurements: As detailed in the previous subsection the generation and load profiles of low-voltage customers were available with hourly resolution and interpolated to a 5 minute sampling time. The voltage profiles of the external high-voltage grid connection's voltage magnitude were available with a 1 minute sampling time. For the three curtailable PV plants, the profiles were created based

on measurements collected at a large PV park that connects to the Stedin grids. This data was also available with 1 minute temporal resolution. Different summer and winter days were selected for the cPV plants, and the data was scaled to match the appropriate nominal power levels. This means, that the profile data used in the simulations has either 1 minute or 5 minute temporal resolution. The detailed plots of the summer and winter day profiles used are given in Appendix B of this report.

4-4   Base Cases and Uncoordinated Controller Results

In the so-called base cases, no high-level voltage control scheme acted on the studied grid, only the AVC relay that switched the primary substation transformer's OLTC, using only the local voltage magnitude measurement of Bus 0076. The metrics for the four simulated base cases are shown in Table 4-1. As expected, the p_{cur} relative curtailment values are all zero as this control action is not used in this case, and the N_{tc} total tap change numbers are similar, because at bus 0076 of the primary substation, the only strongly felt disturbance is the fluctuation of the external grid's voltage.

Table 4-1: Calculated Metrics for the Base Cases (Simple AVC Relay Only)

Test Case	V_{RMSE} pu	A_{viol} pu·s	p_{cur} %	N_{tc} taps
Summer	0.013379	537.586	0.000	26
Winter	0.009001	3.061	0.000	23
Summer Slovervolt	0.013316	515.569	0.000	26
Summer Cpvout	0.009054	20.827	0.000	26

By observing the metrics, it can be seen that the Summer and Summer Slovervolt test cases feature larger voltage limit violation areas. These are mainly overvoltage violations caused by excessive PV generation. The nodal voltage profiles for the Summer test case shown in Figure 4-5, also confirm this fact. It can be seen that the remotely positioned buses' voltage magnitudes become considerably higher during hours when solar generation is at its peak. Only the primary substation's medium voltage buses stay closer to nominal (yellow line of bus 0076 on Figure 4-5 also overlapping a similar blue line of bus 0796) as these are regulated by the AVC relay. Since the Summer and Summer Slovervolt test cases both result in less flat voltage profiles for the majority of the studied grid's nodes, these will have the highest V_{RMSE} values. The solid red line way above the upper voltage limit is the voltage profile of bus 2266, i.e. the location of the external 50 kV connection. This line overlaps the very similar profile of bus 2283, the network's other 50kV bus. The voltage magnitude of these two high voltage buses is uncontrollable due to the large stiffness of the external grid, i.e. only the network's medium voltage buses are controlled, and consequently, only these buses' voltages are included in the V_{RMSE} and A_{viol} metrics.

By observing the results for the Winter and the Summer Cpvout test cases in Table 4-1, it can be seen, that in case less PV power is injected into the grid, the voltage RMSE and violation area values improve. This confirms the fact that the large installed PV capacity is responsible for voltage issues. By observing the voltage profiles for the Winter test case shown in Figure 4-6, it can be seen that the voltages are smoothest and closest to nominal in the time range
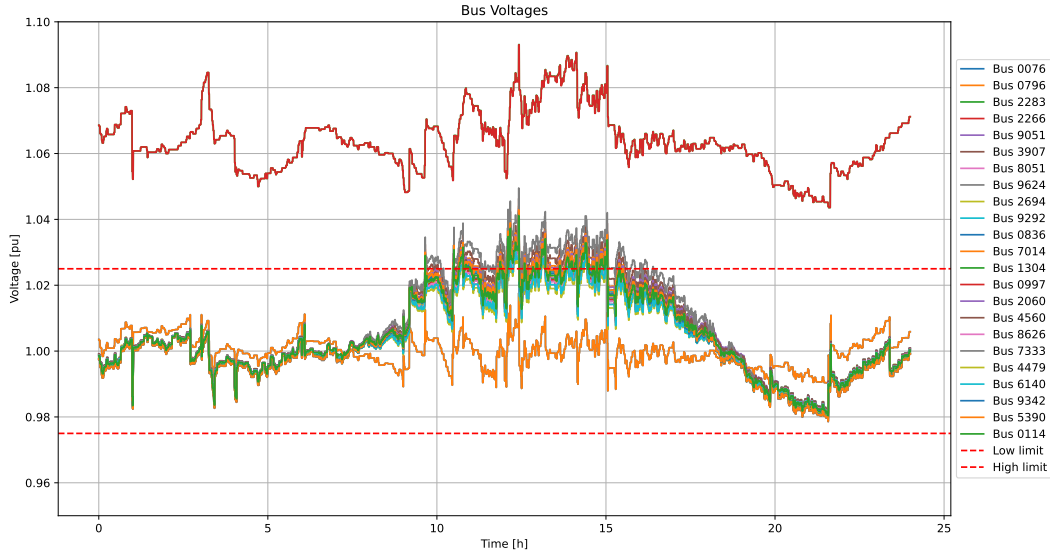
Figure 4-5: Simulated Voltage Profiles for the Base Summer Day Test Case (Simple AVC Relay Only)

between 10 and 14 hours, i.e. during the times when solar plants were able to export some energy, but way below their nominal power, due to bad weather conditions. This illustrates that the presence of Distributed Generation (DG) could actually help with improving voltage profiles to some extent. Besides the high price of PV energy due to scarcity during the winter, this improvement in voltage profiles is also a strong reason to avoid curtailment during the Winter test case if possible. Contrary to the Summer profiles, it can be seen in the graph that the regulated bus 0076's voltage is higher than the rest of the medium-voltage buses in the network, which is due to the high loading, and the resulting voltage drops. The limit violations during the winter day are low limit violations, caused by high loading and fluctuations of the external grid's voltage.

It has to be noted that the external grid's voltage profile is above nominal for the entire winter and summer day, as it can be seen in Figure 4-5 and Figure 4-6. This is likely caused by the large wind park which connects to the high-voltage grid very close to the medium-voltage grid's external connection point. Wind power production does not have a strong daily fluctuation trend like PV, and is able to raise voltages locally, also during the night and other times when there is little sunshine (e.g. winter days).

In order to mitigate overvoltage issues during excessive generation, and improve voltage drops during heavy loads, CC and its combination with local APC for PV plants was implemented. The CC scheme operates at the primary substation with a $T_{\text{s,CC}} = 4$ minutes and the local APCs with $T_{\text{s,APC}} = 10$ s sampling times. Other tuning parameters are given in Appendix C. Similarly to the base cases, the performance metrics of the MPC schemes can also be compared with these results. The calculated metrics for CC and CCAPC are given in Table 4-2.

Compared to the base cases, the V_{RMSE} and A_{viol} metrics improve with both control schemes for all four test cases, when compared with the base results. This indicates that these two control schemes resulted in flatter voltage profiles and fewer limit violations, even with a large PV power injection during the Summer and Summer Slovervolt test cases. It has to be noted
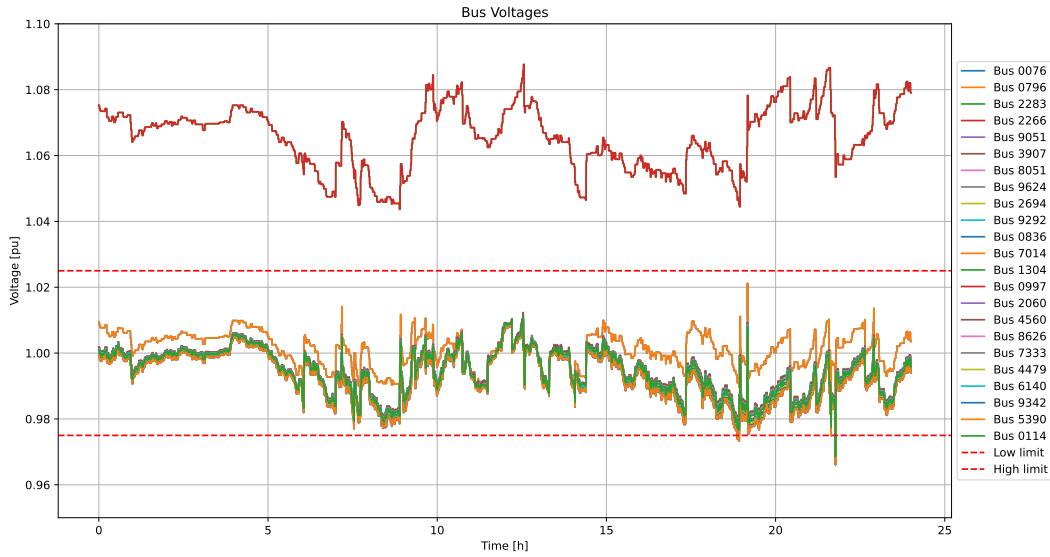
Figure 4-6: Simulated Voltage Profiles for the Base Winter Day Test Case (Simple AVC Relay Only)

Table 4-2: Calculated Metrics for Current Compounding (CC) and its Combination with Local Active Power Curtailment (CCAPC)

Test Case	CC				CCAPC			
	V_{RMSE} pu	A_{viol} pu·s	p_{cur} %	N_{tc} taps	V_{RMSE} pu	A_{viol} pu·s	p_{cur} %	N_{tc} taps
Summer	0.007438	1.118	0.000	25	0.007180	0.467	2.009	25
Winter	0.005684	0.480	0.000	30	0.005684	0.480	0.000	30
Summer Slovervolt	0.008000	2.463	0.000	21	0.007690	0.249	2.871	23
Summer Cpvout	0.007065	0.439	0.000	25	0.006978	0.007	5.596	23

that neither control scheme was capable of completely eliminating limit violations, in any of the test cases. When comparing CC and CCAPC results, it can be seen that the V_{RMSE} and A_{viol} results improved with the introduction of local APC controllers in 3 of the 4 test cases. These three test cases are the ones based on Summer profiles, where overvoltage issues dominated. Active power curtailment is only effective against overvoltage issues, moreover, this local controller type only gets activated when a PV plant's local voltage magnitude is above the V_{crit} threshold. During the Winter test case, this did not happen for any of the curtailable PV plants, so no PV curtailment was used at all, which is also indicated by the zero p_{cur} metrics for both CC and CCAPC. So, PV production is not limited with any of the two control schemes during the Winter, which is the desired behavior, due to the high price of PV energy on these days.

The highest relative curtailment value was observed during the Summer Cpvout test case, which could be explained by the fact that only cPV3 is operational during this time. Out of the three curtailable PV plants, this one is located in the weakest part of the grid, so this has

to be curtailed hardest. Even during the regular summer day, a relative curtailment of 5.646 % was needed at cPV3 (and other plants brought the total p_{cur} value down), which is similar to the Summer Slovervolt results. This means that switching off two large PV plants did not confuse the CC scheme at the primary substation, thanks to the crudeness of the chosen stairstep $V_{\mathrm{set}}\left(P_{\mathrm{prim,supp}}\right)$ function. This is further confirmed by the fact, that the number of tap changes is the same (25) for Summer and Summer Cpvout for CC and very similar (25 and 23 respectively) when local AVC is used as well.

The behavior of the CC scheme's setpoint adjustment as a function of time and active power delivery is given in Figure 4-7 for the Summer test case. It can be seen that the actual points correspond to the originally tuned stairstep function of Figure 3-4, the occasional outliers are due to the fact that the $P_{\mathrm{prim,supp}}$ active power supplied through TR1 changes faster than the 4 minute sampling time of the CC policy.
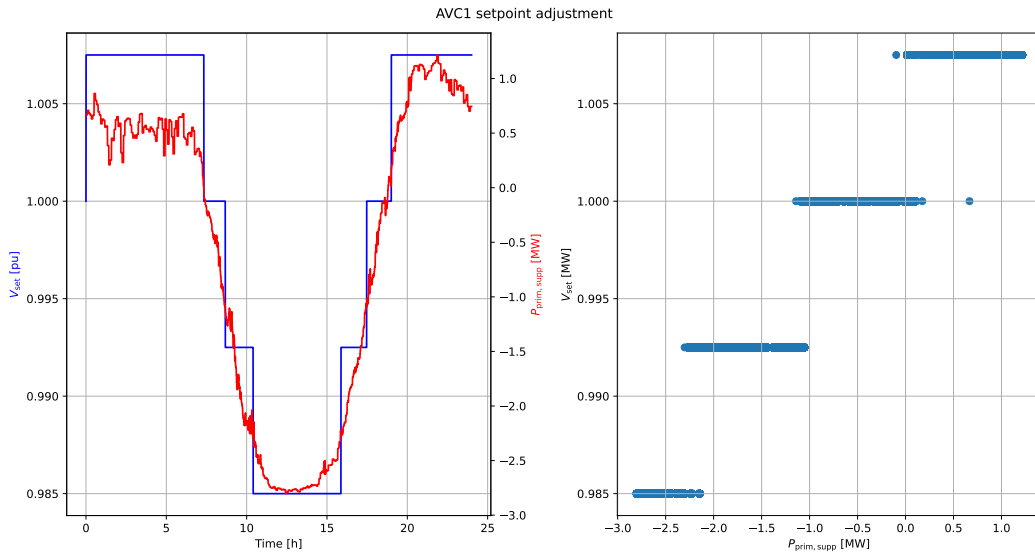
Figure 4-7: AVC Relay Setpoints in the Summer Test Case using CC

The active power curtailments of the three curtailable PV plants are visualized in Figure 4-8 during the Summer Slovervolt test case. It can be seen, that the different plants are curtailed differently, depending on how large their local voltage issue is. As cPV3 is located at the grid's weakest location, this plant has to be curtailed more drastically compared to others. Figure 4-8 also shows that the local APC schemes are able to operate without any chatters (quick overcorrections), thanks to the presence of the integrator, visualized in the block diagram of Figure 3-5.

To sum up, the CC and CCAPC schemes are both able to improve voltage profiles in all 4 test cases when compared to base data. The introduction of APC alongside a CC scheme is able to further improve voltage RMSE and limit violation metrics in the test cases based on summer data. In the Winter case, APC controllers do not affect performance as curtailment is avoided during these days, as desired. Neither CC nor its combination with local APC was able to completely eliminate voltage limit violations in any of the simulated test cases.

Figure 4-8: Curtailment of PV Plants in the Summer Slovervolt Test Case using CCAPC

4-5 Results with Simple MPC: Justification of Integer Taps and Conditional Curtailment

The simple MPC policy does not know anything ahead of future disturbances and does not use conditional curtailment. The $T_{\text{s,MPC}}$ sampling time of the simple and conditional curtailment policy is selected to be 4 minutes in order to only coincide with every fourth change of both the 1 minute and 5 minute sampling time profiles in the s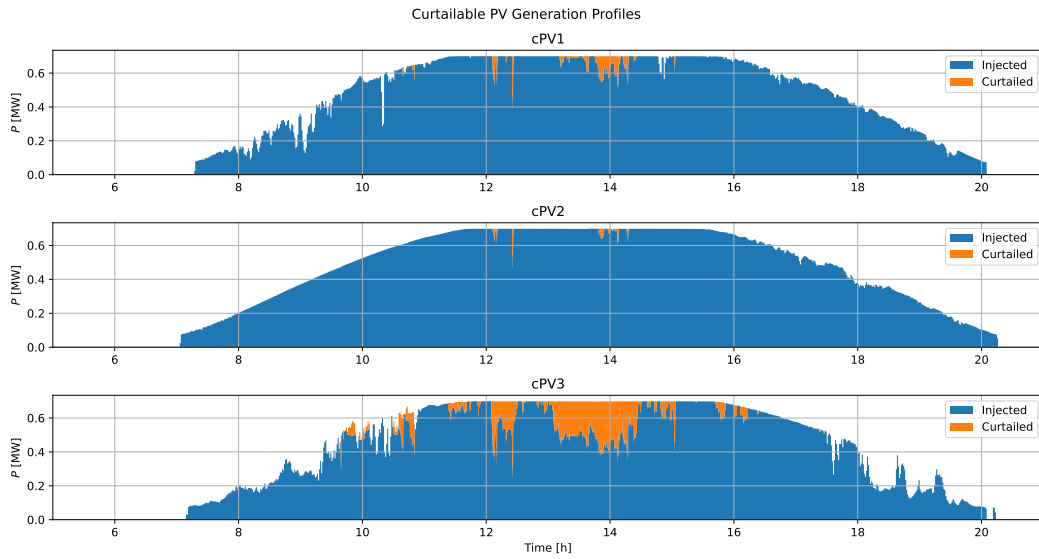imulations, thus making them more realistic due to the presence of intersample phenomena. The rest of the tuning parameters used in the simulations for this policy are given in Appendix C.

The results with this simple MPC policy, both using integer and continuous tap positions are given in Table 4-3. By observing these results it can be stated, that the continuous tap position representation results in lower maximum computation times in all four test cases, due to only having to solve a QP problem instead of a MIQP problem, at each sampling time instant of the simple MPC policy. On the other hand, the largest computation time of 2.125 seconds in the Winter test case with integer taps is still way below the 4 minute sampling time of the control policy. By looking at the N_{tc} total number of tap changes, it can be seen, that the integer tap representation results in more tap changes for all four test cases. This phenomenon could be explained by the fact that the optimal continuous tap positions are values that get rounded back to the original tap value, which effectively results in not enough tap changes being carried out. With the integer tap positions, the optimizer is aware of this discreteness and selects the right position. This is also illustrated in Figure 4-9 for the Summer Slovervolt test case, which figure also shows that the upper limit of TR1's OLTC is hit due to the external grid's overvoltage. The simple MPC scheme with integer tap positions results in better V_{RMSE} metrics when compared with its continuous tap position counterpart, in all four test cases.

In addition to worse V_{RMSE} values, the continuous tap position approximation only makes sense with the simple MPC, as only that scheme gives the opportunity to simplify the opti-

Table 4-3: Calculated Metrics for Simple MPC with Integer and Continuous Taps

Test Case	Simple MPC Integer Taps					Simple MPC Continuous Taps				
	V_{RMSE}	A_{viol}	p_{cur}	N_{tc}	$T_{\mathrm{MPC,max}}$	V_{RMSE}	A_{viol}	p_{cur}	N_{tc}	$T_{\mathrm{MPC,max}}$
	pu	pu·s	%	taps	s	pu	pu·s	%	taps	s
Summer	0.005385	6.661	2.318	54	1.906	0.005759	19.028	1.821	34	0.609
Winter	0.004199	0.300	8.890	51	2.125	0.004635	0.181	7.478	38	0.578
Summer Slovervolt	0.006070	2.469	3.332	42	2.031	0.006326	10.610	2.948	26	0.734
Summer Cpvout	0.004500	0.148	2.453	48	2.094	0.005020	0.117	2.102	34	0.453
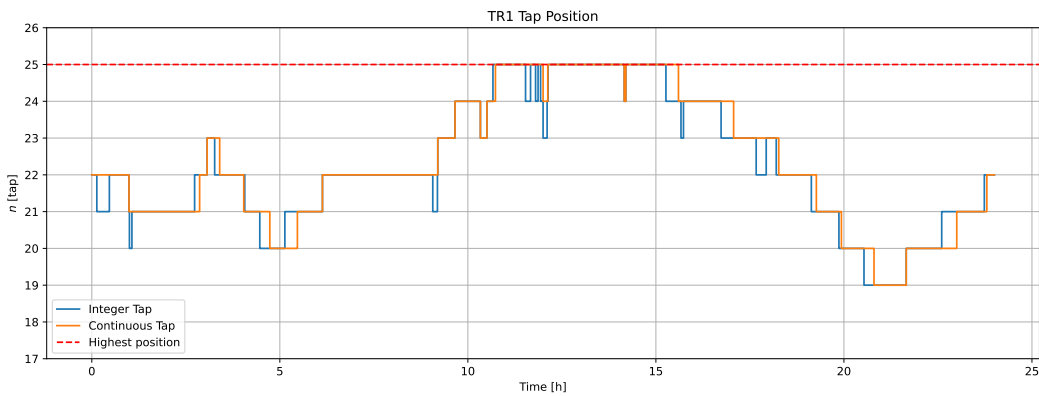
Figure 4-9: OLTC Positions of TR1 in the Summer Slovervolt Test Case using Simple MPC with Integer and Continuous Tap Positions

mization problem to be a QP. The other MPC policies in this study require the solution of MIQP problems regardless of tap position variables, due to the presence of binary variables (necessary for the curtailment logic and intersample dynamic modeling). As the usage of integer tap variables does not place the optimization problem into a simpler class with the more complex MPC schemes, all MPC results shown in the following will be obtained with integer tap positions, unless stated otherwise.

The results in Table 4-3 show high relative PV curtailments for the Winter test case (8.890 % with integer taps), which is not desired, as this would result in a lot of wasted energy, and a lot of compensation to be paid on Stedin's behalf to the PV plant operators. The reason behind these excessive losses is the intersample behavior of the simple MPC scheme, illustrated in Figure 4-10. It can be seen, that at each sampling time instant of the MPC scheme (shown with black vertical dashed lines), the controller calculates a maximum allowed power level for the PV plant that is relatively close to the possible production. The possible production of the plant increases between two sampling instances, so the realized losses are larger than intended.

To deal with the issue of intersample losses, conditional active power curtailment is used, as described in Section 3-2 of Chapter 3. Table 4-4 shows the relative curtailment values and upper limit violation areas, for four controllers: simple MPC with its regular cost function weights, simple MPC with double cost on curtailment, conditional curtailment MPC with the
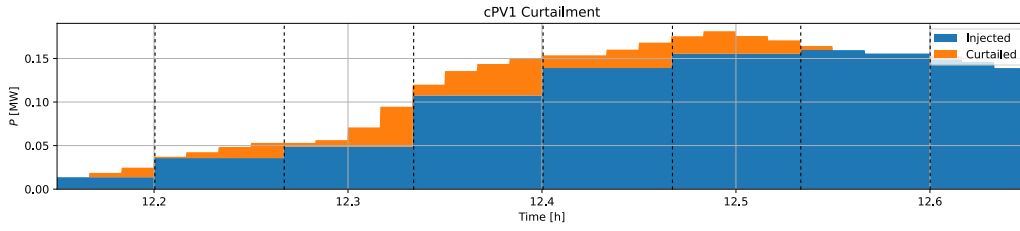
Figure 4-10: Illustration of Intersample Curtailment Losses with Simple MPC in the Winter Test Case

regular R_{cPV} weight matrix used in the curtailment cost, and conditional curtailment MPC with a halved curtailment cost.

Table 4-4: Simple MPC vs. Conditional Curtailment

Test Case	Simple MPC R_{cPV}		Simple MPC $2R_{\text{cPV}}$		Conditional Curtailment R_{cPV}		Conditional Curtailment $0.5R_{\text{cPV}}$	
	p_{cur} %	$A_{\text{viol,high}}$ pu $\cdot$ s	p_{cur} %	$A_{\text{viol,high}}$ pu $\cdot$ s	p_{cur} %	$A_{\text{viol,high}}$ pu $\cdot$ s	p_{cur} %	$A_{\text{viol,high}}$ pu $\cdot$ s
Summer	2.318	0.000	1.665	0.000	0.044	0.000	0.045	0.000
Winter	8.890	0.300	7.180	0.300	0.000	0.300	0.000	0.300
Summer Slovervolt	3.332	0.515	2.134	0.857	0.787	0.555	1.416	0.349
Summer Cpvout	2.453	0.000	1.807	0.000	0.086	0.000	0.105	0.000

The results in Table 4-4 show that doubling the curtailment's cost in simple MPC barely helps with decreasing the relative curtailment losses during the Winter test case (from 8.890 % to 7.180 %) as most energy is wasted between sampling times of the controller. Moreover doubling curtailment costs makes the simple MPC less "brave", when the usage of curtailment would be justified, e.g. during the Summer Slovervolt case. This is confirmed by the increased $A_{\text{viol,high}}$ upper limit violation area. With the usage of conditional curtailment, i.e. only allowing curtailment of a PV plant when its local voltage is above a threshold, it can be seen that the relative curtailment values improve in all 4 test cases when compared with the simple MPC. The losses with conditional curtailment are so low, that they allow cutting the cost on curtailment in half, making the control policy more brave in situations when the usage of said control action is justified. By looking at the conditional curtailment results with half curtailment cost, it can be seen, that it resulted in better upper limit violation values (with zero values during Summer and Summer Cpvout) and lower relative curtailment (with a zero value during Winter) when compared with the simple MPC. For this reason, the MPC policies whose results will be shown in the following all have the conditional curtailment logic incorporated and use the modified $R'_{\text{cPV}} = 0.5R_{\text{cPV}}$ weight matrix in the cost term that punishes active power limitation losses.

4-6   Results with Constraint and Automatic Voltage Control Relay Deadband Tightening
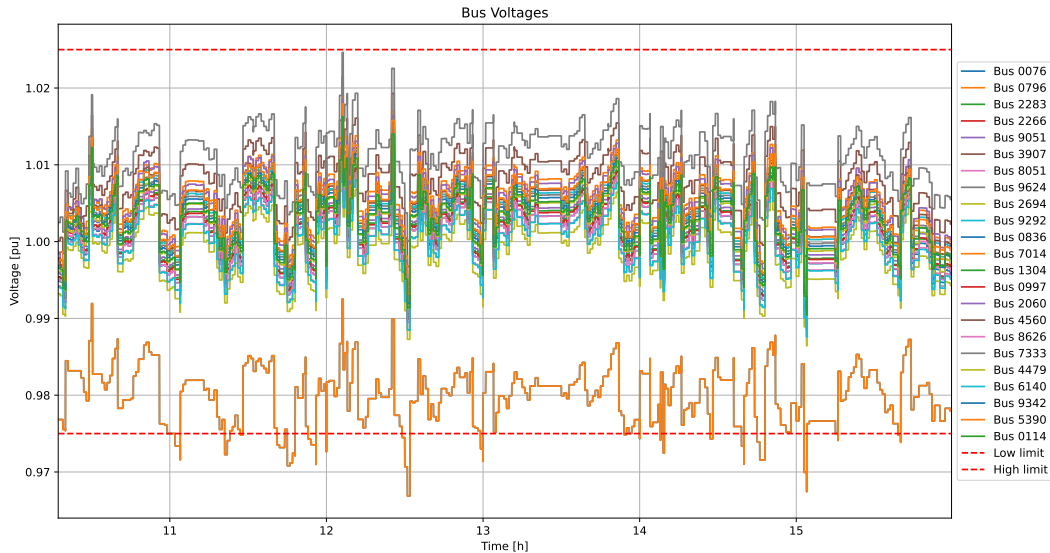

Figure 4-11: Voltage Limit Violations at Buses 0076 and 0796 during the Summer Test Case using Conditional Curtailment MPC

The results with conditional curtailment MPC still have some limit violations, e.g. a large lower limit violation area during the Summer test case (Table 4-4 only showed the higher limit violation area to be zero). By looking at the voltage profiles in Figure 4-11, it can be seen that these violations happen at the primary substation's medium voltage buses, mostly between sampling times of the MPC policy. MPC drives these buses' voltage magnitudes close to the lower limit and the disturbances (low voltage consumption, generation and external grid voltage fluctuation) the control scheme is unaware of, cause the violations. Even though these primary substation buses do not directly connect customers, the pragmatic approach of tightening the voltage limits by $V_{\text{tighten}} = 0.005$ pu and the tightening of AVC relay's deadband to $V'_{\text{db}} = 0.006$ pu were tried to improve limit violations. The weights on voltage limit violations were increased to $w'_{\text{low}} = w'_{\text{high}} = 50$ €/pu with the tightened voltage limits. These ideas are explained in more detail in Section 3-3 of Chapter 3, and the tuning parameter selection for this case study is shown in Appendix C of this report. The results are summarized in Table 4-5.

According to Table 4-5, voltage limit tightening on its own managed to improve the limit violation areas for the Summer and Summer Slovervolt test cases. On the other hand, the limit tightening also results in worse voltage RMSE values for all but the winter test case. When only the AVC relay's deadband is tightened, the V_{RMSE} metrics become better due to the AVC relay being able to perform some justified tap changes earlier that are supposed to happen between the sampling time instants of the MPC policy. The limit violation areas do not improve, as the deadband could not be made tight enough such that the AVC relay is able to react to the disturbances that caused the limit violations at the primary substation's medium-voltage buses. When limit and deadband tightening is applied at the same time,

Table 4-5: MPC Results with Voltage Constraint (Ctighten) and AVC Relay Deadband (Dbtighten) Tightening, and their Combination (Cdbtighten)

Test Case	No Tightening		Ctighten		Dbtighten		Cdbtighten	
	V_{RMSE}	A_{viol}	V_{RMSE}	A_{viol}	V_{RMSE}	A_{viol}	V_{RMSE}	A_{viol}
	pu	pu $\cdot$ s	pu	pu $\cdot$ s	pu	pu $\cdot$ s	pu	pu $\cdot$ s
Summer	0.005489	7.058	0.006005	0.866	0.005430	7.266	0.005874	0.744
Winter	0.004186	0.300	0.004186	0.300	0.004121	0.300	0.004121	0.300
Summer Slovervolt	0.006095	2.304	0.006262	0.475	0.006052	2.304	0.006197	0.338
Summer Cpvout	0.004534	0.148	0.004556	0.148	0.004460	0.352	0.004482	0.352

the V_{RMSE} results are between the values that could be obtained when the two ideas were applied separately. This combination also resulted in the best A_{viol} values for the Summer and Summer Slvoervolt test cases, and the second best A_{viol} value in the Summer Slovervolt test case. For the Winter test case, the limit violation area remained unaffected by all ideas tried here.

4-7   Results with the Incorporation of Ideal Future Knowledge

The previous two subsections focused on the achievable results and possible improvements for realistically implementable MPC policies. The results presented in this section on the other hand will focus on the best possible results that are achievable with MPC-based voltage control. The first step towards these ideal results is to increase the sampling time of the simulated MPC policy to $T_{\text{s,idMPC}} = 1$ minute from the original $T_{\text{s,MPC}} = 4$ minutes, as the sampling time of the highest resolution profile data is also 1 minute. This way, the MPC policy is able to react to the changes of disturbances almost as soon as they happen (after the 1 second time step of the simulation). The results with decreased sampling time conditional curtailment MPC policy (with no future knowledge yet) are given in Table 4-6.

Table 4-6: Conditional Curtailment MPC Results with 1 min Sampling Time and No Future Knowledge

Test Case	V_{RMSE} pu	A_{viol} pu $\cdot$ s	p_{cur} %	N_{tc} taps	$T_{\text{MPC,max}}$ s
Summer	0.005219	0.091	0.057	86	2.125
Winter	0.003831	0.014	0.000	61	2.625
Summer Slovervolt	0.005875	0.025	1.532	48	3.125
Summer Cpvout	0.004147	0.005	0.094	68	2.375

It can be seen that the MPC is able to achieve much lower limit violation areas and very good voltage RMSE values, once the control policy's sampling time is decreased. The curtailment of PV plants is also very low, however, the number of tap changes is much higher compared to any previously shown results, as the MPC tries to use the OLTC to counteract every disturbance, even if they only cause problems for brief time periods. The maximum computation times

of the policy are way below the controller's 1 minute sampling time, even in the Summer Slovervolt case, which resulted in the highest value of 3.125 seconds.

It has to be noted that, for a fair comparison, increasing the sampling time of the CC controller to 1 min in the CCAPC was also tried, however, it did not have a serious effect on the metrics of the scheme. The metrics actually got slightly worse due to some uncoordinated behavior of the CC and APC schemes, which happened as the two control scheme's sampling times were closer to each other, and the CC scheme was more sensitive to quick disturbances.

In order to further improve the metrics of the MPC policy which had the ideally fast sampling times, the MPC policy was made aware of the future fluctuations in generation and consumption in low voltage areas, as well as future changes in the external grid's voltage. In order to incorporate these future disturbances into the predicted voltages, the studied grid's voltage magnitude sensitivities to power injections from low-voltage customers and to the external grid's voltage changes also have to be calculated before solving the cost function minimization. Surprisingly the first results were worse than the ones in Table 4-6, especially in terms of total voltage limit violation areas. This could be attributed to three main reasons:

- **"Intersample Ignorance":** The phenomenon which was named here "intersample ignorance" is caused by the fact that the control actions take effect at the beginning of the MPC policy's sampling time interval, while the $\Delta V_{\mathrm{dist}}(k)$ change in disturbances only takes effect at the end of said interval (right before sampling time instant $k + 1$). In case the controller knows that large disturbances are about to take effect, it chooses actions to counteract them, which might cause limit violations before said disturbance takes effect. An example of a captured intersample ignorance phenomenon is illustrated in Figure 4-12 with annotations for easier understanding. To counteract the effect of this phenomenon, the midpoint (intersample) voltages are also modeled and subjected to voltage limits in the MPC policy's optimization problem. The accurate midpoint voltages are modeled with the help of Mixed Integer Linear (MIL) constraints and the introduction of extra continuous and binary decision variables into the problem. For more details see Section 3-4 of Chapter 3.

- **"AVC Confusion":** The phenomenon named here "AVC confusion" is basically an unwanted intersample tap change, that causes very brief limit violations, as illustrated in Figure 4-13. The cause of the unwanted tap change is a wrong V_{set} adjustment, as this setpoint is always set to the 1-step ahead predicted V_{meas} voltage to keep the relay at rest. With the incorporation of future knowledge, the predicted V_{meas} value already contains the $\Delta V_{\mathrm{dist}}(k)$ disturbance, which hasn't taken its effect at the time of the relay's setpoint adjustment. This causes a mismatch between the relay's setpoint and measured voltage, which eventually leads to the undesired tap change. To mitigate this phenomenon, the AVC relay will be deactivated, and the MPC with its increased sampling time will be the sole controller responsible for voltages in the studied grid.

- **Slightly Weak Voltage Limits:** This reason was only responsible for some very minor limit violations. To eliminate this problem, the increased violation weights of $w'_{\mathrm{low}} = w'_{\mathrm{high}} = 50$ €/pu were used, similarly to the case of voltage limit tightening.

This leads to an MPC policy with integer taps, conditional curtailment, 1 minute sampling time, knowledge of future disturbances, incorporated midpoint voltage dynamics and deactivated AVC relay, which resulted in the metrics shown in Table 4-7. The tuning parameters of
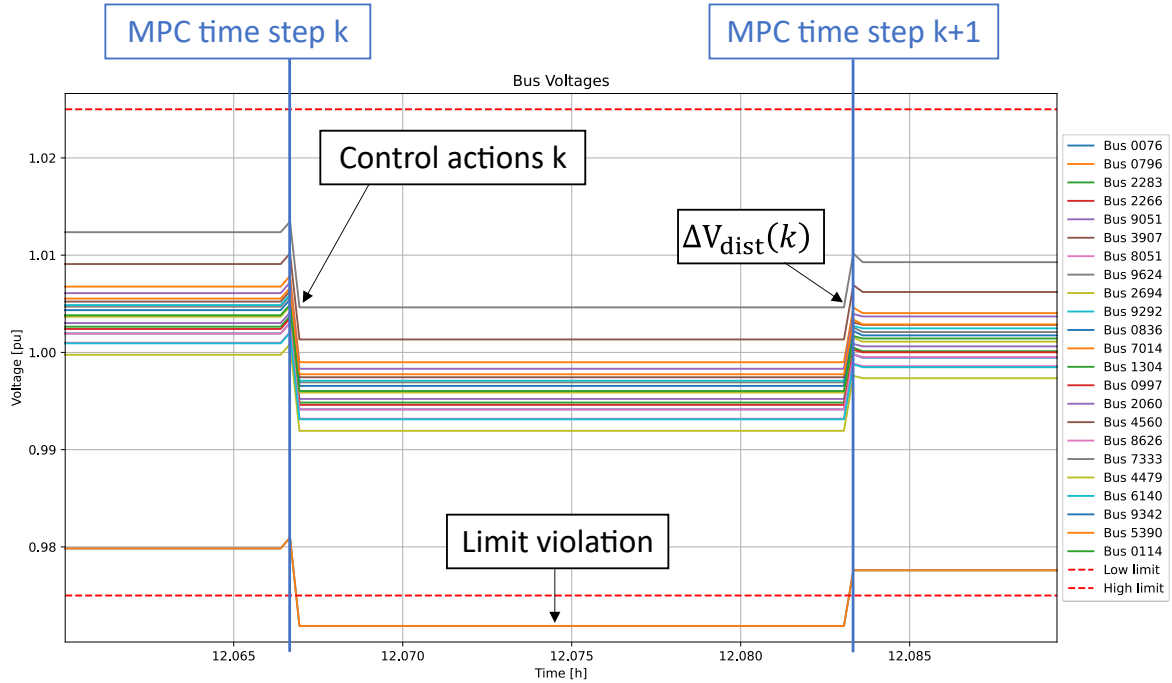
Figure 4-12: Illustration of the "Intersample Ignorance" Phenomenon, Captured during the Summer Test Case

said policy used in this case study are given in Appendix C. In terms of voltage limit violation areas, these are the best results in any of the test cases, more specifically the control policy was able to completely eliminate limit violations, except for the Summer Slovervolt case. The V_{RMSE} values are low in all four test cases, and the curtailment and tap change metrics are both acceptable. It can be seen that the incorporation of future knowledge reduced the number of tap changes, compared to the MPC with 1 minute sampling time that did not have knowledge of the future. As far as computation times are concerned, this policy resulted in the highest values so far, which could likely be attributed to the fact that extra continuous and binary decision variables had to be introduced to model midpoint voltages, which made the problem of cost function minimization larger. The longest computation time of 4.703 seconds was measured during the Summer test case; this value is still way below the 1 minute sampling time of the MPC policy.

Table 4-7: Conditional Curtailment MPC with 1 minute Sampling Time, Future Profiles, Incorporated Midpoint Dynamics, and Deactivated AVC Relay

Test Case	V_{RMSE} pu	A_{viol} pu $\cdot$ s	p_{cur} %	N_{tc} taps	$T_{\mathrm{MPC,max}}$ s
Summer	0.005421	0.000	0.375	50	4.703
Winter	0.003963	0.000	0.000	47	4.016
Summer Slovervolt	0.005984	0.159	1.452	40	4.281
Summer Cpvout	0.004307	0.000	0.165	42	4.422
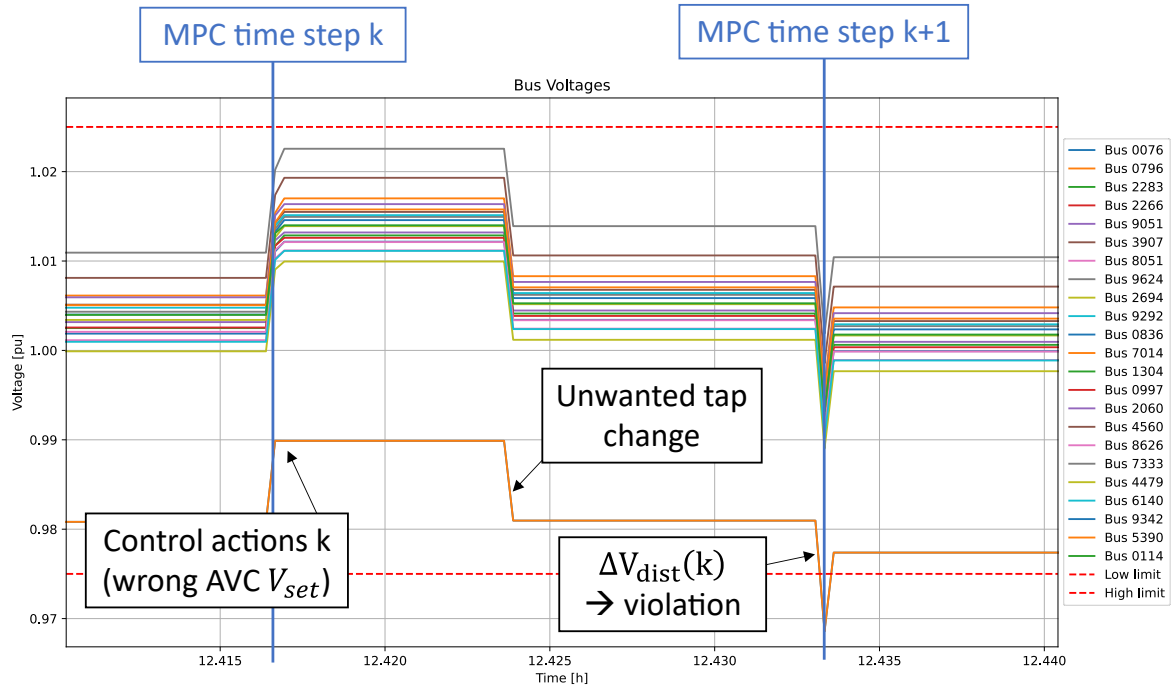
Figure 4-13: Illustration of the "AVC Confusion" Phenomenon, Captured during the Summer Test Case

This ideal assumption of knowing future disturbances over the course of the prediction horizon and incorporating them into the MPC policy also gives the opportunity to test the accuracy of the sensitivity matrix based prediction model for the grid's slow voltage dynamics. The 1 time step ahead prediction error (RMSE) was calculated for the monitored voltage magnitudes at each sampling time step of the MPC in all 4 test cases. Results are shown in Figure 4-14. For easier interpretation, the RMSE for the whole simulated interval was also calculated in all cases, Summer: 0.000299 pu, Winter: 0.000344 pu, Summer Slovervolt: 0.000420 pu, Summer Cpvout: 0.000298 pu. It can be seen that these results are all at least an order of magnitude lower than the best achievable V_{RMSE} values shown in Table 4-7. Figure 4-14 shows that even the largest voltage prediction RMSE values, which are slightly above 0.004 and only happen occasionally are lower than most V_{RMSE} values achieved by the controllers. This proves that the sensitivity matrix based model is a good choice for voltage prediction in MPC-based grid voltage control schemes.

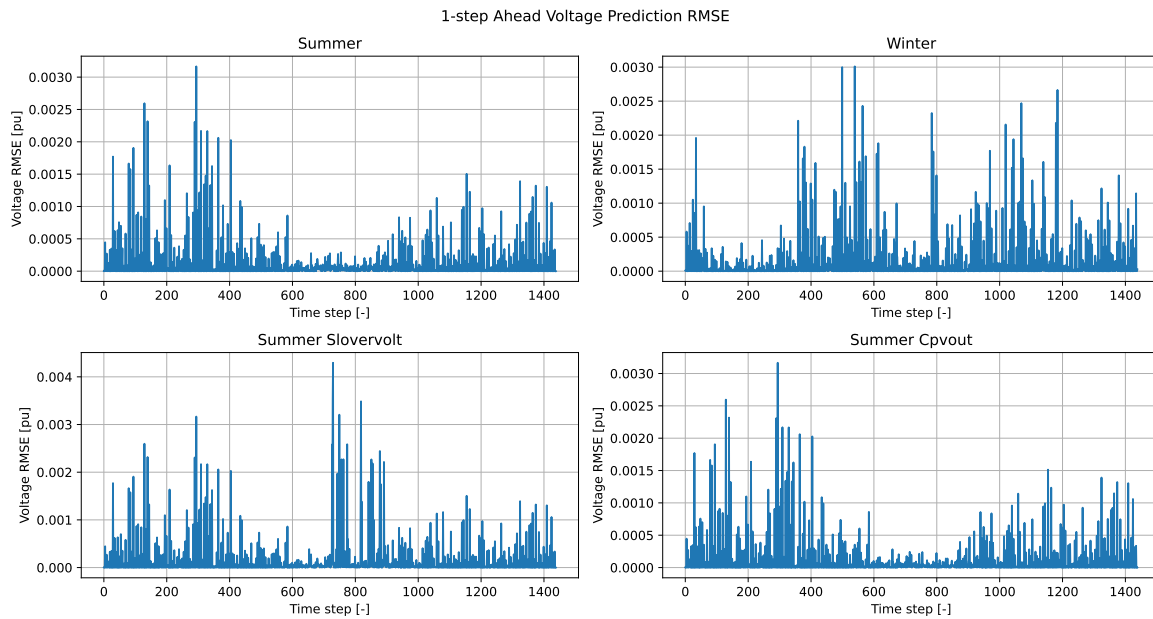**Figure 4-14:** 1-step Ahead Voltage Prediction RMSE Values of the Sensitivity Model

4-8   Comparison of Uncoordinated and Model Predictive Control Schemes

In order to better show the differences between the uncoordinated (CCAPC) and the MPC schemes, the metrics of the following 3 controller's results will be compared in this section:

- **CCAPC:** Current compounding applied at the primary substation with a 4 minutes sampling time. The three curtailable PV plants are fitted with local active power curtailment controllers, all operating with a sampling time of 10 seconds.

- **Realistic MPC:** MPC policy that uses conditional curtailment and tightened voltage constraints (half curtailment weights, 5-fold increase in voltage limit violation weights). The policy is implemented with a sampling time of 4 minutes. As its name suggests, the implementation of this policy would realistically be possible in the studied grid section, as it does not rely on ideal knowledge of future disturbances.

- **Ideal MPC:** MPC policy, that uses conditional curtailment (with the halved R'_{cPV} weight matrix), is aware of future disturbances over the course of the prediction horizon, models and limits midpoint voltages, uses voltage limit violation weights with a 5 fold increase. This policy is implemented with a sampling time of 1 minute, and the primary substation's AVC relay was turned off to avoid the previously described "AVC confusions". As its name suggests, this policy shows what are the best achievable results with an MPC policy, and the implementation of this controller in its current form, is not realistic due to its dependence on future information.

In the following, the three compared control policies are referred to as CCAPC, Realistic MPC, and Ideal MPC in this section.
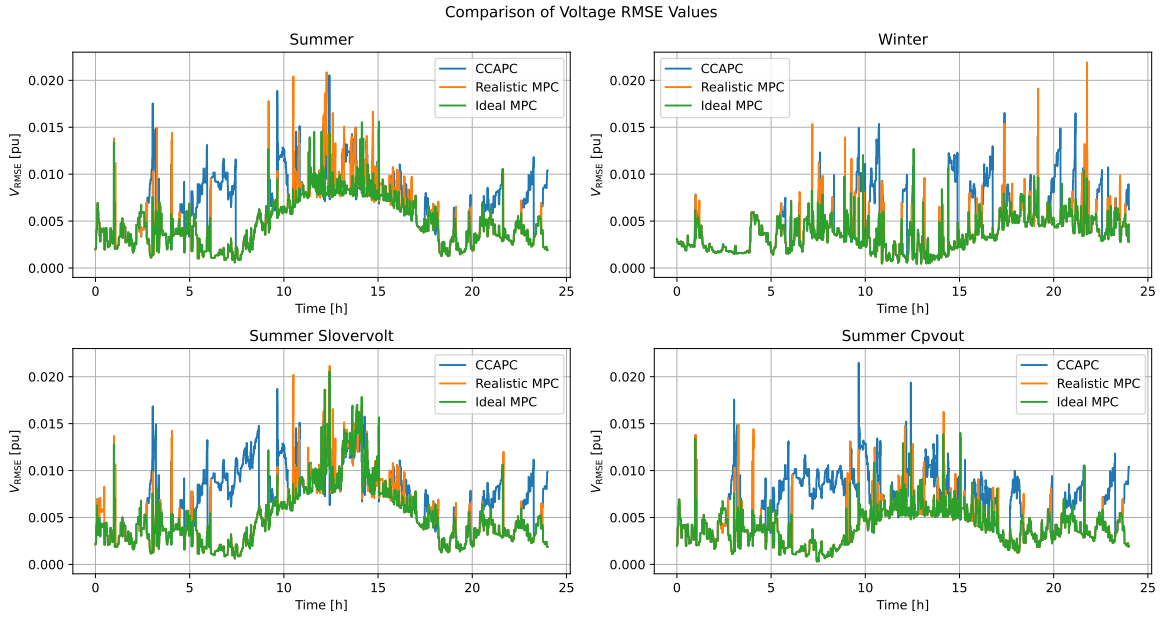
Comparison of Voltage RMSE Values

Figure 4-15: Comparison of Voltage RMSE Values as a Function of Time

Table 4-8: Comparison of Total Voltage RMSE (V_{RMSE}) Values

Test Case	CCAPC	Realistic MPC	Ideal MPC
Summer	0.007180 pu	0.006005 pu	0.005421 pu
Winter	0.005684 pu	0.004186 pu	0.003963 pu
Summer Slovervolt	0.008000 pu	0.006262 pu	0.005984 pu
Summer Cpvout	0.007065 pu	0.004556 pu	0.004307 pu

The voltage RMSE values of each control policy for each test case are shown in Figure 4-15 as a function of time. It can be seen that the CCAPC scheme gives the highest and the Ideal MPC the lowest values in all four test cases, and the Realistic MPC gives values in between. The total V_{RMSE} values calculated for the whole simulated time interval are given in Table 4-8, and these results show the same trend as the graphs. By further observing Figure 4-15, it can be seen that except for the Winter Case, the V_{RMSE} values reach their highest values around noon, due to the large solar production. The Winter case gives the lowest RMSE results around the same time, as in that case the PV generation helps improve voltage profiles. In the early morning (between 5:00 and 8:00) and evening (after 20:00) it can be seen that the CCAPC results are higher in the Summer, Summer Slovervolt and Summer Cpvout cases. Similar results can be seen for the Winter case at e.g. 15 and 20 hours. This mismatch between the CCAPC and MPC results could be explained by the crude tuning of the CC policy's stairstep function, especially for the cases when there is large consumption in the studied grid.

The A_{viol} total limit violation areas can be compared by looking at Figure 4-16. The Ideal MPC policy clearly excels in this field, as it was completely eliminates limit violations, except for the Summer Slovervolt test case, where it still managed to produce the best results. The Realistic MPC has the worst performance from this aspect in 3 of the 4 test cases with the
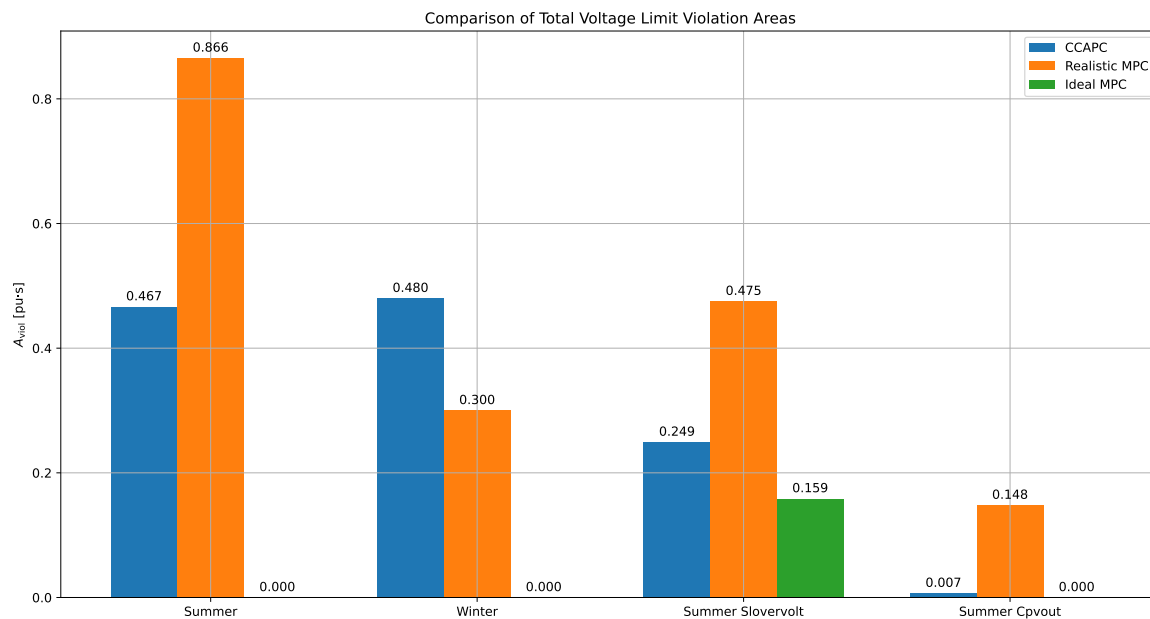
Figure 4-16: Comparison of Total Voltage Limit Violation Areas

exception being Winter. The reason behind CCAPC outperforming the Realistic MPC is the intersample limit violations which still could not be totally eliminated with the tightened voltage constraints (only reduced).

As far as control actions are concerned the comparison between the p_{cur} relative PV curtailments are shown in Figure 4-17, and the N_{tc} total number of tap changes can be compared in Figure 4-18. It can be seen, that no control policy limits PV export during the Winter test case, which is beneficial. In the other three test cases, the CCAPC always wasted more power than the two MPC schemes. During the curtailable PV outages, the MPC schemes were able to adapt to the situation, while the CCAPC just increased curtailment locally (at cPV3), hence the largest value of 5.596 %. Both MPC schemes use very little curtailment in these cases. In the Summer and Summer Slovervolt Cases, the Ideal MPC achieves less curtailment compared to the Realistic MPC. This could be attributed to smaller sampling times and knowledge of future disturbances. As far as tap changes are concerned, the MPC policies use the OLTC more (sometimes twice as much) than CCAPC in all test cases, as it can be seen in Figure 4-18. The reasons behind this are the crudeness of the CC controller's stairstep function and the cheapness of tap change actions in MPC policies. The incorporation of future knowledge seems to cut down on N_{tc} values, as shown by the values achieved with ideal MPC. While more tap switchings lead to the faster wear of the OLTC on TR1, this is forgivable, because ensuring smooth, limit violation free voltage profiles and avoiding unnecessary curtailments are more important control goals. Knowing this, it can be stated, that out of the three controllers compared here, the Ideal MPC seems to deliver the best performance.

Table 4-9 shows the maximum computation times for the two MPC policies. It can be seen, that the Ideal MPC policy takes longer to compute, due to the extra (binary and continuous) decision variables, that make the cost function minimization problem larger. It has to be
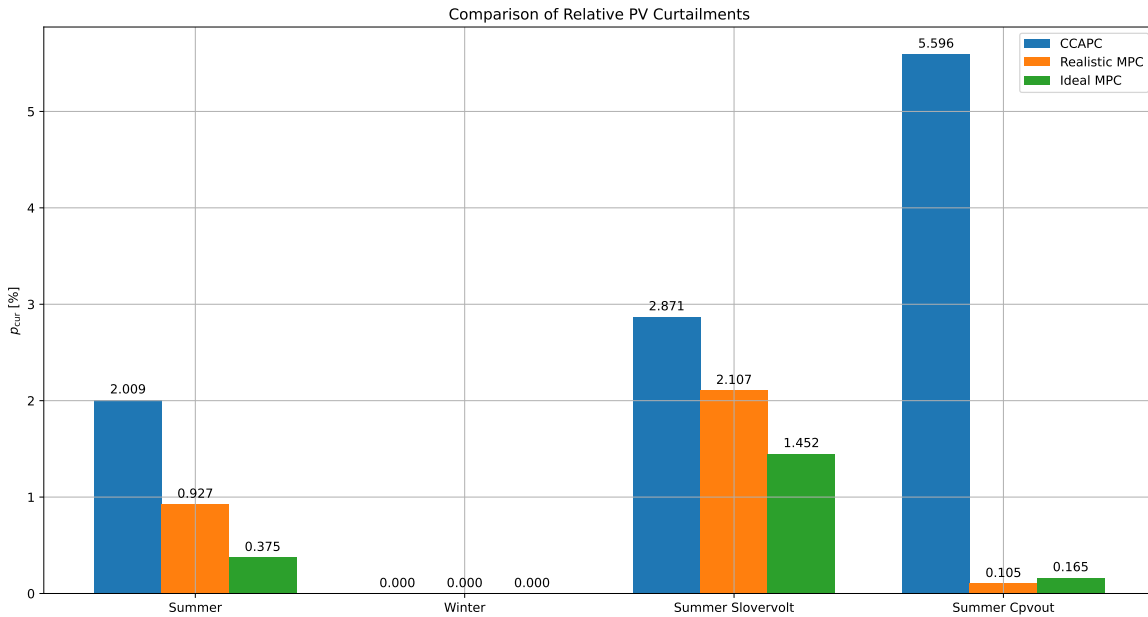
Figure 4-17: Comparison of Relative PV Curtailment Values

noted though that even the highest computation time of 4.703 seconds is way below the 1 minute sampling time of the Ideal MPC policy. So, in case good predictions of future disturbances would somehow be available, the Ideal MPC policy would be implementable for the studied grid section from a computational point of view. As this is the best-performing controller out of the 3 compared, research in the field of load, generation and voltage profile forecasting might be beneficial for grid operators (Stedin in this case). Further research could also be conducted, on how this policy scales to larger grids, as these controllers here were only designed for a small section of the actual medium voltage distribution grid of Stedin.

Table 4-9: Comparison of Maximum MPC Computation Times ($T_{\mathrm{MPC,max}}$)

Test Case	Realistic MPC	Ideal MPC
Summer	2.094 s	4.703 s
Winter	1.875 s	4.016 s
Summer Slovervolt	3.094 s	4.281 s
Summer Cpvout	2.172 s	4.422 s

The CCAPC scheme's computational times are not shown in Table 4-9 as these values are negligibly small when compared with MPC policies. For this reason, they were not measured during the simulations. Besides the advantage in computational demand, the CCAPC scheme also comes at a much lower infrastructural cost, as - contrary to centralized MPC - there is no need for the installation an extensive communication network in the electric grid.

Having the compared metrics of the three controlled schemes it can be clearly seen, that only the ideal MPC is able to deliver a performance that is objectively better than CCAPC regarding the V_{RMSE}, A_{viol} and p_{cur} performance metrics. The realistically implementable MPC (without disturbance predictions) is not able to perform better than the simple uncoordinated
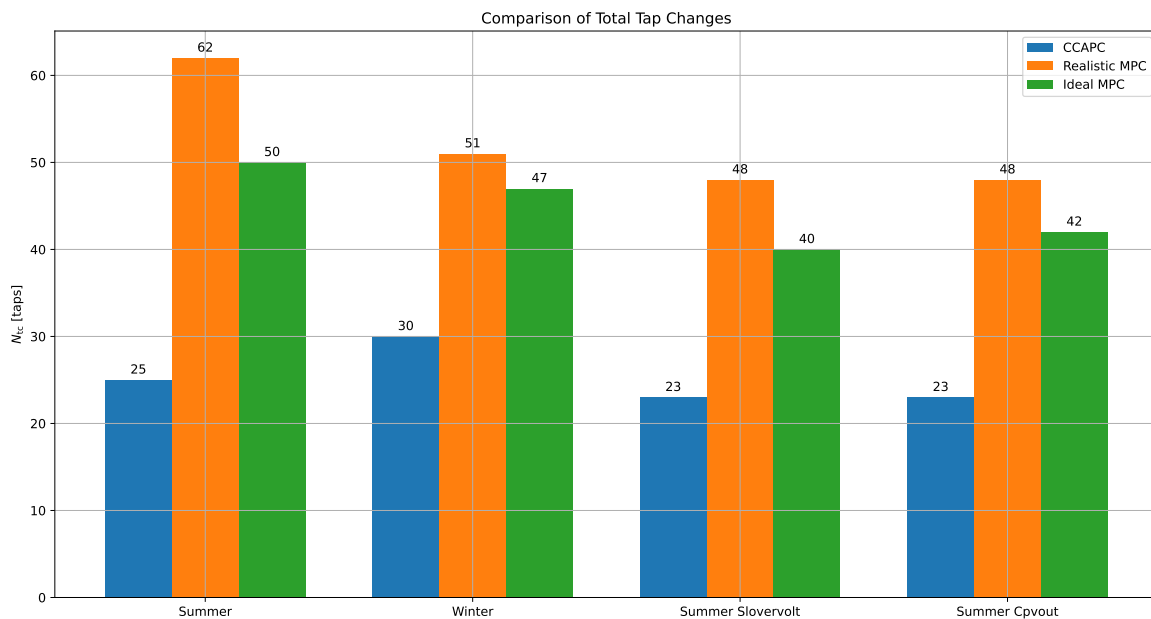
Figure 4-18: Comparison of Tap Changes

CCAPC policy regarding said performance metrics and also results in the most number of tap changes in all 4 test cases. This means that an MPC-based voltage control scheme should only be considered for the studied grid section, in case accurate forecasts are available for the disturbance quantities. Even in that case, the computational demands, extra tap changes, and infrastructural costs of deploying said policy should be assessed in more detail.

4-9   Conclusions

This chapter focused on presenting the case study that was conducted as part of the MSc project. The first three sections presented the building blocks that were necessary to conduct the simulations of the studied control policies. The rest of the chapter focused on the results achieved by the different voltage controllers that were considered in this MSc project.

The first section gave a very brief overview of academic benchmark grids, and stated, that this study uses a small section of an actual medium voltage Stedin distribution grid, in order to specifically demonstrate how the control policies would act in the company's networks. Then the most important characteristics of the studied grid were presented, including its structure, means to influence voltages, and sources of disturbances.

The second section showed the Python-Powerfactory co-simulation framework in which the simulations of this study were conducted. This simulation framework is based on the cooperation of a grid model stored in PowerFactory and several Python scripts and was created to better focus on the grid's slow voltage dynamics. The data exchange between different software, and the working principle of the simulation's main Python script were explained in detail.

The third section focused on the profile data collected for the simulations and the test cases

that were constructed using them. The profile data was based on real-life measurements. The generation and load profiles of customers in low voltage areas were only available with an hourly resolution and were interpolated to 5 minutes using a SRGAN-based method found in the literature. The four constructed test cases were: a typical summer day (Summer), a typical winter day (Winter), the typical summer day with overvoltage at the external grid connection (Summer Slovervolt), and the typical summer day with 2 out of 3 large curtailable PV plants out of operation (Summer Cpvout).

From the fourth to the eighth section of this chapter, the simulations' numerical results are presented. The fourth section contains results for the base cases (when only the central substation's AVC relay acted based on one voltage measurement) and the results for the CC and CCAPC controllers. These results were needed as the designed MPC policies need to be compared against a baseline and alternative control methods. The fifth section showed the results with simple MPC and justified the usage of integer variables in the optimization problem for tap positions, as they resulted in better performance and an acceptable increase in computational demand. The section also showed conditional PV curtailment results, more specifically how it helped with avoiding unnecessary energy waste, especially during the Winter test case. For this reason, integer tap positions and conditional curtailment were applied by default in any subsequent control policies shown. The sixth section shows the results of two ideas, that were tried to lessen the problem of intersample limit violations: the tightening of voltage constraints and the tightening of the AVC relay's deadband. The voltage limit tightening seemed to work better. The seventh section showed how ideal MPC performance could be achieved, firstly by increasing the sampling time and secondly by incorporating knowledge about future disturbances into the MPC policy. To avoid undesired intersample phenomena, intersample voltages had to be modeled and subjected to limits, and the AVC relay of TR1 had to be activated. The eight section compared CCAPC to a realistically implementable and an ideal MPC policy. Several metrics were visualized and compared. The MPC policies had better performance in terms of voltage smoothness, voltage limit violations, and relative PV curtailment. The ideal MPC demonstrated the potential gains, one could get from investing more research into forecasting algorithms on generation, load and voltage profiles. The CCAPC scheme used fewer tap changes, and it also came with the benefit of less computational and infrastructural costs.

Chapter 5

Conclusions

This chapter concludes the report, presents the most important aspects of this MSc project, and provides ideas for improving the given work during future research. The first section gives a short summary of the project. In the second section, the findings of this thesis are listed and the research questions, formulated in the first chapter's problem statement are answered. The last section lists possible directions for future research.

5-1 Summary

This project investigated the application of Model Predictive Control (MPC) to the problem of voltage regulation in active medium voltage distribution grids. The relevance of the topic could be backed by the increasing installed photovoltaic (PV) and other renewable generation capacity, which due to their smaller scale and localized nature is usually connected to distribution grids. The increased generation capacity in distribution grids causes more voltage problems with conventional voltage control schemes, so research on new control approaches is necessary. Voltage control is more challenging in electric networks that have lines with high R/X ratios, as nodal voltages mainly depend on active power flows and reactive power injection is ineffective in counteracting voltage disturbances. Underground cable networks, typical in Western European electricity distribution networks, usually have high R/X ratios. The installed PV and other renewable capacity shows a growing tendency in the Netherlands, including the networks of Stedin, a Dutch Distribution System Operator (DSO), who supported this project.

The following voltage control schemes were studied in the project: In order to compare MPC with simpler (easier to implement) schemes, Current Compounding (CC) and its combination with local Active Power Curtailment (APC) were simulated. These controllers were selected as at the time of writing this thesis, Stedin is having success using a CC policy and plans to increase the controllability of large PV plants. The planned model predictive control policies all used a quadratic cost function, with linear equality and inequality constraints. The inequality constraints came from the hard physical limitations of control actions, and the soft

limits of voltage magnitudes. Soft voltage magnitude limits were used to ensure the feasibility of the cost function minimization problem at all times. The linear equality constraints came from using the sensitivity matrix-based model for grid voltage prediction. This required the calculation of sensitivity matrices at every sampling time step of the MPC policy. The question whether the discreteness of On-Load Tap Changer (OLTC) mechanisms should be considered in the MPC policy (in the form of integer decision variables) was investigated. The application of a conditional curtailment logic (similar to local APC controllers) was tested in MPC policies, in order to avoid unnecessary wasting of valuable energy. This logic was described and incorporated in the MPC's optimization problem with the help of Mixed Integer Linear (MIL) constraints, which to the author's best knowledge was being done for the first time and therefore is one of the contributions of this MSc project. Two simple, realistically implementable, ideas were tested to improve the intersample voltage limit violation problems of MPC: voltage limit tightening and Automatic Voltage Control (AVC) relay deadband tightening. The idea of incorporating knowledge on all future disturbances was also tested, which to the author's best knowledge is also something that was being done for the first time, therefore this idea is also a contribution of this thesis. Unwanted intersample phenomena were observed with this approach, and two necessary measures were introduced to counteract these: the incorporation of midpoint voltage magnitudes and the deactivation of the AVC relay. This direction showed the importance of research on profile forecasting algorithms. Finally, the performance of three control schemes was compared: the easy-to-implement, uncoordinated CCAPC, a more realistically implementable MPC and an MPC operating in ideal conditions (with access to accurate forecasts).

The results of this project were produced with the help of numerical simulations. A section of a real Stedin medium-voltage grid was selected and after some slight modifications (addition of extra PV plants), the performance of different voltage control schemes was compared. The studied grid carried the typical characteristics of a Dutch medium voltage distribution grid, as it was an underground cable network with relatively large R/X ratios. The means to influence voltage magnitudes were: the primary substation transformer's OLTC and the active power limitation of large PV plants. The simulations were conducted with the help of DIgSILENT Power Factory, a commercial power system modeling software, and Python, a general-purpose programming language. PowerFactory and the written Python scripts exchanged data using the DIgSILENT Python API. The created simulation framework made the simulation of slow grid voltage dynamics possible. The profile data used in the simulations were based on real Stedin measurements, which were available with either 1 minute or 1 hour sampling times. The profile data with the 1 hour sampling time was interpolated to 5 minute sampling time with the help of a Super Resolution General Adversarial Network (SRGAN) based interpolation model, found in the literature under [100]. To the author's best knowledge, this is the first time this interpolation method was used in order to increase the accuracy of profile data in a model predictive voltage control study. The numerical simulation based case study with the added novelty of the SRGAN-based interpolation is the third contribution of this MSc project.

5-2   Overview of Findings and Answers to the Research Questions

In the author's opinion, the most important findings of this MSc project were the following:

- The consideration of integer tap positions is necessary during the cost function minimization of the MPC policies, as it results in significantly better performance (when compared with a continuous approximation), even though the computational costs grow when using integer optimization.

- A conditional curtailment logic can be incorporated into MPC-based voltage control strategies, which is similar to the conditional curtailment logic of local APC controllers. Curtailment of a PV plant is only allowed if its local voltage magnitude is above a tuneable critical value. The formulation of this logic in the MPC policy's minimization problem can be done with the introduction of extra binary decision variables and MIL constraints. This logic helps avoid unjustifiable PV curtailment, and therefore it helps with saving energy.

- The benefits of incorporating knowledge on future disturbances into MPC policies, and hence the importance of research on forecasting these quantities were shown. Two important intersample phenomena were observed, that caused unwanted voltage limit violations. The problem of the MPC policy being unaware of intersample voltages ("intersample ignorance") can be solved with the modeling and limitation of midpoint (intersample) voltage magnitudes, which can be done with the help of binary variables and MIL constraints. Unwanted tap changes could occur due to the wrong setpoint adjustment of the AVC relay ("AVC confusion"). To eliminate this phenomenon, the AVC relay can be deactivated, when ideal future knowledge MPC policies are used, as the sampling time of said policies is lower anyway.

In Chapter 1, two research questions were formulated, for which the following answers can be given, based on the results and findings of the work presented in the previous chapters of this report:

- **How can complex distribution networks (like Stedin's medium voltage distribution networks) be modeled and simplified to be effectively used with MPC-based voltage regulation?**

  This question has already been mostly answered by the literature survey as most studies found on the topic of model predictive grid voltage regulation used the grid's sensitivity model to predict future voltages of the network [6, 103, 75, 64, 62, 54, 30, 31]. For this reason, the MPC policies that were considered in this MSc project also used the sensitivity matrix-based model. This establishes a linear relationship between the network's nodal voltage magnitudes and the changes in control actions and disturbances. The popularity of the model likely lies behind the fact that this linear relationship looks similar to the state equation of a discrete-time linear system, for which it is easiest to create model predictive controllers. Due to the model's linearity, the prediction model only adds linear equality constraints to the MPC's cost function minimization, and hence does not spoil said optimization problem's convexity. The model's parameters, the grid's sensitivity matrices, come from the linearization of the power flow equations. Due to the nonlinear nature of said equations, the sensitivity model is only accurate in the close vicinity of the current point of operation. For this reason, the sensitivity matrices were re-calculated at every sampling time step of the MPC policy, using the

built-in tools of PowerFactory (the simulation software of choice). MPC scheme that did not incorporate future knowledge needed access to the voltage magnitudes' sensitivity matrices to TR1's tap changes, and to the active power injection of curtailable PV plants. It was also shown with simulations, that in order to get a good performance with MPC, the discreteness of the primary substation transformer's OLTC should be considered in the cost function minimization problem, making it an Mixed Integer Quadratic Programming (MIQP) problem from an optimization point of view. The usage of integer variables in optimization problems comes with extra computational demands as opposed to the continuous approximation approach. When knowledge of future disturbance profiles was also assumed, the monitored voltage magnitudes' sensitivities to the external grid's voltage fluctuations and to the power injection of low-voltage customers were also required. These calculations add to the MPC polices' computational demands. In the future other sensitivity calculation methods (e.g. the enhanced Z-bus [64]), and their effect on the controller's performance and computational cost could be explored. The inclusion of ideal future knowledge in the MPC policy allowed the testing of the sensitivity matrix-based grid model's prediction capabilities. The average root mean square errors of the 1-step ahead predicted voltages were at least an order of magnitude lower than the average voltage RMSE values achieved with the best control scheme (the Ideal MPC). Even the occasional peak prediction errors, were lower or comparable to the the voltage RMSE values of said controller.

- **How effective is a MPC-based voltage control policy in mitigating the voltage disturbances caused by load, DG, and external grid voltage variation in an active MV distribution grid?**

The answer to this question lies in the comparative results of the CCAPC, Realistic MPC, and Ideal MPC schemes, presented in Section section 4-8 of Chapter 4. By looking at the V_{RMSE} voltage root mean square error results, it can be seen, that the Ideal MPC scheme resulted in the smallest (best) values followed, by the results of the Realistic MPC, and finally CCAPC. This means that the two MPC schemes are able to produce smoother voltage profiles, i.e. more nodal voltages are closer to the nominal value of 1 pu, for longer times. As far as the A_{viol} total voltage limit violation areas are concerned, only the Ideal MPC scheme seems to deliver better results than the uncoordinated CCAPC scheme, which means that the inclusion of future disturbance profiles is needed to perform better than a simpler scheme: The Ideal MPC scheme was able to completely eliminate all limit violations in 3 of the 4 test cases, and also result the smallest total limit violation area in the Summer Slovervolt test case, when no control scheme was able to completely eliminate overvoltages. This happened due to TR1's OLTC hitting its upper limit, i.e. due to the loss of important control action. As far as the Realistic MPC's limit violations are concerned, they were the highest values in 3 of the 4 test cases, and the second highest in the fourth (Winter) case, even though the voltage limits were tightened in order to decrease limit violations with this scheme. All in all, the results show that only the ideal MPC scheme is truly more effective than CCAPC against the effects of the disturbances (loading, distributed generation, and external grid voltage variation) in the studied grid. This means that the implementation of an MPC-based voltage control scheme should only be considered for the studied grid, in case accurate short-term forecasts are possible to be obtained

for the mentioned disturbance quantities. On the other hand, the studied grid was able to accept PV power with less severe voltage limit violations using both CCAPC and MPC-based schemes, compared to the base (simple AVC relay only) test cases. This means that the application of either voltage control scheme helped improve the grid's PV hosting capacity, and therefore they could both be considerable alternatives to grid reinforcement.

5-3   Future Research Directions

Considering the work and results shown in this report, the following directions could be considered for future research:

- Gathering profile data with higher temporal resolution and doing more simulations using them. This way, more accurate insight could be gained into the performance of the studied control policies, and the drawn conclusions would be based on simulations that reflect the dynamic performance of the real grid. Having profile data with higher temporal resolution for the low-voltage customers' generation and low profiles would eliminate the need to use the SRGAN interpolation method. Extra profile data would also allow the construction of more diverse test cases, as the currently studied four test cases were only based on the profiles of two days (one recorded during the winter and one recorded during the summer).

- Creating a more detailed dynamic model and higher accuracy simulations (e.g. RMS or EMT simulations) for the studied grid. This would give further insight whether the simplifications used in the constructed simulation framework are valid or not.

- Exploration of the grid's storage capabilities, and their incorporation into the MPC policy, as it would provide a better control action alternative to PV curtailment when dealing with overvoltages. The energy which would be lost with regular PV curtailment, could be injected into the grid later when it would no longer contribute to overvoltage events. At the time of writing this thesis, Dutch DSO companies are forbidden from installing battery energy storage systems into their grids, and have restricted control abilities over the connected batteries, as these actions would interfere with the energy market. For this reason, alternative storage capabilities such as smart electric vehicle charging stations, and the heat storage of buildings with controlled heat pumps could be considered. Starting points for this direction could for example be [107, 6, 62, 54].

- Studying the reactive power capabilities of distributed generation units. Even though the grid's nodal voltages have very little sensitivity to reactive power flows, the studied grid's reactive power import could be minimized with the coordination of the reactive power injection capabilities of distributed generation units, such as PV plants. This would improve the DSO's power factor, and make the company a better customer for the Transmission System Operator (TSO) that provides external high voltage grid connections.

- Measuring, predicting, and limiting currents that flow in the cables. Currently, the studied grid's installed PV capacity does not necessitate active overload control, however,

if MPC policies were able to account for this, the installed PV (and other distributed generation) capacity could be increased, making the grid less dependent power import from the external grid.

- Studying the short-term generation, load, and external grid voltage profile forecasting models/algorithms. The simulations have clearly shown the benefits of incorporating future knowledge on these quantities into the MPC policy. In those cases, however, exact knowledge was assumed on said disturbance profiles over the course of the prediction horizon. It would be interesting to see, how well the MPC policy would perform with realistically obtainable forecasts on said disturbance quantities. Starting points could for example be [29, 37, 106, 20, 39, 56].

- Exploring the usage of a commercial solver, such as Gurobi [45] for the cost function minimization problem. Right now, the cost function minimization problems are handed by the Mindtpy toolbox in Python, which decomposes the problem into Mixed Integer Linear Programming (MILP) and Nonlinear Programming (NLP) subproblems which are solved iteratively one after another. The decompositions and subsequent solver calls for the MILP and NLP subproblems are handled in Python which makes the whole process slow. With the usage of a fast commercial solver capable of handling the MIQP problems as they are, it is suspected that lower computation times could be achieved for the MPC policies.

- Exploring the usage of different sensitivity computation algorithms, such as the enhanced Z-bus method, that promise faster sensitivity computations. Starting points could for example be [63, 59, 75].

- Scaling the developed MPC policies for the actual grid, on which the studied grid of this project was based. It could be checked whether the policies are still computationally feasible with the large medium voltage grid.

- Developing a systematic tuning method for the MPC schemes. In this study, the MPC policies were hand-tuned, iteratively, using many subsequent simulations, which was a time-consuming procedure. It would be beneficial to develop a systematic approach that would also scale well to larger grids, as it would make the deployment of the control scheme much easier. A good starting point would be [36], as the authors of that paper give a systematic method to tune the weights in a linear cost function of a hybrid MPC-based emergency voltage control scheme.

- The tuning of the CC and local APC controllers is kept deliberately simple for easier reproducibility. Finding their optimal tuning and seeing how much it improves the performance of these simple uncoordinated controllers would also be interesting to see.

- Investigating the performance of the studied MPC policies when combined with a grid state estimator. All MPC policies in this study assumed full knowledge of the controlled grid's state which is only realistic with very small power systems. In practice, this full knowledge of the grid's state is obtained by using state estimators, which need time to converge and could corrupt the performance of the model predictive controllers. A starting point could for example be [43].

- Checking the performance of the studied controllers, especially the two contribution ideas of conditional curtailment and incorporation of ideal future knowledge on academic benchmark grids (e.g. CIGRÉ MV [10]). This would ensure better comparability with other similar voltage control schemes that can be found in the literature.

Appendix A

Parameters of the Studied Grid

This appendix chapter contains the detailed data of the studied grid, that was used in the numerical simulations of this study. For ease of interpretation, the grid's single line diagram is also shown here in Figure A-1. The nominal line-to-line voltages of the different busbars are given in Table A-1. The parameters of the lines are given in Table A-2, with the referred cable types described in Table A-3. The two high-voltage to medium-voltage (HV/MV) transformers, more specifically TR1 and TR2 of the primary substation are described in Table A-4. The relevant parameters of the a-eberle REG-D [2] Automatic Voltage Control (AVC) relay used at the primary substation are shown in Table A-5. The curtailable PV plants are described in Table A-6. The nominal generation and consumption of MV load elements (that describe low-voltage customers) are given in Table A-7 alongside the power factors, and the MV/LV transformers' parameters are listed in Table A-8. The load elements are described in Table A-9, and the external (high-voltage grid connection), which acted as the slack bus in the studies is described in Table A-10.
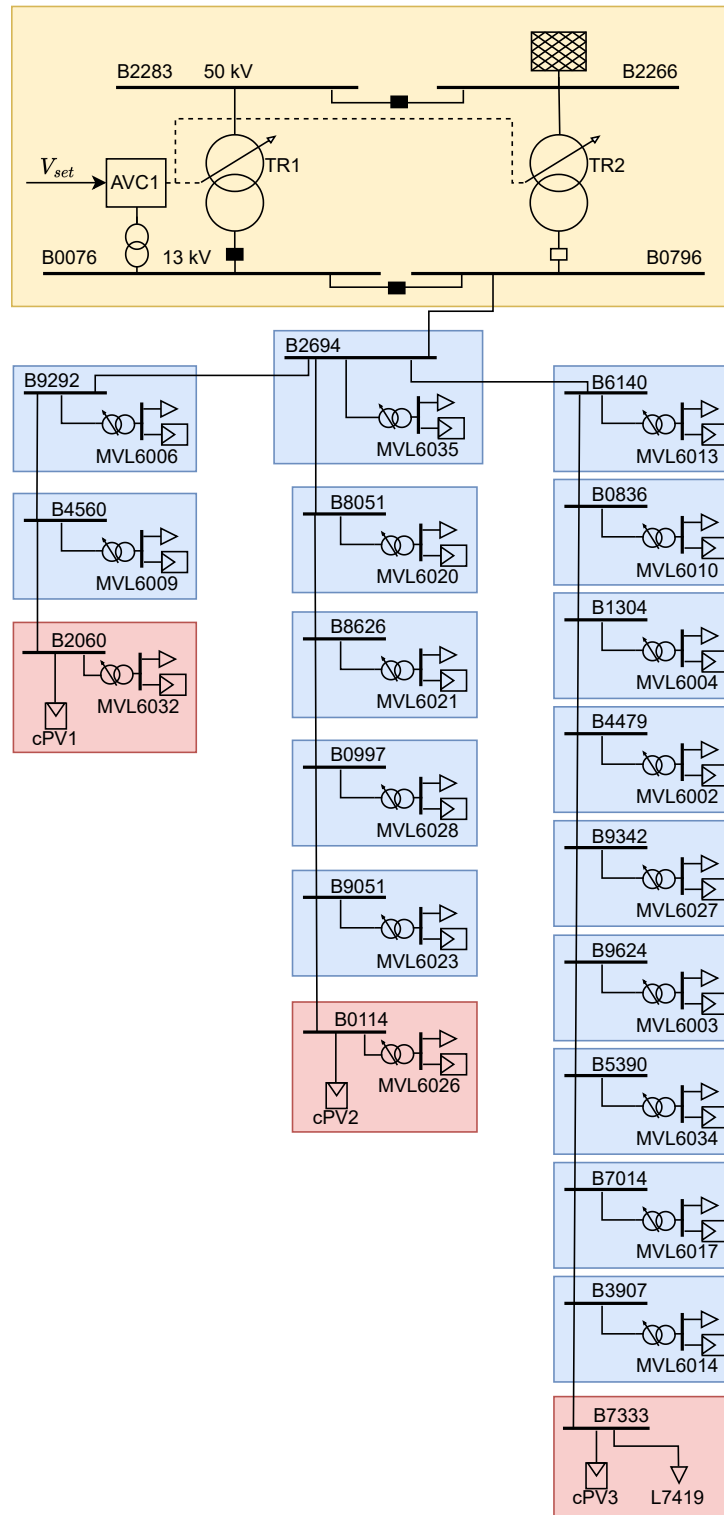
Figure A-1: Single Line Diagram of the Studied Grid

Table A-1: Busbar Data

Name	Nominal Voltage [kV]	Name	Nominal Voltage [kV]	Name	Nominal Voltage [kV]
B2266	50	B8051	13	B4479	13
B2283	50	B8626	13	B9342	13
B0076	13	B0997	13	B9624	13
B0796	13	B9051	13	B5390	13
B9292	13	B0114	13	B7014	13
B4560	13	B6140	13	B3907	13
B2060	13	B0826	13	B7333	13
B2694	13	B1304	13		

Table A-2: Line Data

From	To	Type	Laying	Length [km]
B0796	B2694	3x 95 Cu GPLK 12.5	Ground	5.382
B2694	B9292	3x 25 Cu GPLK 12.5	Ground	1.538
B9292	B4560	3x 95 Cu GPLK 12.5	Ground	0.384
B4560	B2060	3x 95 Cu GPLK 12.5	Ground	0.959
B2694	B8051	3x 50 Cu GPLK 12.5	Ground	0.482
B8051	B8626	3x 50 Cu GPLK 12.5	Ground	0.404
B8626	B0997	3x 50 Cu GPLK 12.5	Ground	0.243
B0997	B9051	3x 50 Cu GPLK 12.5	Ground	0.315
B9051	B0114	3x 50 Cu GPLK 12.5	Ground	0.431
B2694	B6140	3x 50 Cu GPLK 12.5	Ground	0.466
B6140	B0836	3x 35 Cu GPLK 12.5	Ground	0.575
B0836	B1304	3x1x150 Al XLPE 12/20 trefoil	Ground	0.653
B1304	B4479	3x 35 Cu GPLK 12.5	Ground	0.458
B4479	B9342	3x 35 Cu GPLK 12.5	Ground	0.297
B9342	B9624	3x 95 Cu GPLK 12.5	Ground	0.372
B9624	B5390	3x 95 Cu GPLK 12.5	Ground	0.823
B5390	B7014	3x 95 Cu GPLK 12.5	Ground	1.373
B7014	B3907	3x 35 Cu GPLK 12.5	Ground	1.351
B3907	B7333	3x 25 Cu GPLK 12.5	Ground	1.659

Table A-3: Cable Types

Type	R' [Ω/km]	X' [Ω/km]	B' [μS/km]	I_{nom} [kA]
3x 25 Cu GPLK 12.5	0.810	0.113	59.690	0.110
3x 35 Cu GPLK 12.5	0.579	0.107	69.115	0.135
3x 50 Cu GPLK 12.5	0.430	0.100	72.257	0.145
3x 95 Cu GPLK 12.5	0.220	0.091	91.106	0.220
3x1x150 Al XLPE 12/20 trefoil	0.205	0.125	75.398	0.290

Table A-4: HV/MV Transformer Data (TR1 and TR2)

Rated apparent power S_{rated} [MVA]	31.5
Nominal high voltage $V_{HV,nom}$ [kV]	50.25
Nominal low voltage vol$V_{LV,nom}$ [kV]	13
Short circuit voltage V_{short} [%]	14.23
Copper losses P_{Cu} [kW]	83
Vector group	YNd11
Tap side	HV
Min/nominal/max tap [−]	1/13/25
Turn ratio change / tap [%]	1

Table A-5: AVC Relay Data: a-eberle REG-D [2]

Parameter	Interpretation	Value	Unit
K_{i}	Integrator gain	-1.667	tap/pu
V_{db}	Deadband	0.01	up

Table A-6: Curtailable PV Plant Data

Name	Nominal Active Power [MW]	Power Factor [-]
cPV1	0.7	1
cPV2	0.7	1
cPV3	0.7	1

Table A-7: MV Load Data (Lumped LV areas)

Name	Transformer Type	$P_{l,nom}$ [MW]	pf$_l$ [-]	$P_{PV,nom}$ [MW]	pf$_{PV}$ [-]
MVL6006	13/0.4kV 250kVA	0.144	0.98 ind	0.1	1
MVL6009	13/0.4kV 250kVA	0.144	0.98 ind	0.1	1
MVL6032	13/0.4kV 1000kVA	0.576	0.98 ind	0.1	1
MVL6035	13/0.4kV 400kVA	0.230	0.98 ind	0.1	1
MVL6020	13/0.4kV 400kVA	0.230	0.98 ind	0.1	1
MVL6021	13/0.4kV 400kVA	0.230	0.98 ind	0.1	1
MVL6028	13/0.4kV 400kVA	0.230	0.98 ind	0.1	1
MVL6023	13/0.4kV 400kVA	0.230	0.98 ind	0.1	1
MVL6026	13/0.4kV 400kVA	0.230	0.98 ind	0.1	1
MVL6013	13/0.4kV 300kVA	0.173	0.98 ind	0.1	1
MVL6010	13/0.4kV 630kVA	0.363	0.98 ind	0.1	1
MVL6004	13/0.4kV 400kVA	0.23	0.98 ind	-	-
MVL6002	13/0.4kV 400kVA	0.230	0.98 ind	0.1	1
MVL6027	13/0.4kV 400kVA	0.230	0.98 ind	0.1	1
MVL6003	13/0.4kV 400kVA	0.230	0.98 ind	0.1	1
MVL6034	13/0.4kV 400kVA	0.230	0.98 ind	0.1	1
MVL6017	13/0.4kV 150kVA	0.086	0.98 ind	0.1	1
MVL6014	13/0.4kV 630kVA	0.3692	0.98 ind	-	-

Table A-8: MV/LV Transformer Data

Type ($V_{MV,nom}/V_{LV,nom}\ S_{rated}$)	V_{short} [%]	P_{Cu} [kW]
13/0.4kV 150kVA	4	2.1
13/0.4kV 250kVA	4	2.8
13/0.4kV 300kVA	4	3.3
13/0.4kV 400kVA	4	4.0
13/0.4kV 630kVA	4	5.4
13/0.4kV 1000kVA	6	9.9

Table A-9: Load Data

Name	$P_{l,nom}$ [MW]	pf$_l$ [-]
L7419	0.15	0.98 ind

Table A-10: External Grid (Slack Bus) Data

Nominal Voltage Magnitude [pu]	Voltage Phasor Angle [°]	S_k [MVA]	R/X [-]
1	0	750	0.1

Profile Data Used in the Simulations

This appendix chapter contains the profile data that was used in the numerical simulation of the MSc project. All the data is based on real measurements of Stedin.

B-1   External Grid Voltages

The high voltage external grid connection's voltage profiles recorded during the Summer and Winter days are shown in Figure B-1. The data was recorded with a 1 min sampling time. It can be seen that the voltages are above the nominal 1 pu, for the whole day, with both profiles, which is likely caused by the fact that the high voltage grid connects a large wind farm close to the studied medium voltage grid's external connection.
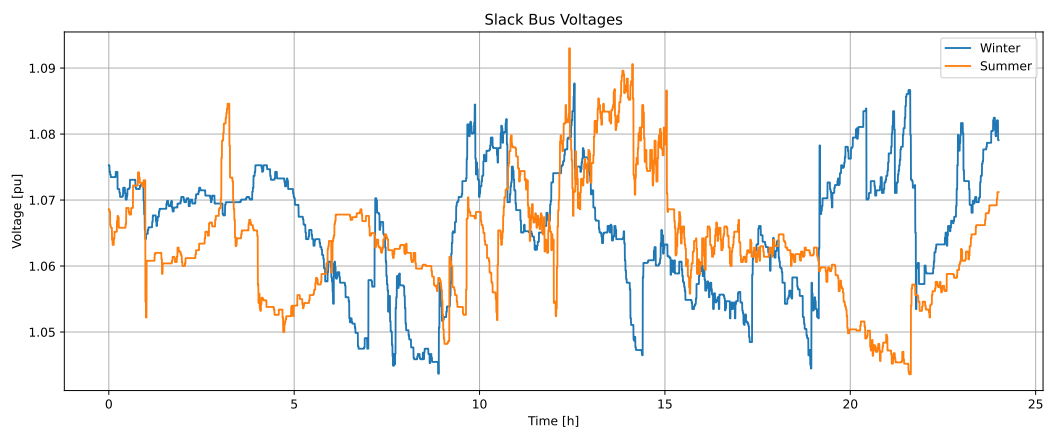
Figure B-1: Profiles for the External High-Voltage Grid Connection's Voltage Magnitude

B-2   Load Profiles

The load profiles for the low-voltage consumers are shown in Figure B-2 for the Summer, and in Figure B-3 for the Winter day. These measurements were recorded with 1 hour sampling times and interpolated to 5 minute data points using the SRGAN method of [100]. It can be seen that in both cases, loading is heavier during the evening. The winter loadings are in general higher than the summer values.
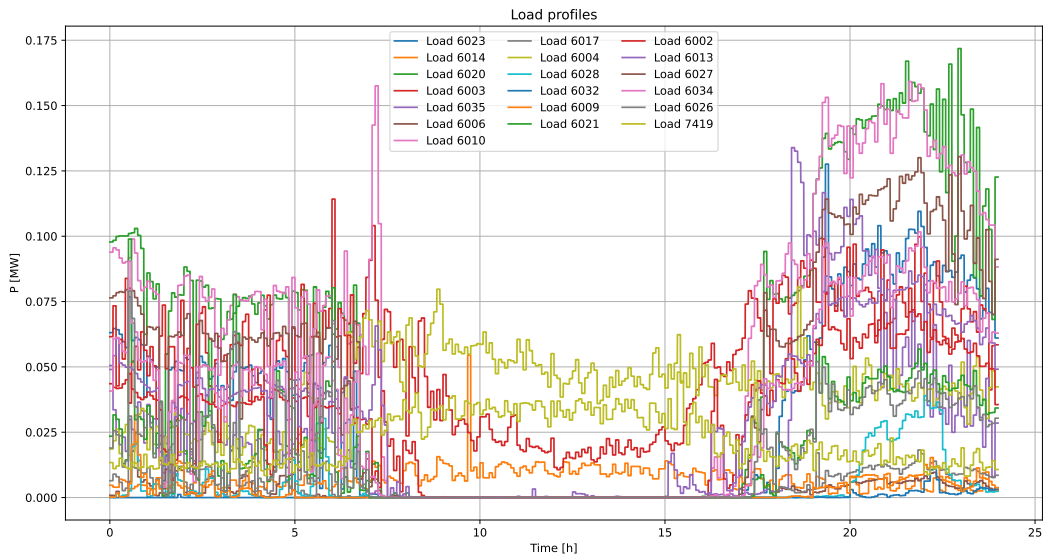
Figure B-2: Summer Load Profiles
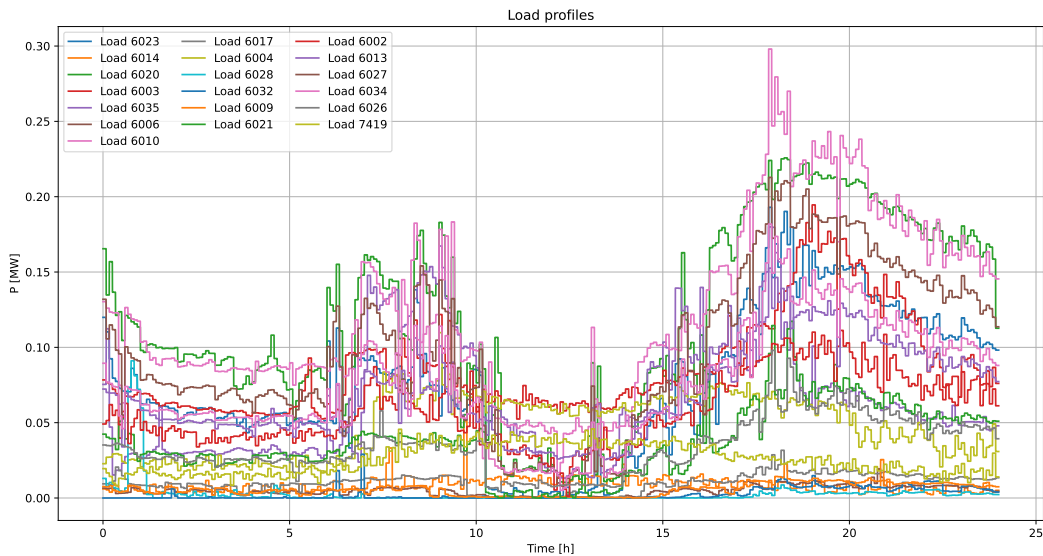
Figure B-3: Winter Load Profiles

B-3   Household (Low-Voltage) Solar Generation

The generation profiles for the household solar cells of low-voltage customers are shown in Figure B-4 for the Summer, and in Figure B-5 for the Winter day. These measurements were recorded with 1 hour sampling times and interpolated to 5 minute data points using the SRGAN method of [100]. It can be seen that photovoltaic (PV) generation is only available during the day (when loading is low), and that much more energy is produced during Summer.
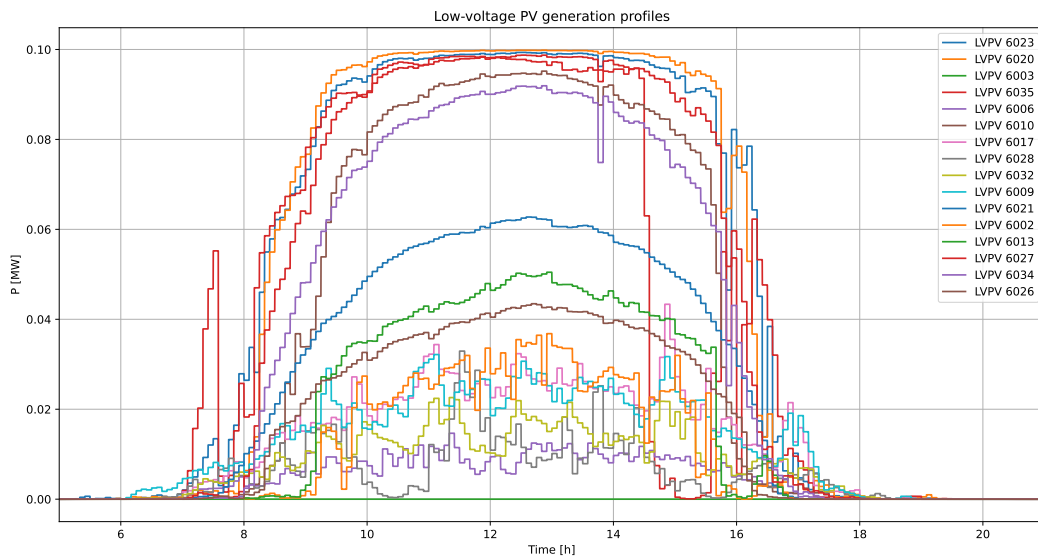
Figure B-4: Summer Generation Profiles of Household (Low-Voltage) Solar Panels
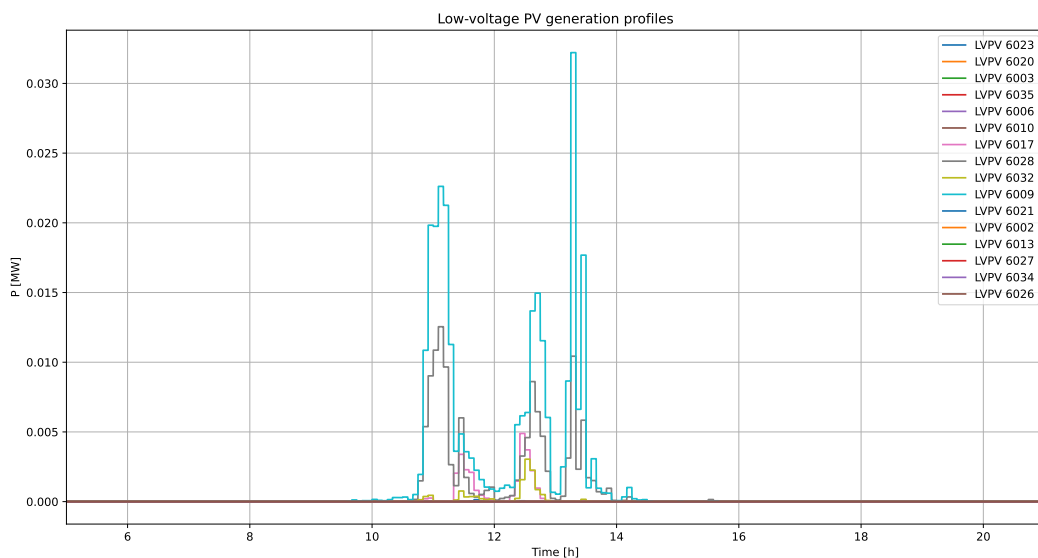
Figure B-5: Winter Generation Profiles of Household (Low-Voltage) Solar Panels

B-4   Curtailable Solar Plants

The generation profiles for the large curtailable solar plants that directly connect to the medium-voltage grid are given in Figure B-6 for the Summer day, and in Figure B-7 for the Winter day. These are based on different daily profiles of a large solar park that connects to Stedin's grid. The data was recorded with 1 minute sampling time. It can be seen, that during the summer day, the generation is capped at a maximum value, as the inverter of the PV park that served as the basis of these profiles reached its peak power capabilities. It can also be seen, that a lot less power is being produced during the Winter day.

Figure B-6: Summer Generation Profiles of Curtailable Solar Plants

Figure B-7: Winter Generation Profiles of Curtailable Solar Plants

Appendix C

Tuning of the Control Policies in the Case Study

This appendix chapter gives the tuning parameters of the control policies that were used in the case study conducted as part of this MSc thesis. Besides giving the values of said parameters it is also briefly explained how said values were obtained, usually in the form of an iterative procedure using many subsequent simulations.

C-1 Simple Model Predictive Voltage Controller

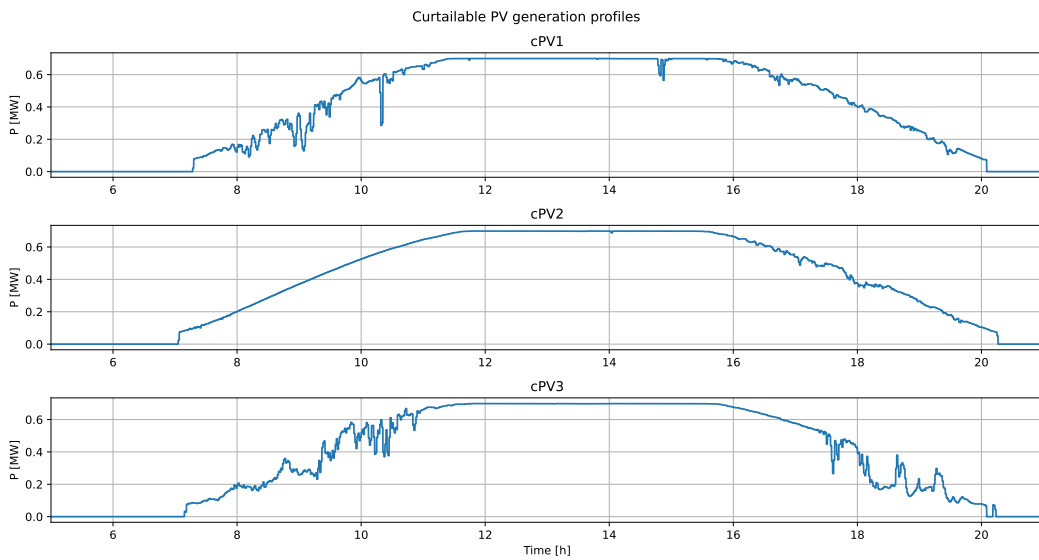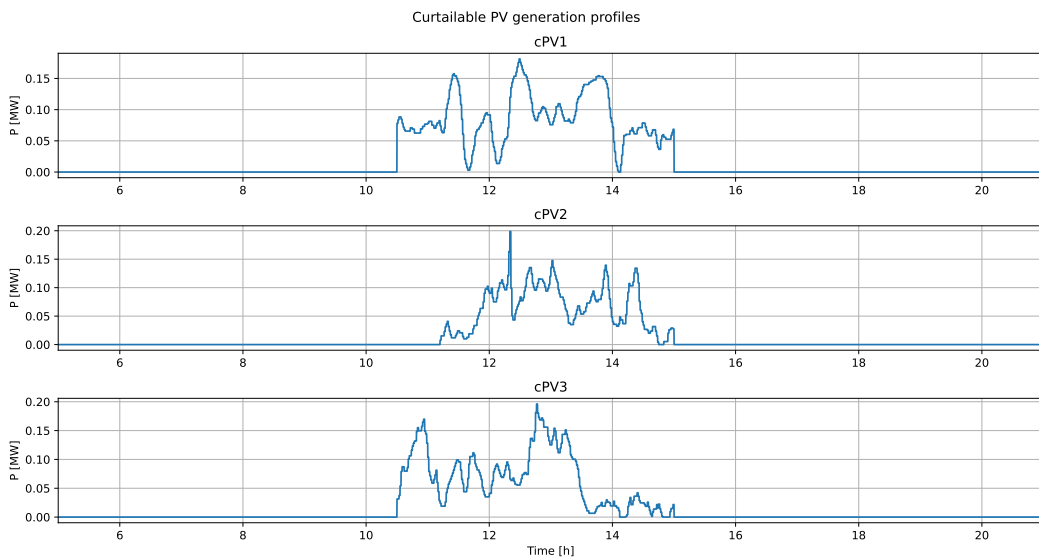The simple Model Predictive Control (MPC) policy is applied to the studied grid with the chosen $T_{\text{s,MPC}}$ sampling time of 4 minutes as shown in Table C-1. The profile data in the simulations was available with 5 minute and 1 minute temporal resolutions, so by selecting this sampling time of 4 minutes there are intersample phenomena to be observed, while the controller's actions only coincide with profile data changes every 20 minutes, making the simulations more realistic. With this sampling time, there is also plenty of time to solve the optimization problem of the cost function minimization. The rest of the tuning parameters for the simple MPC scheme applied in the case study are also given in Table C-1.

In Table C-1 I_V, I_n, and I_{cPV} are identity matrices, with sizes corresponding to the number of monitored buses, controlled On-Load Tap Changer (OLTC)s, and curtailable photovoltaic (PV) plants respectively. In case of the studied grid section, these are 21x21, 1x1, and 3x3 identity matrices respectively. According to Table C-1 the prediction horizon is 5 steps long, and the 4 minutes sampling time means that the controller is looking 20 minutes ahead into the future. During the tuning of the cost function, the Q_V weight matrix on voltage deviations was chosen to be identity and was kept constant. The other weights on control actions and limit violations were adjusted relative to this. If the controller was using one action too "bravely" (e.g. too many tap changes or too much curtailment), the coefficient in front of their identity matrix was increased. Otherwise, if it was felt that a control action could be used more toward the goal of voltage regulation, the coefficient in front of its corresponding

Table C-1: Tuning Parameters and Chosen Values for the Simple Voltage MPC Scheme

Parameter	Interpretation	Value	Unit
$T_{\text{s,MPC}}$	Sampling time of the simple MPC policy	4	minutes
N_{p}	Length of the prediction horizon	5	time steps
Q_V	Weight matrix of voltage errors	I_V	€/pu^2
R_n	Weight matrix of tap change cost	$0.002I_n$	€/tap^2
R_{cPV}	Weight matrix of active power curtailment cost	$0.05I_{\text{cPV}}$	€/MW^2
w_{low}	Weight in lower voltage limit violation cost term	10	€/pu
w_{high}	Weight in upper voltage limit violation cost term	10	€/pu
V_{low}	Lower voltage limit	0.975	pu
V_{high}	Upper voltage limit	1.025	pu
n_{min}	Minimum tap position	1	-
n_{max}	Maximum tap position	25	-
Δn_{min}	Lower limit on tap changes at once	-2	taps
Δn_{max}	Upper limit on tap changes at once	2	taps

identity matrix was decreased, making the usage of said action cheaper. The weights on limit violations were selected such that the controller avoids voltage limit violations in normal operating conditions. The minimum and maximum voltage limits are the ones described in Chapter 1 of this study. The tap position limits stem from the physical limitations of the said control device, and the limits on tap change were tuned so that only single and double tap changes are possible at once (i.e. at one sampling time step of the MPC policy).

C-2   Conditional Curtailment

The V_{crit} critical voltage (above which curtailment is allowed) and R'_{cPV} reduced curtailment weight matrix parameters for the conditional curtailment MPC are given in Table C-2. The rest of the parameters are the same as the ones selected for the simple MPC given in Table C-1.

Table C-2: Tuning Parameters and Chosen Values of the Conditional Curtailment MPC

Parameter	Interpretation	Value	Unit
V_{crit}	Critical voltage	1.015	pu
R'_{cPV}	Reduced weight matrix in curtailment cost	$0.5R_{\text{cPV}} = 0.025I_{\text{cPV}}$	€/MW^2

C-3   Voltage Limit Tightening

The chosen amount with which the voltage limits were tightened in this scheme and the increased weights on limit violations are given in Table C-3. Similarly to the previously shown values, these parameters were also tuned iteratively using many simulations. Besides the tightened voltage limits, this is a conditional curtailment MPC, so the rest of the tuning parameters can be found in the previously presented Table C-1 and Table C-2.

Table C-3: Tuning Parameters and Chosen Values of Voltage Limit Tightening MPC

Parameter	Interpretation	Value	Unit
V_{tighten}	Amount with which the voltage limits are tightened	0.005	pu
w'_{low}	Increased weight on lower limit violations	$5w_{\text{low}=50}$	€/pu^2
w'_{low}	Increased weight on upper limit violations	$5w_{\text{high}} = 50$	€/pu^2

C-4   Automatic Voltage Control Relay Deadband Tightening

The tightened deadband value used in the case study is given in Table C-4. As previously shown in Table A-4, the primary substation transformer's OLTC in the studied grid is able to change the nominal turns ratio in 1% increments. This means that one tap-change changes the Automatic Voltage Control (AVC) relay's V_{meas} measured voltage magnitude by roughly 1%. This is just a rough approximation as the actual amount depends on the grid's state and can only be determined after solving the power flow equations. The AVC relay is at rest when voltages lie within the $V_{\text{set}} \pm V_{\text{db}}$ deadband around the voltage setpoint. The original value for V_{db} is 0.01 per unit, which means that if the AVC relay acts its correction will roughly drive V_{meas} as close to V_{set} as possible. V_{db} was tightened to be $V'_{\text{db}} = 0.006$ pu, as this way, the V_{meas} will still likely end up in the $V_{\text{set}} \pm V'_{\text{db}}$ deadband around the setpoint, after a corrective tap change. Thus the tap-hunting phenomenon is likely avoided with this tuning, while the whole control scheme is able to react to smaller disturbances as well, therefore being more resilient against them.

Table C-4: Tuning Parameters and Selected Values of AVC Relay Deadband Tightening

Parameter	Interpretation	Value	Unit
V'_{db}	Tightened deadband of the AVC relay	0.006	pu

Besides the tightened AVC relay deadband this scheme used a conditional curtailment MPC whose tuning parameters are given in Table C-1 and Table C-2.

C-5   Ideal MPC: Incorporation of Future Knowledge

The $T_{\text{s,idMPC}}$ sampling time of the ideal MPC policy is decreased to be the same as the sampling time of the profile with the highest temporal resolution used in the simulated test cases: 1 minute. Its value is given in Table C-5. The rest of the tuning parameters are given in the previously presented Table C-2 (V_{crit} critical voltage and reduced R'_{cPV} curtailment weight matrix), Table C-3 (increased w'_{low}, w'_{high} limit violation weights), and Table C-1 (the rest of the parameters).

Table C-5: Tuning Parameters and Selected Values of the Ideal MPC

Parameter	Interpretation	Value	Unit
$T_{\text{s,idMPC}}$	Sampling time of the Ideal MPC	1	minutes

It has to be noted that with the increased sampling time, and the same $N_{\text{p}} = 5$ time steps control horizon the MPC policy looks only 5 minutes into the future instead of 20 minutes.

However, the prediction horizon's length was not increased in order to keep the number of decision variables in the cost function minimization problem and thus the ideal MPC policy's computation time relatively low.

C-6 Simple Control Schemes

C-6-1 Current Compounding

To make a fair comparison with MPC-based voltage control schemes Current Compounding (CC) was applied with the same 4 minutes sampling time in the case study. The chosen $T_{s,CC}$ sampling time value is given in Table C-6.

Table C-6: Tuning Parameters and Selected Values of the Current Compunding (CC) Scheme

Parameter	Interpretation	Value	Unit
$T_{s,CC}$	Sampling time of Current Compounding	4	minutes

The CC scheme's setpoint adjustment function will be tuned by equally distributing 5 voltage setpoints over the range of minimum and maximum active powers supplied by the primary substation's transformer. In the case study, the maximum active power supplied through the primary substation's transformer was measured during the winter day test case: 2.000 MW, and the minimum during the summer day: -2.805 MW. In the latter case, power flowed back to the external high-voltage grid, hence the negative sign. These values were rounded to 2.5 and -3.5 MW respectively, to account for cases that are more extreme than the edge cases of our test days. These power limit values were used during the tuning of the current compounding scheme. The 5 voltage values were equidistantly selected between $V_{low} + V_{db}$ and $V_{high} + V_{db}$, where V_{low} and V_{high} are the considered voltage limits and V_{db} is the deadband of the AVC relay. This way it is ensured that the AVC relay always acts in case there is a (lower or upper) voltage limit violation at the primary substation's monitored bus, as it can't adjust the setpoint as much as it would make (a part of) the deadband lie outside the voltage limits. The voltage setpoints with their corresponding power ranges are given in Table C-7 and the resulting stairstep function is also visualized in Figure 3-4.

Table C-7: Voltage Setpoints of the Current Compounding Scheme

$P_{prim,supp}$ range		V_{set}
Min. active power [MW]	Max. active power [MW]	AVC setpoint [pu]
$-\infty$ (-3.5)	-2.3	0.985
-2.3	-1.1	0.9925
-1.1	0.1	1
0.1	1.3	1.0075
1.3	∞ (2.5)	1.015

As it can be seen in Table C-7, in case the transformer's $P_{prim,supp}$ power delivery goes outside the range of the assumed -3.5 and 2.5 MW, the policy still gives an adjusted voltage setpoint for the AVC relay, indicated by the $-\infty$ and ∞ power limits. Figure 3-4 illustrates the stairstep (piecewise affine) shape of the CC scheme's tuned setpoint adjustment function.

Stedin uses a similar policy in its medium voltage distribution grid that served as the basis for this MSc project's studied grid. Since this study only considers a section of the actual medium-voltage grid, the setpoint adjustment function here had to be modified. The tuning of the CC scheme used with the large grid also uses a similar stairstep function, but the active power ranges and the different voltage setpoints are more arbitrary as they were specifically hand-tuned to fit the exact grid. In this study, the more systematic equally distributed power ranges and setpoints are used for easier reproducibility.

C-6-2 Local Active Power Curtailment

The tuning parameters for the local Active Power Curtailment (APC) schemes are given in Table C-8. Each curtailable PV plant's local APC scheme had the same tuning parameter choices as it is indicated in the table by $\forall j \in \mathcal{I}_{\text{cPV}}$. The reason behind this is the fact, that all three curtailable PV plants in the studied grid section have the same nominal power and are all quite far from the primary substation. They are in a similar area, so their generation profile is also quite similar. Choosing the same voltage values for each plant also makes the tuning much easier, due to fewer adjustable parameters.

Table C-8: Tuning Parameters and Selected Values of Local Active Power Curtailment Controllers

Parameter	Interpretation	Value	Unit
$T_{\text{s,APC}}$	Sampling time of local active power curtailment	10	seconds
$V_{\text{crit},j} \quad \forall j \in \mathcal{I}_{\text{cPV}}$	Critical voltage	1.015	pu
$V_{\text{max},j} \quad \forall j \in \mathcal{I}_{\text{cPV}}$	Maximum voltage	1.025	pu
$K_{\text{i},j} \quad \forall j \in \mathcal{I}_{\text{cPV}}$	Integrator gain	0.05	MW/s

The local APC schemes were implemented with the sampling time of 10 seconds as they had to operate considerably faster than the CC scheme acting at the central substation (with a 4 min sampling time). This is chosen like this, as CC affects all nodal voltages of the studied grid (thanks to the tap changes it triggers) while local APC has more localized effects. The critical voltage choice is the same as it was with conditional curtailment MPC, and the maximum voltage above which no power export is allowed is chosen to be the V_{high} upper voltage limit of this study. The $K_{\text{i},j}$ integrative gains were hand-tuned iteratively using many simulations. Balance had to be found as too large $K_{\text{i},j}$ values make the controller chatter, while too low integrative gains produce an unreasonably slow response.

Bibliography

[1] Pyomo website, 2023. http://www.pyomo.org/, Last accessed on 2023-02-21.

[2] A. Eberle GmbH & Co. KG. REG-D Relay for Voltage Control & Transformer Monitoring, 2016. First Edition.

[3] J.M. Akker, Herman Blok, Chris Budd, Rob Eggermont, Alexander Guterman, Domenico Lahaye, Jesper Lansink Rotgerink, Keith Myerscough, Corien Prins, Thijs Tromper, and Wander Wadman. A case study in the future challenges in electricity grid infrastructure. 02 2012.

[4] Alo Allik and Andres Annuk. Interpolation of intra-hourly electricity consumption and production data. In *2017 IEEE 6th International Conference on Renewable Energy Research and Applications (ICRERA)*, pages 131–136, 2017.

[5] AG Bakirtzis. Sensitivity computation for power flow control in electric power systems. *Electric power systems research*, 22(2):77–84, 1991.

[6] Pavan Balram, Ola Carlson, et al. Predictive voltage control of batteries and tap changers in distribution system with photovoltaics. In *2016 Power Systems Computation Conference (PSCC)*, pages 1–7. IEEE, 2016.

[7] P Bauer and SWH De Haan. Solid state tap changers for utility transformers. In *1999 IEEE Africon. 5th Africon Conference in Africa (Cat. No. 99CH36342)*, volume 2, pages 897–902. IEEE, 1999.

[8] A Giovanni Beccuti, Tobias Geyer, and Manfred Morari. A hybrid system approach to power systems voltage control. In *Proceedings of the 44th IEEE Conference on Decision and Control*, pages 6774–6779. IEEE, 2005.

[9] Alberto Bemporad and Manfred Morari. Control of systems integrating logic, dynamics, and constraints. *Automatica*, 35(3):407–427, 1999.

[10] K Benchmar Strunz, E Abbasi, R Fletcher, N Hatziargyriou, R Iravani, and G Joos. Tf c6. 04.02: Tb 575-benchmark systems for network integration of renewable and distributed energy resources; cigre: Paris, france, 2014. Technical report, ISBN 978-285-873-270-8.

[11] David E Bernal, Qi Chen, Felicity Gong, and Ignacio E Grossmann. Mixed-integer nonlinear decomposition toolbox for pyomo (mindtpy). In *Computer Aided Chemical Engineering*, volume 44, pages 895–900. Elsevier, 2018.

[12] Steven W Blume. *Electric power system basics for the nonelectrical professional*, chapter 1. John Wiley & Sons, 2016.

[13] Steven W Blume. *Electric power system basics for the nonelectrical professional*, chapter 4. John Wiley & Sons, 2016.

[14] Abdullah Bokhari, Ali Alkan, Rasim Dogan, Marc Diaz-Aguiló, Francisco de León, Dariusz Czarkowski, Zivan Zabar, Leo Birenbaum, Anthony Noel, and Resk Ebrahem Uosef. Experimental determination of the zip coefficients for modern residential, commercial, and industrial loads. *IEEE Transactions on Power Delivery*, 29(3):1372–1381, 2014.

[15] Hoseinali Borhan, Ardalan Vahidi, Anthony M. Phillips, Ming L. Kuang, Ilya V. Kolmanovsky, and Stefano Di Cairano. Mpc-based energy management of a power-split hybrid electric vehicle. *IEEE Transactions on Control Systems Technology*, 20(3):593–603, 2012.

[16] Michael L. Bynum, Gabriel A. Hackebeil, William E. Hart, Carl D. Laird, Bethany L. Nicholson, John D. Siirola, Jean-Paul Watson, and David L. Woodruff. *Pyomo–optimization modeling in python*, volume 67. Springer Science & Business Media, third edition, 2021.

[17] CENELEC, EN50160:2022. Voltage characteristics of electricity supplied by public distribution networks, 2022.

[18] Luigi Chisci, J Anthony Rossiter, and Giovanni Zappa. Systems with persistent disturbances: predictive control with restricted constraints. *Automatica*, 37(7):1019–1028, 2001.

[19] Christian D'Adamo, Samuel Jupe, and Chad Abbey. Global survey on planning and operation of active distribution networks-update of cigre c6. 11 working group activities. In *CIRED 2009-20th International Conference and Exhibition on Electricity Distribution-Part 1*, pages 1–4. IET, 2009.

[20] Swaechchha Dahal, Gunne John Hegglid, and Thomas Øvyang. Improved load and generation forecasting for extended day-ahead estimates in the nordic grid. In *CIRED 2023 27th International Conference & Exhibition on Electricity Distribution*, 2023.

[21] Jan Dentler, Somasundar Kannan, Miguel Angel Olivares Mendez, and Holger Voos. A real-time model predictive position control with collision avoidance for commercial low-cost quadrotors. In *2016 IEEE Conference on Control Applications (CCA)*, pages 519–525, 2016.

[22] DIgSILENT GmbH. DIgSILENT Interface Documentation: DGS Interface, 2010. Document version 003.

[23] DIgSILENT GmbH. DIgSILENT PowerFactory Application Guide: Dynamic Modelling Tutorial, DIgSILENT Technical Documentation, 2013. Revision r887.

[24] DIgSILENT GmbH. DIgSILENT PowerFactory Application Guide: DPL Tutorial, DIgSILENT Technical Documentation, 2014. Revision r1152.

[25] DIgSILENT GmbH. DIgSILENT PowerFactory Application Guide: Python Tutorial, DIgSILENT Technical Documentation, 2014. Revision r1530.

[26] DIgSILENT GmbH. Power Factory 2019 User Manual, chapter 47, 2018. Document version r5185.

[27] DIgSILENT GmbH. PowerFactory 2018 Python Function Reference, 2018. Revision 2.

[28] DIgSILENT Gmbh. Powerfactory website, 2023. https://www.digsilent.de/en/powerfactory.html, Last accessed on 2023-02-23.

[29] Vahid Rasouli Disfani, Pablo Ubiratan, and Jan Kleissl. Model predictive on-load tap changer control for high penetrations of pv using high resolution resources assessment with sky imager. In *2016 IEEE Power and Energy Society General Meeting (PESGM)*, pages 1–5. IEEE, 2016.

[30] Arunima Dutta, Sanjib Ganguly, and Chandan Kumar. Voltage control in active distribution networks and an approach based on model predictive control. In *2019 8th International Conference on Power Systems (ICPS)*, pages 1–6. IEEE, 2019.

[31] Arunima Dutta, Sanjib Ganguly, and Chandan Kumar. Model predictive control based coordinated voltage control in active distribution networks utilizing oltc and dstatcom. In *2020 IEEE International Conference on Power Electronics, Drives and Energy Systems (PEDES)*, pages 1–6. IEEE, 2020.

[32] Jawad Faiz and Behzad Siahkolah. Solid-state tap-changer of transformers: Design, control and implementation. *International Journal of Electrical Power & Energy Systems*, 33(2):210–218, 2011.

[33] Marcello Farina, Antonio Guagliardi, Federico Mariani, Carlo Sandroni, and Riccardo Scattolini. Model predictive control of voltage profiles in mv networks with distributed generation. *Control Engineering Practice*, 34:18–29, 2015.

[34] P Frase and S Morita. Distributed generation in liberalised electricity markets. international energy agency, 9, rue de la f. ed. eration. 75739 paris, cedex 15. Technical report, France, Tech. Rep, 2002.

[35] Luis Felipe Gaitán, Juan David Gómez, and Edwin Rivas-Trujillo. Quasi-dynamic analysis of a local distribution system with distributed generation. study case: The ieee 13 nodes system. *TecnoLógicas*, 22(46):140–157, 2019.

[36] Tobias Geyer, Mats Larsson, and Manfred Morari. Hybrid emergency voltage control in power systems. In *2003 European Control Conference (ECC)*, pages 1893–1898. IEEE, 2003.

[37] Shibani Ghosh, Saifur Rahman, and Manisa Pipattanasomporn. Distribution voltage regulation through active power curtailment with pv inverters and solar generation forecasts. *IEEE Transactions on Sustainable Energy*, 8(1):13–22, 2016.

[38] Francisco Gonzalez-Longatt and José Luis Rueda Torres. *Advanced smart grid functionalities based on powerfactory*. Springer, 2018.

[39] Jorge Á González Ordiano, Simon Waczowicz, Veit Hagenmeyer, and Ralf Mikut. Energy forecasting tools and services. *Wiley Interdisciplinary Reviews: Data Mining and Knowledge Discovery*, 8(2):e1235, 2018.

[40] John J Grainger. *Power system analysis*, chapter 9. McGraw-Hill, 1999.

[41] John J Grainger. *Power system analysis*, chapter 6. McGraw-Hill, 1999.

[42] John J Grainger. *Power system analysis*, chapter 1. McGraw-Hill, 1999.

[43] John J Grainger. *Power system analysis*, chapter 15. McGraw-Hill, 1999.

[44] Adam Greenhall, Rich Christie, and Jean-Paul Watson. Minpower: A power systems optimization toolkit. In *2012 IEEE Power and Energy Society General Meeting*, pages 1–6. IEEE, 2012.

[45] Gurobi Optimization, LLC. Gurobi Optimizer Reference Manual, 2023. https://www.gurobi.com.

[46] Xue Han, Anna Magdalena Kosek, Daniel Esteban Morales Bondy, Henrik William Bindner, Shi You, David Victor Tackie, Jasmin Mehmedalic, and Fannar Thordarson. Assessment of distribution grid voltage control strategies in view of deployment. In *2014 IEEE International Workshop on Intelligent Energy Systems (IWIES)*, pages 46–51. IEEE, 2014.

[47] William E Hart, Jean-Paul Watson, and David L Woodruff. Pyomo: modeling and solving mathematical programs in python. *Mathematical Programming Computation*, 3(3):219–260, 2011.

[48] TJ Tengku Hashim, Azah Mohamed, and Hussain Shareef. A review on voltage control methods for active distribution networks. *Prz. Elektrotech*, 88(6):304–312, 2012.

[49] Tor Aksel N Heirung, Joel A Paulson, Jared O'Leary, and Ali Mesbah. Stochastic model predictive control—how does it work? *Computers & Chemical Engineering*, 114:158–170, 2018.

[50] Simon Hilpert, Cord Kaldemeyer, Uwe Krien, Stephan Günther, Clemens Wingenbach, and Guido Plessmann. The open energy modelling framework (oemof)-a new approach to facilitate open science in energy system modelling. *Energy strategy reviews*, 22:16–25, 2018.

[51] CM Hird, H Leite, N Jenkins, and H Li. Network voltage controller for distributed generation. *IEE Proceedings-Generation, Transmission and Distribution*, 151(2):150–156, 2004.

[52] Saber Izadpanah Toos. Impact of tap changing transformer on voltage stability, 11 2019.

[53] Johannes Jargstorf, Ward Boeraeve, and Piet Lauwers. Voltage regulation on primary substations to increase hosting capacity. In *CIRED 2023 27th International Conference & Exhibition on Electricity Distribution*, 2023.

[54] Yibao Jiang, Can Wan, Jianhui Wang, Yonghua Song, and Zhao Yang Dong. Stochastic receding horizon control of active distribution networks with distributed renewables. *IEEE Transactions on Power Systems*, 34(2):1325–1341, 2018.

[55] Konstantinos Kavvadias, Ignacio Hidalgo Gonzalez, Andreas Zucker, and Sylvain Quoilin. Integrated modelling of future eu power and heat systems-the dispa-set v2. 2 open-source model. 2018.

[56] Hussain Kazmi and Zhenmin Tao. How good are tso load and renewable generation forecasts: Learning curves, challenges, and the road ahead. *Applied Energy*, 323:119565, 2022.

[57] Prabha S Kundur and Om P Malik. *Power system stability and control*, chapter 7. McGraw-Hill Education, 2022.

[58] Aadil Latif, Mohsin Shahzad, Peter Palensky, and Wolfgang Gawlik. An alternate powerfactory matlab coupling approach. 09 2015.

[59] Yingqi Liang, Junbo Zhang, and Dipti Srinivasan. Power system sensitivity matrix estimation by multivariable least squares considering mitigating data saturation. In *IECON 2020 The 46th Annual Conference of the IEEE Industrial Electronics Society*, pages 1676–1683, 2020.

[60] C-C Liu and Khoi T Vu. Analysis of tap-changer dynamics and construction of voltage stability regions. *IEEE Transactions on circuits and systems*, 36(4):575–590, 1989.

[61] G.X. Luo and A. Semlyen. Efficient load flow for large weakly meshed networks. *IEEE Transactions on Power Systems*, 5(4):1309–1316, 1990.

[62] Yongqing Lv, Xiaobo Dou, Qiangsheng Bu, Xiaochun Xu, Pengpeng Lv, Congyue Zhang, and Zongqiang Qi. Tube-based mpc of hierarchical distribution network for voltage regulation considering uncertainties of renewable energy. *Electric Power Systems Research*, 214:108875, 2023.

[63] Salish Maharjan, Ashwin M Khambadkone, and Jimmy C-H Peng. Enhanced z-bus method for analytical computation of voltage sensitivities in distribution networks. *IET Generation, Transmission & Distribution*, 14(16):3187–3197, 2020.

[64] Salish Maharjan, Ashwin M. Khambadkone, and Jimmy Chih-Hsien Peng. Robust constrained model predictive voltage control in active distribution networks. *IEEE Transactions on Sustainable Energy*, 12(1):400–411, 2021.

[65] Andrew Makhorin. Glpk (gnu linear programming kit). *http://www.gnu.org/s/glpk/glpk.html*, 2008.

[66] Egoitz Martinez, Iosu Fernandez, and Jose Maria Canales. Thyristor based solid state tap changer for distribution transformers. In *2013 IEEE 11th International Workshop of Electronics, Control, Measurement, Signals and their application to Mechatronics*, pages 1–5. IEEE, 2013.

[67] Carlos Mateo, Giuseppe Prettico, Tomás Gómez, Rafael Cossent, Flavia Gangale, Pablo Frías, and Gianluca Fulli. European representative electricity distribution networks. *International Journal of Electrical Power & Energy Systems*, 99:273–280, 2018.

[68] David Q Mayne, María M Seron, and SV Raković. Robust model predictive control of constrained linear systems with bounded disturbances. *Automatica*, 41(2):219–224, 2005.

[69] Juraj Medanic, Marija Ilic-Spong, and John Christensen. Discrete models of slow voltage dynamics for under load tap-changing transformer coordination. *IEEE Transactions on Power Systems*, 2(4):873–880, 1987.

[70] Alexandra Meier. Integration of renewable generation in california: Coordination challenges in time and space. *IEEE*, 10 2011.

[71] Steffen Meinecke, Džanan Sarajlić, Simon Ruben Drauz, Annika Klettke, Lars-Peter Lauven, Christian Rehtanz, Albert Moser, and Martin Braun. Simbench—a benchmark dataset of electric power systems to compare innovative solutions based on power flow analysis. *Energies*, 13(12):3290, 2020.

[72] Federico Milano. Hybrid control model of under load tap changers. *IEEE transactions on power delivery*, 26(4):2837–2844, 2011.

[73] Arvin Morattab, Ouassima Akhrif, and Maarouf Saad. Decentralised coordinated secondary voltage control of multi-area power grids using model predictive control. *IET Generation, Transmission & Distribution*, 11(18):4546–4555, 2017.

[74] R.R. Negenborn, Bart De Schutter, Marco Wiering, and J. Hellendoorn. Experience-based model predictive control using reinforcement learning. 02 2023.

[75] Hoa Minh Nguyen, Jose Luis Rueda Torres, Aleksandra Lekić, and Hoan V Pham. Mpc based centralized voltage and reactive power control for active distribution networks. *IEEE Transactions on Energy Conversion*, 36(2):1537–1547, 2021.

[76] Harsha V Padullaparti, Quan Nguyen, and Surya Santoso. Advances in volt-var control approaches in utility distribution systems. In *2016 IEEE Power and Energy Society General Meeting (PESGM)*, pages 1–5. IEEE, 2016.

[77] Harsha Vardhana Padullaparti, Quan Nguyen, and Surya Santoso. Advances in volt-var control approaches in utility distribution systems. pages 1–5, 07 2016.

[78] Nikolaos Papazacharopoulos. Voltage control in mv distribution networks with a large share of distributed renewable generation. 2014.

[79] Fabrizio Pilo, Giuditta Pisano, Sandra Scalari, Diego Dal Canto, Alfredo Testa, Roberto Langella, Roberto Caldon, and Roberto Turri. Atlantide-digital archive of the italian electric distribution reference networks. 2012.

[80] Ghanim Putrus and Edward Bentley. Integration of distributed renewable energy systems into the smart grid. *Electric Renewable Energy Systems*, pages 487–518, 2016.

[81] Marshall D Rafal and William F Stevens. Discrete dynamic optimization applied to on-line optimal control. *AIChE Journal*, 14(1):85–91, 1968.

[82] J.B. Rawlings, D.Q. Mayne, and M. Diehl. *Model Predictive Control: Theory, Computation, and Design*, chapter 1. Nob Hill Publishing, 2017.

[83] J.B. Rawlings, D.Q. Mayne, and M. Diehl. *Model Predictive Control: Theory, Computation, and Design*, chapter 2. Nob Hill Publishing, 2017.

[84] J.B. Rawlings, D.Q. Mayne, and M. Diehl. *Model Predictive Control: Theory, Computation, and Design*, chapter 6. Nob Hill Publishing, 2017.

[85] J.B. Rawlings, D.Q. Mayne, and M. Diehl. *Model Predictive Control: Theory, Computation, and Design*, chapter 3. Nob Hill Publishing, 2017.

[86] Jose Rodriguez and Patricio Cortes. *Predictive control of power converters and electrical drives*. John Wiley & Sons, 2012.

[87] Krzysztof Rudion, Antje Orths, Zbigniew A Styczynski, and Kai Strunz. Design of benchmark of medium voltage distribution network for investigation of dg integration. In *2006 IEEE Power Engineering Society General Meeting*, pages 6–pp. IEEE, 2006.

[88] SK Salman and IM Rida. Ann-based avc relay for voltage control of distribution network with and without embedded generation. In *DRPT2000. International Conference on Electric Utility Deregulation and Restructuring and Power Technologies. Proceedings (Cat. No. 00EX382)*, pages 263–267. IEEE, 2000.

[89] SK Salman and ZG Wan. Fuzzy logic-based avc relay for voltage control of distribution network with and without distributed/embedded generation. In *2007 IEEE Lausanne Power Tech*, pages 2128–2132. IEEE, 2007.

[90] Francisco Sanchez Gorostiza and Francisco Gonzalez-Longatt. Integration digsilent - python. an introduction., 12 2019.

[91] Džanan Sarajlić and Christian Rehtanz. Overview of distribution grid test systems for benchmarking of power system analyses. In *2020 AEIT International Annual Conference (AEIT)*, pages 1–6. IEEE, 2020.

[92] Charles R Sarimuthu, Vigna K Ramachandaramurthy, KR Agileswari, and Hazlie Mokhlis. A review on voltage control methods using on-load tap changer transformers for networks with renewable energy sources. *Renewable and Sustainable Energy Reviews*, 62:1154–1161, 2016.

[93] Peter W Sauer, Mangalore A Pai, and Joe H Chow. *Power system dynamics and stability: with synchrophasor measurement and power system toolbox*, chapter 7. John Wiley & Sons, 2017.

[94] Kevin P Schneider, BA Mather, BC Pal, C-W Ten, Greg J Shirek, Hao Zhu, Jason C Fuller, José Luiz Rezende Pereira, Luis F Ochoa, Leandro Ramos de Araujo, et al. Analytic considerations and design basis for the ieee distribution test feeders. *IEEE Transactions on power systems*, 33(3):3181–3188, 2017.

[95] Dariush Shirmohammadi, H Wayne Hong, A Semlyen, and GX Luo. A compensation-based power flow method for weakly meshed distribution and transmission networks. *IEEE Transactions on power systems*, 3(2):753–762, 1988.

[96] Statistics Netherlands (CBS). Renewable electricity share up by 20 percent in 2022, 2023. https://www.cbs.nl/en-gb/news/2023/10/renewable-electricity-share-up-by-20-percent-in-2022, Last accessed on 2023-03-25.

[97] Matthias Stifter, Roman Schwalbe, Filip Pröstl Andrén, and Thomas Strasser. Steady-state co-simulation with powerfactory. 05 2013.

[98] Brian Stott and Ongun Alsac. Fast decoupled load flow. *IEEE transactions on power apparatus and systems*, (3):859–869, 1974.

[99] Harald G Svendsen and Ole Chr Spro. Powergama: A new simplified modelling approach for analyses of large interconnected power systems, applied to a 2030 western mediterranean case study. *Journal of Renewable and Sustainable Energy*, 8(5):055501, 2016.

[100] Rui Tang, Jonathon Dore, Jin Ma, and Philip HW Leong. Interpolating high granularity solar generation and load consumption data using super resolution generative adversarial network. *Applied Energy*, 299:117297, 2021.

[101] Reinaldo Tonkoski and Luiz AC Lopes. Impact of active power curtailment on overvoltage prevention and energy production of pv inverters connected to low voltage residential feeders. *Renewable energy*, 36(12):3566–3574, 2011.

[102] Minh-Quan Tran, Trung Thai Tran, Phuong H Nguyen, and Guus Pemen. Sparse identification for model predictive control to support long-term voltage stability. *IET Generation, Transmission & Distribution*, 17(1):39–51, 2023.

[103] Gustavo Valverde and Thierry Van Cutsem. Model predictive control of voltages in active distribution networks. *IEEE Transactions on Smart Grid*, 4(4):2152–2161, 2013.

[104] S Vigneshwaran and T Yuvaraja. Voltage regulation by solid state tap change mechanism for distributing transformer. *International Journal of Engineering Research & Technology (IJERT)*, 4(02), 2015.

[105] Andreas Wächter and Lorenz T Biegler. On the implementation of an interior-point filter line-search algorithm for large-scale nonlinear programming. *Mathematical programming*, 106:25–57, 2006.

[106] Jingyao Wang. Power system short-term load forecasting. In *Proceedings of the 2017 5th International Conference on Machinery, Materials and Computing Technology (ICMMCT 2017)*, pages 250–253. Atlantis Press, 2017/04.

[107] Yun Wang, Dong Liu, and Qing-Sheng Li. A hybrid system based cps model and control of loads in active distribution network. In *2016 IEEE International Conference on Power System Technology (POWERCON)*, pages 1–8. IEEE, 2016.

[108] Zhengfa Zhang, Filipe Faria da Silva, Yifei Guo, Claus Leth Bak, and Zhe Chen. Double-layer stochastic model predictive voltage control in active distribution networks with high penetration of renewables. *Applied Energy*, 302:117530, 2021.

[109] Marek Zima and Göran Andersson. Stability assessment and emergency control method using trajectory sensitivities. In *2003 IEEE Bologna Power Tech Conference Proceedings,*, volume 2, pages 7–pp. IEEE, 2003.

Glossary

List of Acronyms

TSO	Transmission System Operator
DSO	Distribution System Operator
ANM	Active Network Management
OLTC	On-Load Tap Changer
AVC	Automatic Voltage Control
DG	Distributed Generation
PV	photovoltaic
MPC	Model Predictive Control
QP	Quadratic Programming
NLP	Nonlinear Programming
MILP	Mixed Integer Linear Programming
MIQP	Mixed Integer Quadratic Programming
MINLP	Mixed Integer Nonlinear Programming
MIL	Mixed Integer Linear
MLD	Mixed Logical Dynamical
PWA	Piecewise Affine
RMPC	Robust Model Predictive Control
SMPC	Stochastic Model Predictive Control
CC	Current Compounding
APC	Active Power Curtailment
SRGAN	Super Resolution General Adversarial Network

List of Symbols

A_{viol}	area of total voltage limit violations
G_{ii}, B_{ii}	conductance and susceptance in diagonal element i of the network's admittance matrix
J, $\tilde{J}$	Jacobian matrices of the power flow equations
K_{i}	integrative gain
M^k, C^k	mismatch and correction vectors for iteration k of the Newton-Raphson algorithm
N_{p}	length of the prediction horizon in time steps
P_{LV}	active power injection of low voltage customers
P_{S}, P_{l}, P_{PV}	active power quantities in the illustrative simple feeder example (supplied, consumed by the load, injected by the solar plant respectively)
P_{all}	vector containing the allowed active power limits for curtailable PV plants
$P_{\mathrm{cPV,mid}}$	vector containing the midpoint active power injections of curtailable PV plants
P_{cPV}	vector consisting the active power outputs of curtailable PV plants
P_{cur}	vector of active powers lost due to the curtailment of PV plants
P_{nom}	vector of nominal power outputs for the curtailable PV plants
P_{poss}	vector containing the possible active power outputs of curtailable PV plants
$P_{\mathrm{prim,supp}}$	active power supplied through the primary substation's transformer
P_i, Q_i	scheduled active and reactive power of bus i in the power flow equations respectively
Q_V	weight matrix on voltage devitaions from the reference
Q_{S}, Q_{l}, Q_{c}	reactive power quantities in the illustrative simple feeder example (supplied, consumed by the load, injected by the compensator respectively)
R_n, R_{cPV}	weight matrices on control actions (tap changes and PV curtailment respectively)
S_n, S_{PcPV}, S_{PLV}, S_{sl}	the monitored voltage magnitudes sensitivity to tap changes, active power injections of curtailable PV plants and low-voltage customers, and voltage fluctuations of the external grid (slack bus) respectively
$T_{\mathrm{MPC,max}}$	maximum MPC computation time
$T_{\mathrm{s,APC,j}}$	sampling time of curtailable PV plant j's active power curtailment scheme
$T_{\mathrm{s,CC}}$	samping time of the current compounding scheme
$T_{\mathrm{s,MPC}}$	sampling time of MPC voltage controllers
$T_{\mathrm{s,idMPC}}$	sampling time of the ideal MPC policy with future knowledge of disturbances
V	vector of monitored voltage magnitudes in the MPC schemes
V_{RMSE}	voltage root mean square error
V_{crit}	critical voltage, above which the curtailment of a PV plant is allowed
V_{db}	deadband of the automatic voltage control relay
V_{high}	upper limit on monitored voltage magnitudes
V_{low}	lower limit on monitored voltage magnitudes

V_{mid}	vector of monitored midpoint voltage magnitudes in the MPC scheme that incorporates midpoint voltages
V_{set}, V_{meas}	voltage setpoint and measurement of automatic voltage control relays
V_{tighten}	the amount with which voltage limits were tightened
V_i	voltage magnitude of bus i in the power flow equations
$V_{\text{cPV},j}$	local voltage magnitude of the jth PV plant
$\mathbf{I}$	current phasor in the illustrative feeder example
$\mathbf{V}_{\text{S}} = V_{\text{S}}\angle\varphi_{\text{S}}$, $\mathbf{V}_{\text{R}} = V_{\text{R}}\angle\varphi_{\text{R}}$	voltage phasors of the sending and receiving side in the illustrative simple feeder example
$\mathbf{Y}$	admittance / admittance matrix of the grid
$\mathbf{Z}$, R, X	cable impedance, resistance and reactance in the illustrative simple feeder example
$\mathbf{a}$, $\mathbf{a}_{\text{nom}}$, $\mathbf{y}_t$	off-nominal, nominal turns ratio, and series admittance in a transformer's π-model respectively
ε	machine precision parameter used in mixed-integer linear constraints
$\varepsilon_{\text{low}}, \varepsilon_{\text{high}}$	slack variables for the implementation of soft voltage limits
b_{cur}	binary auxiliary variable, for the incorporation of conditional curtailment into the MPC policies
b_{mid}	binary auxiliary variables for the calculation of midpoint voltages
n	tap position of the on-load tap changer mechanism
n_{min}, n_{nom}, n_{max}	minimum, nominal, and maximum on-load tap changer positions respectively
p_{cur}	relaitve PV curtailment
$w_{\text{low}}, w_{\text{high}}$	weights on lower and upper limit violations respectively
z_{cur}, z_{cPV}	auxiliary continuous variables for the calculation of midpoint voltages